

JOÃO PAULO MONTICELLI

**WEATHERING STUDY OF THE GNEISSIC ROCK MASS FROM THE
MONTE SECO TUNNEL REGION, SOUTHEASTERN BRAZIL**

São Paulo

2019

JOÃO PAULO MONTICELLI

**WEATHERING STUDY OF THE GNEISSIC ROCK MASS FROM THE
MONTE SECO TUNNEL REGION, SOUTHEASTERN BRAZIL**

Dissertation presented to the Graduate
Program in Civil Engineering at the
Polytechnic School of the University of
São Paulo to obtain the degree of Master
of Science

Concentration area:
Geotechnical Engineering

Advisor:
Prof. Dr. Marcos Massao Futai

São Paulo
2019

Autorizo a reprodução e divulgação total ou parcial deste trabalho, por qualquer meio convencional ou eletrônico, para fins de estudo e pesquisa, desde que citada a fonte.

Este exemplar foi revisado e corrigido em relação à versão original, sob responsabilidade única do autor e com a anuência de seu orientador.

São Paulo, _____ de _____ de _____

Assinatura do autor: _____

Assinatura do orientador: _____

Catálogo-na-publicação

Monticelli, João Paulo

WEATHERING STUDY OF THE GNEISSIC ROCK MASS FROM THE MONTE SECO TUNNEL REGION, SOUTHEASTERN BRAZIL / J. P.

Monticelli -- versão corr. -- São Paulo, 2019.

154 p.

Dissertação (Mestrado) - Escola Politécnica da Universidade de São Paulo. Departamento de Engenharia de Estruturas e Geotécnica.

1.Weathering of gneissic rocks 2.Tunnel 3.Fall of blocks 4.Geologic and geotechnical investigations 5.Cordierite I.Universidade de São Paulo. Escola Politécnica. Departamento de Engenharia de Estruturas e Geotécnica II.t.

Dedico este trabalho aos meus pais, irmãos e ao meu tio Tadeu.

ACKNOWLEDGMENTS

I would like to thank my parents, Paulina and João Jerônimo, and my sister and brother, Tatiana and Murilo, for all their support during this journey, sharing knowledge, experiences and affection.

Special thanks to my advisor Prof. Marcos Massao Futai, known by few as Marcão, for having provided me with an incredible life experience, academic and professional, and for having oriented and provided me all the necessary support for the development of the scientific initiation, graduation work and master's thesis. Thank my co-authors/advisors, Pedro (3), Rogério (4) and Joel (5) for the support in the development of each chapter of this dissertation.

Thank also to all which made part or currently are in the GeoInfraUSP research group: Silvia, Pedro, Willian, Renato, André, Uilian, Sérgio, Vitor (Cancro), Vitor, Luana, Andrei and Adrian. Thanks also to the technicians, Benedito, Jordana, Verônica, Mirna and Adílson for the works that directly or indirectly affected this study.

Gratitude to my uncle Tadeu (in memoriam) for receiving my "technical visits" with great affection and willingness to teach the practical life side of his works along of the Brazil.

Thanks also to all my friends (Otávio, Karina, Alan, Duilio, Atié, Juliana, João, Júlio, Natália, Lucca, Natasha, Carol and many others) for the hours shared at the pubs discussing subjects since geology to the Brazilian political problems.

AGRADECIMENTOS

Eu gostaria de agradecer os meus pais, Paulina e João Jerônimo, e os meus irmãos, Tatiana e Murilo, por todo apoio durante essa jornada dividindo conhecimento, experiências e carinho.

Agradeço especialmente ao meu orientador Prof. Marcos Massao Futai, conhecido por poucos como Marcão, por ter me proporcionado uma incrível experiência de vida, acadêmica e profissional, e por ter me orientado e concebido todo o apoio necessário ao desenvolvimento dos trabalhos de iniciação científica, de formatura e de dissertação de mestrado. Agradeço aos meus coautores/coorientadores, Pedro (3), Rogério (4) e Joel (5) pelo suporte no desenvolvimento de cada capítulo dessa dissertação.

Agradeço também a todos que fizeram parte ou estão atualmente do grupo de pesquisa GeoInfraUSP: Silvia, Pedro, Willian, Renato, André, Uilian, Sérgio, Vitor (Cancro), Vitor, Luana, Andrei e Adrian. Agradeço também aos técnicos, Benedito, Jordana, Verônica, Mirna e Adílson pelos trabalhos que direta ou indiretamente afetaram esse estudo.

Gratidão ao meu tio Tadeu (*in memoriam*) por receber as minhas “visitas técnicas” com muito carinho e disposição para ensinar o lado prático da vida em suas obras pelo Brasil.

Agradeço também a todos meus amigos (Otávio, Karina, Alan, Duílio, Atié, Juliana, João, Júlio, Natália, Lucca, Natasha, Carol e muitos outros) pelas horas compartilhadas as mesas de bares discutindo assuntos desde geologia aos problemas políticos brasileiros.

“Geology has an overwhelming sadness that can never be got rid of. This sadness comes
from the idea that time works against them”

Salvador Dalí

ABSTRACT

This study refers to a qualitative and quantitative weathering characterization of a gneiss rock mass (weathering profile, intact rock and discontinuity) in a tropical region. The rock mass was excavated for a construction of an unlined railway tunnel, which during its useful life began to present block instability problems linked to the weathering and the time of exposure of the rock.

The weathering of the rock mass and its weathering grades are approached in the geological and geotechnical points of view, covering bibliographical review on the subject, field inspection, direct and indirect investigations, and laboratory tests: petrographic analysis, X-ray diffraction, physical properties and durability index, sclerometry, ultrasonic test, uniaxial and diametral compression.

Keywords: Tunnel, weathering, weathering indexes, petrographic analyses, gneiss, fall of blocks

RESUMO

Este estudo se refere à caracterização qualitativa e quantitativa do intemperismo de um maciço rochoso gnáissico (perfil de intemperismo, rocha intacta e descontinuidades) em uma região tropical. O maciço foi escavado para a construção de um túnel ferroviário não revestido, que ao longo da vida útil começou a apresentar problemas de instabilidade de blocos vinculados ao intemperismo e ao tempo de exposição da rocha.

O intemperismo do maciço rochoso e os seus graus de alteração foram abordados do ponto de vista geológico e geotécnico, levando-se em consideração uma ampla revisão bibliográfica sobre o tema, inspeção de campo, investigações diretas e indiretas, e os seguintes ensaios laboratoriais: análise petrográfica, difratometria de raios X, índices físicos e de durabilidade, esclerometria, ultrassom, compressão uniaxial e diametral.

Palavras Chave: Túnel, intemperismo, índices de alteração, análise petrográfica, gnaisse, queda de blocos.

LIST OF FIGURES

Figure 3.1 - Site of the Monte Seco Tunnel. Southeast Brazil (A), Colatina Lineament Domain (B) and in detail, the local geological map (C) (modified from Vieira et al. 2014).	29
Figure 3.2 - Mapping of lineament traces (A), rose diagram and identification of main sets of lineaments traces (B), and histogram of respective lengths in km (C).	31
Figure 3.3 - Characterization of discontinuity sets by geological mapping (A) showing the contours of pole concentrations (B) and rose diagram (C) of the geological structures.	32
Figure 3.4 - Topographic features and their relationship with weathering, erosion and drainages in the Monte Seco site. The Vitória-Minas Railroad (VMR) and the local highway (BR 101) are represented by red and black lines, respectively.	33
Figure 3.5 - Type and intensity of weathering in the Monte Seco Tunnel in the summer (red) and winter (blue) (modified after Dearman et al. 1978).	34
Figure 3.6 - Classification of heterogeneity in petrographic facies B1, B2 and B3 for the gneissic rock of the Monte Seco Tunnel.	34
Figure 3.7 - Examples of discontinuities apparent on TLS point cloud (A), the contours of pole concentrations (B) and rose diagram obtained (C) of the geological structures (modified after Cacciari and Futai 2017).	36
Figure 3.8 - Sectors A, B, C and D used for the analysis of the weathering conceptual model (A) and the distribution of the volumetric fracturing intensity for F1, F2 and F3 discontinuity sets, and for rock mass (F1+F2+F3) (B) (modified after Cacciari et al. 2017).	37
Figure 3.9 - Location of the first 340 m of the Monte Seco tunnel and geotechnical investigation performed at tunnel site (Cacciari and Futai 2016).	38
Figure 3.10 - Geotechnical profile from SR-01, 02 and 03, the correspondent geoelectrical profile 1 and the drilling boreholes illustrating the contrast between the weathering horizon along the valley.	39
Figure 3.11 - Geoelectrical profiles illustrating the contrast between the weathering horizon along the valley (GP 2 to 7) and geoelectrical anomalies related to the sectors A, B, C and D of the TLS mapping.	41
Figure 3.12 - Geoelectrical profile perpendicularly to the tunnel axis (GP 8) and geoelectrical anomaly related to the sector C.	42

Figure 3.13 - Contact between weathering horizons I and III, close to the Monte Seco Tunnel site.	42
Figure 3.14 Representative weathering samples of F1 (A), F2 (B) discontinuity sets and foliation Sn (C) and photomicrographs illustrating mineral weathering. The discontinuity wall is positioned at the top of D1 (A) and to the right side of D5 (B) and D13 (C).	46
Figure 3.15 Relationship between average residual friction (ϕ_r) estimated by the Ja parameter and apparent porosity (η) of the discontinuity wall samples.	47
Figure 3.16 Distribution of the volumetric fracturing intensity (F1+F2+F3) (modified after Cacciari et al., 2017) and indication of the sectors A, B, C and D used for analyzing the conceptual weathering model.	50
Figure 3.17 Weathering profile indicating sectors A, B, C and D. Illustration of the formation of Horizon II (very to intermediately weathered rock mass) and advance of weathering via F1 and F2 discontinuity sets, and sheet fractures related to foliation opening (F3 - Sn). Horizon I – Transported Soil, and Horizon III – Weakly weathered rock mass.	51
Figure 4.1 - Site of the Monte Seco Tunnel. Southeast Brazil (A), Colatina Lineament Domain (B) and in detail, the local geological map (C) (modified from Vieira et al. 2014).	61
Figure 4.2 - Relationship between strength ratio and durability index for some igneous and metamorphic rocks in accordance with a general classificatory approach of weathering grades.	64
Figure 4.3 - Photomicrographs illustrating: A) facies B1; B) facies B2; C) facies B3; D) biotite altered to chlorite and iron oxides and hydroxides; E) cordierite altered to pinite, chlorite, sericite and iron oxides and hydroxides; F) plagioclase and orthoclase altered to sericite; G) intermineral fissures in facies B1; H) fissured weathered matrix of facies B2 impregnated with iron oxides and hydroxides, and I) fissured weathered matrix of facies B3, fissures currently found empty. Abbreviations: Fi – intramineral fissure, Fe – intermineral fissure, Ft – transmineral fissure and Fr – radial fissure; V- voids; Qz – quartz, Cr – cordierite, Fk – orthoclase, Pl – plagioclase, Bt – biotite, Pn – pinite, Chl – chlorite, Sr – sericite and Ox./Hx. – iron oxides and hydroxides.	70
Figure 4.4 - Relationship between micropetrography index (I_p) and porosity (η) for the gneissic rock facies B1, B2 and B3.	72
Figure 4.5 - Photos after all the SDT cycles for each petrographic facies and weathering grade. Petrographic facies: (A) B1, (B) B2 and (C) B3. Weathering grades: W1 (fresh to	

slightly weathered), W2 (moderately weathered) and W3 (highly to completely weathered).	75
Figure 4.6 - The behavior of I_d according to the weathering grade of each petrographic facies along the five SDT cycles. It is shown in detail the mutual behavior of the facies for weathering grades (A) W1 (fresh to slightly weathered), (B) W2 (moderately weathered) and (C) W3 (highly to completely weathered). Slake durability classes (Gamble, 1971): VH (very high); H (high), MH (medium high), M (medium), L (low), VL (very low) with the value of the alterability parameter (10 – 4) (Celada et al. 2014).	76
Figure 4.7 - Relationships between the uniaxial compressive strength (UCS) and strength ratio (R_s) with porosity (η) (A and D), micropetrographic index (I_p) (B and E) and durability index (I_d) (C and F), presenting the general weathering grades classification for the intact rock of the Monte Seco Tunnel. Weathering grades: I: fresh, II: slightly weathered, III: moderately weathered, IV: highly weathered and V: completely weathered.....	77
Figure 4.8 - Relationship between UCS and I_d RMR rating values along the 1 st cycle (A), 2 nd cycle (B) and 3 rd to 5 th cycle (C). Weathering grades: fresh (I), slightly weathered (II), moderately weathered (III), highly weathered (IV) and completely weathered (V).	83
Figure 4.9 - Relationship between the R_s and I_d along the weathering grades with the alterability equation proposed for granite and gneissic rocks, I_{d4} (A) and compared with Celada et al. (2014) (B).	84
Figure 5.1 - Micromorphological and textural description of weathered minerals based on the shape and volume of the alteromorphs (Modified from Delvigne 1998).	95
Figure 5.2 - Weathering profile adopted to study the Monte Seco Tunnel rock mass....	97
Figure 5.3 - Flowchart of the methodology.	100
Figure 5.4 - Flowchart of the methodology of the additional step: cordierite alteromorph characterization.....	101
Figure 5.5 - Photomicrographs of the mineral weathering stages and weathering process in fissured quartz (Qz), orthoclase (Fk) and plagioclase (Pl) (A – C). Biotite (Bt) undergoing incipient weathering, producing goethite (Gth) along some cleavages (D) and interlayered chlorite (Chl) and probably smectite in an advanced weathering stage (E). Cordierite (Cr) undergoing weathering, producing pinite (Pn) and chlorite with an incipient wedge effect (G) in an advanced weathering condition or producing interlayered pinite, chlorite and probably smectite, with sericite (Sr) with an extreme wedge effect (F).	

Hypersthene (Hp) (H) and garnet (Gr) (I) producing high quantities of goethite. In the images, (D – G) depict the fissuring process due to the textural modification of the biotite and cordierite alteromorphs. The voids are represented by the letter V, while the mineral weathering stages (0 – 4) are denoted inside the brackets.....	103
Figure 5.6 - Illustration of a X-ray diffraction test showing some of the final weathering products, in this case, smectite, illite and kaolinite.	104
Figure 5.7 - Dominant weathering process affecting the gneissic rock minerals.....	106
Figure 5.8 - Textural and micromorphological gneissic rock mineral classification. ..	107
Figure 5.9 - Photomicrographs of the cordierite evolution stages (0, 1, 2, 3 and 4) with respect to the petrographic intramineral weathering indexes.	110
Figure 6.1 - Illustration of the criterion used for the petrographic weathering index application (modified after Monticelli et al. 2019a). Yellow boxes represent what could be classified as UM, while the blue boxes are related to the criterion applied based on textural and micromorphological modifications.....	128
Figure 6.2 - Photomicrographs illustrating the evolution of the fissures in facies B1 (sample numbers 1-5), B2 (sample numbers 6-10) and B3 (sample numbers 11-15) according to the $I_{p\ mod}$ and the comparison between the initial (Table 6.2) and the general (I-V) weathering grade classifications. The samples numbers 1 to 15 are denoted in white, and the values of $I_{p\ mod}$ are denoted in red. Intramineral (F_i), intermineral (F_e) and transmineral (F_t) fissures are indicated.....	130
Figure 6.3 - Relationship between physical properties, porosity and bulk density, for the petrographic facies of the gneissic rock mass.	131
Figure 6.4 - Relationships among the average values of the petrographic index, physical properties (bulk density and porosity), compression wave velocity and rebound number with the general weathering grades.	133
Figure 6.5 - Results of sclerometry tests carried out in heterogeneously weathered rock blocks. Rebound numbers were obtained from the rock block surface ($R_{L\ sur}$), the extracted sample ($R_{L\ cp}$) and the average values of the extracted samples ($R_{L\ int}$).	134
Figure 6.6 - Photographic record after the UCS and ITS tests for the completely weathering grade of petrographic facies B1 (A), B2 (B) and B3 (C). Illustrations of the typical compressive stress-strain (displacement) curves from the UCS (D) and ITS (E) tests highlighting the different weathering grade behaviours.....	136
Figure 6.7 - Comparison between parallel and transverse tensile strength values obtained for the extreme weathering grades.....	137

Figure 6.8 - Relationships between the UCS, tensile strength and elastic modulus with the bulk density and porosity.....	139
Figure 6.9 - Relationships between the UCS, tensile strength and elastic modulus with the rebound number and compression wave velocity.....	140
Figure 6.10 - Relationships between the tensile strength (a) and elastic modulus (b) with the UCS.	141
Figure 6.11 - Relationships between the mechanical parameters (UCS, ITS and E) and the modified petrographic weathering indexes, UC_{mod} (a) and $I_{p\ mod}$ (b).....	142
Figure 6.12 - The degradation curves of rock mechanical parameters due to weathering of the Monte Seco Tunnel and of similar lithotypes.....	146

LIST OF TABLES

Table 3.1 - Joint alteration number – Ja (Barton et al. 1974)	45
Table 3.2 - Joint weathering number and physical properties	47
Table 3.3 – Weathering agents affecting the tunnel.....	49
Table 4.1 - Intact rock weathering grades (Modified after Hoek and Brown, 1997; BS 5930 1999, ISRM, 2015)	67
Table 4.2 - Durability classifications	68
Table 4.3 - Description of the petrographic facies of the gneissic rock	69
Table 4.4 - Physical and petrographic properties observed in thin sections.....	71
Table 4.5 - Durability and strength of the gneissic rock from the Nova Venécia Complex	78
Table 4.6 - General weathering grade classification of the gneissic rock of the Monte Seco tunnel	81
Table 4.7 - The alterability parameter for a granite and gneissic rocks.....	85
Table 5.1 - Intact rock weathering grades (Modified after Hoek and Brown, 1997; BS 5930, 1999, ISRM, 2015)	99
Table 5.2 - Weathering grade characterization and additional thin section work.....	100
Table 5.3 - Evolutionary stages of the cordierite alteromorphs.....	109
Table 5.4 - Petrographic aspects of the weathering grades.....	113
Table 6.1 - Description of the petrographic facies of the gneissic rock	125
Table 6.2 - Intact rock weathering grades (modified after Hoek and Brown, 1997; BS 5930, 1999 and ISRM, 2015)	126
Table 6.3 - The porosity and uniaxial compression strength values.....	145
Table 6.4 - Weathering grades of gneissic rock matrix in terms of petrographic modifications	147

SUMMARY

1. INTRODUCTION.....	21
2. OBJECTIVES AND DISSERTATION STRUCTURE.....	22
3. CONCEPTUAL WEATHERING MODEL OF GNEISSIC ROCK MASSES IN TROPICAL CLIMATE CONDITIONS	25
Abstract.....	25
3.1 Introduction.....	26
3.2 Geological settings.....	28
3.3 Terrestrial laser scanning analyses	35
3.4 Weathering profile	37
Indirect and direct investigations	38
Weathering of discontinuity walls.....	42
Conceptual model of weathering advance in the Monte Seco Tunnel region.....	48
3.5 Conclusions.....	52
3.6 References.....	53
4. RELANTIONSHIP BETWEEN DURABILITY INDEX AND THE UNIAXIAL COMPRESSIVE STRENGTH IN DIFFERENT WEATHERING GRADES OF A GNEISSIC ROCK MASS	59
Abstract.....	59
4.1 Introduction.....	60
4.2 UCS and SDT in RMR 2014 update.....	62
4.3 Characterization of weathering grades.....	62
4.4 Materials and methods	65
4.5 Results and discussion	68
4.5.1 Petrographic and physical characterization of the gneissic rock.....	68
4.5.2 Durability and strength characterization of the gneissic rock	74
4.5.3 RMR ratings of Id ₂ and UCS.....	81
4.6 Conclusion	85
4.7 References.....	87

5. TEXTURAL AND MICROMORPHOLOGICAL CHARACTERIZATION OF TROPICAL WEATHERING EFFECTS ON CORDIERITE IN GNEISSIC ROCK ...	91
Abstract.....	91
5.1 Introduction.....	92
5.2 Geological and weathering conditions.....	96
5.2 Materials and methods	97
5.4 Results.....	101
5.4.1 Gneissic textural and micromorphological characterization.....	101
5.4.2 Cordierite textural and micromorphological characterization.....	108
5.4.3 Petrographic aspects and weathering grade characterization	111
5.5 Discussion and conclusion.....	114
5.6 References.....	115
6. THE INFLUENCE OF WEATHERING GRADES ON GNEISSIC ROCK	119
Abstract.....	119
6.1 Introduction.....	120
6.2 Background.....	121
6.3 Materials and methods	123
6.4 Influence of weathering on the petrographic and physical properties of gneissic rocks	129
6.5 Influence of weathering on strength and deformability.....	134
6.6 Discussion.....	142
6.7 Conclusion	149
6.8 References.....	150
7. GENERAL REMARKS.....	153

1. INTRODUCTION

The Monte Seco Tunnel, pertaining to the Vitória – Minas Railroad (VMR) responsible for the transportation of ore from the region of Belo Horizonte (BH) to Vitória (VT), southeast Brazil, was excavated in a gneissic rock mass. Given the favorable conditions at the time of the construction (1950s), neither shotcreting nor anchoring were used for treating the rock mass. In recent years, however, as reported by the railroad maintenance team, the instability of blocks in this and in other tunnels of the VMR have been reported. Although they do not indicate a generalized risk, this problem can cause severe logistic damages to cargo transport. This theme has recently motivated researchers from the GeoInfraUSP (EPUSP) to develop studies to evaluate the geomechanical behavior of the Monte Seco Tunnel.

The block instability observed in the Monte Seco Tunnel results from several factors related to the tropical climate that have caused the degradation of geological-geotechnical parameters of the rock mass, such as the joints shear strength and the intact rock durability and tensile strength, causing blocks to loosen from the roof and walls, particularly in fractured and weathered zones, making excavation unsafe over the years. In this manner, it is important to investigate how weathering affects certain regions of the tunnel and others do not. And, in the affected areas of the rock mass, to study deeply the rock matrix weathering process and to characterize his weathering grades.

The study developed for this dissertation demonstrates that geological-geotechnical investigations, with emphasis on structural geology and rock characterization by petrographic analyses and laboratories test are of fundamental importance for civil engineering works in tropical regions, where the weathering affects in an anisotropic and heterogeneous way the rock mass to great depths, affecting progressively its mechanical properties. Besides that, the use of a standardized classification of the textural and micromorphological modifications of the minerals can improve the criteria among the engineering geologists in the petrographic weathering index analyses applied to weathering grades assessment.

The fractures and foliation are the structures responsible for the weathering advance in the rock mass. The genesis of these structures has influence on the type and intensity of fracturing, in the weathering of their walls and the water infiltration along the tunnel. Among the analyzed sectors (A, B, C and D), which showed different weathering aspects,

sector C, a fault zone, is the most susceptible to weathering and consequently block instability.

The gneissic rock mass presents three petrographic facies B1, B2 and B3, which characterize the heterogeneity of the lithotype banding. The effect of the heterogeneity was analyzed along the weathering grades in terms of petrographic analysis, physical properties, durability sclerometry, ultrasonic test, uniaxial compressive strength and indirect tensile strength. Comparatively to facies B1 and B2, facies B3 was placed at the start of the moderately weathered grade according with the weathering indexes considered and the related petrographic and mechanical properties.

Among the principles minerals of the gneissic rock observed in thin sections, such as quartz, feldspars, biotite and garnet, the cordierite mineral is the one with the greatest alterability. The appearance of the Meso-alteromorph texture in the cordierite and biotite minerals in the weathering grades III and IV, respectively, contribute to the generation of intra to transmineral fissures, and the resulting changes reflects the fragility mechanism of the crystalline fabric, which are the major responsible for the gneissic rock mechanical degradation.

The heterogeneity characterization and the relationship between petrographic and physical-mechanical weathering indexes of gneissic rocks are usually limited in the literature as well as the bond loss effects of the cordierite weathered mineral. For these reasons, it's believed that this dissertation brings some pioneer aspects of the characterization of weathering grades of gneissic rocks.

2. OBJECTIVES AND DISSERTATION STRUCTURE

The objectives of this dissertation aim, basically:

- (i) Separate the tunnel regions with similar weathering aspects and correlate this condition to the falling of blocks;
- (ii) Characterize, qualitatively and quantitatively, the weathering grades of the gneissic rock mass, considering its petrographic facies, through petrographic analyses, physical-mechanical tests, and weathering indexes;
- (iii) Identify the minerals - and modifications in their crystal fabric - responsible for the weathering processes and the degradation of gneissic rock in the tropical environment.

Chapters 3, 4, 5 and 6 of this dissertation presents the studies which allowed to achieve the objectives mentioned above. It should be noted that each of these chapters corresponds to an eventual publication in well-known scientific journals. Chapter 7 summarizes the general remarks of all the work.

The development of the chapters considered several steps:

- 1) Analysis of the basic geological surveys and the studies developed by the researchers of the GeoInfra USP Project in the Monte Seco Tunnel region;
- 2) Qualitative characterization of the weathering grades of the gneissic rock and quantification of these grades in terms of petrographic analyzes and the following tests: physical indices, slake durability, sclerometry, ultrasonic, uniaxial and diametral compression.
- 3) Organization and interpretation of test results considering weathering indexes;
- 4) Integration of the information obtained in the previous items to develop the dissertation chapters in the format of articles for submission. The authors are designated at the footnote in each chapter beginning.

3. CONCEPTUAL WEATHERING MODEL OF GNEISSIC ROCK MASSES IN TROPICAL CLIMATE CONDITIONS¹

Abstract

The Monte Seco Tunnel is part of the Vitória-Minas Railway in Brazil and is used for transporting iron ore. It was excavated in the 1950s through a gneissic rock mass of the Nova Venécia Complex. Rock falls currently occur in tunnels along this railway, affecting ore transport logistics. Rock block falls in the Monte Seco Tunnel are controlled by subvertical fracturing, foliation and weathering. Fractures and foliation are the structures responsible for the weathering advance in the rock mass. The genesis of these structures influences the type and intensity of fracturing, the weathering of their walls and the water infiltration along the tunnel. The analyzed sectors showed different weathering aspects. A fault zone was identified as the most susceptible to weathering and, consequently, to block instability. In this paper, geological investigations that utilized geoelectrical imaging and 3D terrestrial laser scanning mapping, focusing on the structural geology, led to the development of a conceptual model of weathering advance in the Monte Seco Tunnel.

Keywords: weathering, structural geology, gneissic rock mass, tunnel.

¹Authors: Monticelli J. P., Cacciari P. P., Futai M. M.

3.1 Introduction

The Monte Seco Tunnel, of the Vitória-Minas Railway (VMR), is used to transport ore from the region of Belo Horizonte (BH) to Vitória (VT) in southeastern Brazil and was excavated in a gneissic rock of the Nova Venécia Complex (Vieira et al. 2014). Given the favorable conditions at the time of construction (1950s), neither shotcrete nor anchoring were used for treating the rock mass. In recent years, however, the instability of blocks in this and in other tunnels of the VMR has been reported by the railroad maintenance team. Although they do not indicate a generalized risk, this problem can cause severe damage to cargo transport logistics. This issue has recently motivated researchers from the GeoInfraUSP (EPUSP) to develop studies to evaluate the geomechanical behavior at the site laboratory of the Monte Seco Tunnel (Cacciari et al. 2013; Monticeli et al. 2015; Cacciari and Futai 2016, 2017).

The block instability observed in the Monte Seco Tunnel results from several factors related to the tropical climate and have caused degradation of geological and geotechnical parameters of the rock mass, such as the shear strength of the joints and the durability and tensile strength of the intact rock, causing blocks to loosen from the roof and walls over the last several years, particularly in fractured and weathered zones, making the tunnel potentially unsafe. Hence, a detailed study of the geological characteristics that have influenced the weathering evolution in the tunnel is fundamental to re-evaluating the rock mass behavior.

The weathering of rock masses is widely recognized to depend on intrinsic factors, such as the nature of the rock, and extrinsic factors, such as the climate, topography, time of exposure and geotectonic evolution. The climate influence is manifested via the oscillation of temperature and rainfall, which is the most influential factor that determines the type and intensity of weathering processes. The topography controls the infiltration and drainage of rainwater along weathering profiles, causing erosion and deposition. The rock mass is more or less resistant to physical and chemical processes according to its genesis and geological history. In addition to lithology, another important geological aspect is the presence of certain structures, such as fractured and faulted zones (Saunders and Fookes 1970; Deere and Patton 1971; Dearman et al. 1978).

Geological structures, i.e., fissures, fractures, fault zones, geological contacts, and foliation, which result from the evolution of geotectonic regimes in geological history,

are the link that connect weathering agents from the surface with the deepest portions of the rock masses, promoting the variation in the weathering profile sequence and geometry and the building of landscape features (Delvigne 1998; Modenesi-Gauttieri et al. 2002; Turkington et al. 2005; Place et al. 2016). This connection could even be related to endogenous processes (Dewandel et al. 2017), which are more significant at greater depths in underground excavations.

The genesis of the rock mass, chronology of the structures present, and in situ stress fields are relevant aspects in the weathering advance to the subsurface, as the flow of water, the main weathering agent, is governed by the opening of discontinuities in fractured crystalline rock masses (Freeze and Cherry 1979). The crosscutting of fractures and the current stress field could induce reactivation of certain discontinuity sets, which leads to displacement and dilation. The increase in aperture would consequently increase transmissivity along specific paths in the fracture network (Barton et al. 1995; Ferrill et al. 1999; Konzuk and Kueper 2004; Morin and Savage 2003), influencing the weathering pattern in the subsurface and spatial variation in the weathering profiles. Differences in weathering intensity with geological time may also influence the change in hydraulic conductivity of weathering profile horizons (Lachassagne and Wyns 2011).

A rock mass undergoes specific geotectonic regimes throughout its history, which could promote the development of a complex weathering pattern that is structurally controlled in the subsurface. This pattern is not usually considered in the main classification models of weathering profiles applied to engineering geology. To characterize weathering in the subsurface, it is fundamental to characterize the conditioning properties at different scales and under different points of view, gathering detailed and varied information about weathering advance and evolution (Ehlen 2005).

In this article, information on the genesis of geological structures, weathering profiles, and weathering along discontinuity walls in a study area is collected and compared with discontinuity and signal return intensity (or backscatter) maps from terrestrial laser scanning (TLS) point clouds and geoelectrical imaging profiles in the same area. In this case, it was possible to correlate the genesis of geological structures with the fracture intensity observed along the tunnel, the moisture identified on the walls and roof, the geoelectrical anomalies and the weathering conditions of the discontinuity walls, allowing for a better understanding of the preferred weathering paths and,

consequently, the advance of weathering profiles and patterns inside the Monte Seco Tunnel.

The data interpretation indicated that the tunnel has four sectors, A, B, C and D, with different weathering aspects. The weathering advanced via F1 and F2 discontinuity sets in sectors A and C and via foliation S_n in sector B, while sector D does not exhibit weathering agents. The F2 discontinuity set of Precambrian age was reactivated during the Cretaceous, forming a fault zone identified in sector C. Neotectonism (Cenozoic) is responsible for the change in the drainage pattern in the study area and for originating F1 discontinuity set, which currently controls water infiltration in sectors A and C. The sheet fractures are closely related to opening along foliation S_n in the tunnel site and transport weathering agents in sector B. These geologic features trigger the destabilization of rock blocks that impact iron ore transport logistics of the VMR.

3.2 Geological settings

The regional study of the structural geology covered the main tectonic events that occurred in the study area. The photointerpretation of the regional structural framework of the basement was carried out using *Quantum GIS* software, connecting the domains of Folha Aracruz (SE-24-Y-D-IV) and Colatina (SF-24-Y-C-VI) (Figure 3.1). The final product, represented at a 1:100.000 scale, used 2.666 km² of aerial photos to obtain the trace lineaments.

The Monte Seco Tunnel was excavated in a gneissic rock of the Nova Venécia Complex in the northern portion of the Mantiqueira Province (Araçuaí fold belt system), on the Brazilian Atlantic coast (Figure 3.1 A) (Almeida et al. 1981; Pedrosa-Soares et al. 2001). The overall geology and structural framework of this province is related to the Brasiliano orogenic cycle, which includes a succession of accretionary and collisional episodes that were mainly active during the Proterozoic to Paleozoic and were responsible for the creation of Gondwanaland (Brito Neves and Fuck 2013). Lineaments associated with shear zones are well recognized in the study area and are marked by the change in orientation from NE and NNE in the Ribeira domain to N-S and NNW in the Araçuaí domain (Braun 1982).

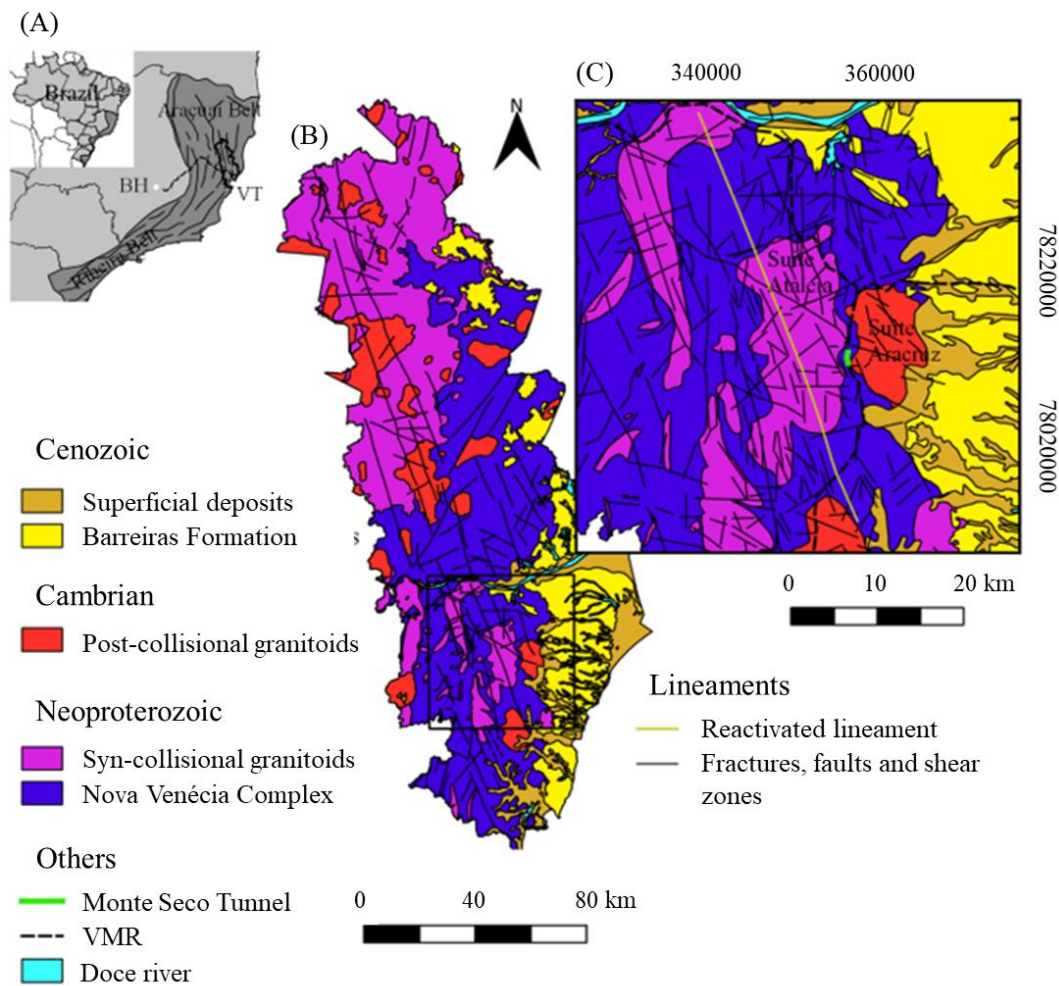


Figure 3.1 - Site of the Monte Seco Tunnel. Southeast Brazil (A), Colatina Lineament Domain (B) and in detail, the local geological map (C) (modified from Vieira et al. 2014).

This structural rearrangement is related to the Vitória Ecoporanga Shear Zone (VESZ), locally named the Colatina Lineament, a NNW-trending network of fractures, faults and shear zones that crosses the state of Espírito Santo from Vitória to Atelia, totaling 280 km in length (Vieira et al. 2014). These are the main structures that characterize the Monte Seco Tunnel area (Figure 3.1 B). The crystalline basement of the study area consists mainly of Neoproterozoic rocks (Precambrian), including highly deformed gneissic rocks of the Nova Venécia Complex in contact with syn-collisional granitoids due to tectonic movement. Cambrian rocks are also present and consist of a variety of post-collisional granitoids of Paleozoic age, sedimentary deposits of the Barreiras Formation, and alluvial, colluvial and coastal deposits of Cenozoic age (Figure 3.1 C). Mesozoic magmatism is represented by dike swarms that rarely outcrop in the study area and are therefore not shown in our maps.

The geological and structural evolution of this area is marked by a series of deformation phases and structural reactivations accompanied by magmatic episodes, periods of denudation and erosion, seismicity and intraplate activity, some of which are well-established and some of which are still controversial. Regionally, 299 lineaments were identified and are represented in the map in Figure 3.2A. The lineament attitudes and lengths were measured, resulting in the principal orientations WNW, NNW, NNE, ENE and E-W (Figure 3.2B and C). The Monte Seco Tunnel was previously investigated by field measurements, and three discontinuity sets and gneissic foliation were recognized (Figure 3.3) (Cacciari and Futai, 2017).

The NNW lineaments stand out in the study area because of their frequency and length; similarly, the WNW and NNE trends are less distinctive yet also stand out. However, only the NNW-trending lineaments result in a significant expression in the tunnel structural mapping. Foliation and F2 discontinuity set show the same trend of the regional NNW lineaments, which correspond to the regional-scale trend from the Neoproterozoic to the Paleozoic. Ductile structures, such as the gneissic foliation, formed during the Brasiliano/Pan-African orogenic cycle, and the brittle structures formed after the lateral shift of the orogeny in the early Cambrian (Alkmim et al. 2006; Vieira et al. 2014).

According to Valente et al. (2012), the set of fractures NNW mapped in Suite Atelia as a dextral transtensional strike-slip fault zone that originated in the Brasiliano (represented in orange in Figure 3.1C) was reactivated by a brittle and extensional regime early in the Cretaceous. This was accompanied by the intrusion of small-scale dike swarms dated to 136 Ma. The Monte Alegre alignment (AFZ) fracture set, whose genesis is connected to the Colatina Lineament located S of Vitória (capital of the state of Espírito Santo), shows features that indicate assimilation of the tectonic movements, reactivating some of these structure planes as NNW-SSE normal faults (Calegari et al. 2016). The reactivations and dike intrusions that occurred preferentially along the Precambrian structures of the Colatina Lineament are interpreted as analogous to the dike swarms of the Ponta Grossa Arch in southern Brazil: the result of an aulacogen or aborted rift related to the opening of the Atlantic Ocean in the Cretaceous (Sial et al. 1987; Novais et al. 2004; Vieira et al. 2013).

The ENE and EW lineaments are less significant in frequency and length at a regional scale, showing approximately the same trend of the F1 discontinuity set in the

Monte Seco Tunnel (Figures 3.2 and 3.3). F1 discontinuity set is a transversal structure relative to foliation and F2 discontinuity set, showing angular relations and geometric patterns of conjugate pairs of shear joints with extension cracks, and are related to a normal fault in an extensional regime. Thus, these discontinuities probably initiated in the Cretaceous in brittle and extensional regimes. However, the ENE and EW lineaments have been considered to be related to the evolution of the Brazilian Continental Coastal Basins and resurgent tectonics, which started in the Paleogene and has been continually active during the Neogene and the Holocene. Such lineaments correspond to the initial phase of the neotectonic intraplate activity in Brazil, as registered by the initial deposition of the Barreiras Formation (Hasui 1990).

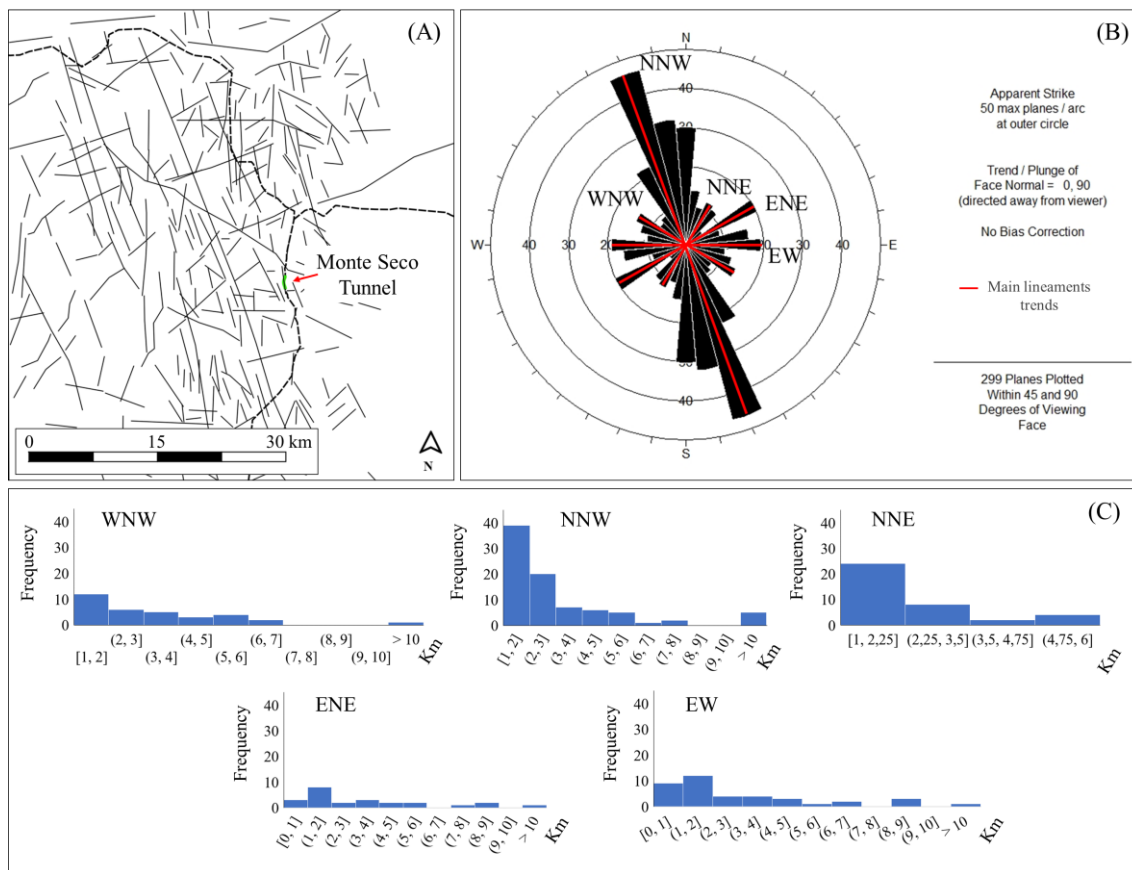


Figure 3.2 - Mapping of lineament traces (A), rose diagram and identification of main sets of lineaments traces (B), and histogram of respective lengths in km (C).

Some of the NE- to ENE-trending normal faults of southeastern Brazil, recognized by Riccomini et al. (1989) and Riccomini and Assumpção (1999), are associated with a distensional tectonic event whose minor tensile axis is oriented along the NW-SE quadrant. The normal faults in the weathered basement rock, as observed by Calegari et

al. (2016), and in the superficial deposits, as observed by Mello et al. (2005) and Hatushika et al. (2005), were related to this stress state, in accordance with the orientation of F1 fractures in the Monte Seco region.

F3 discontinuity set, with no superficial expression due to its low dip angles, terminates at both the F1 and F2 structures, sometimes crossing them, as noticed during field inspections at the tunnel site. F3 is considered to be a set of sheet fractures related to the aperture of the foliation as a consequence of the hilly topography of the area.

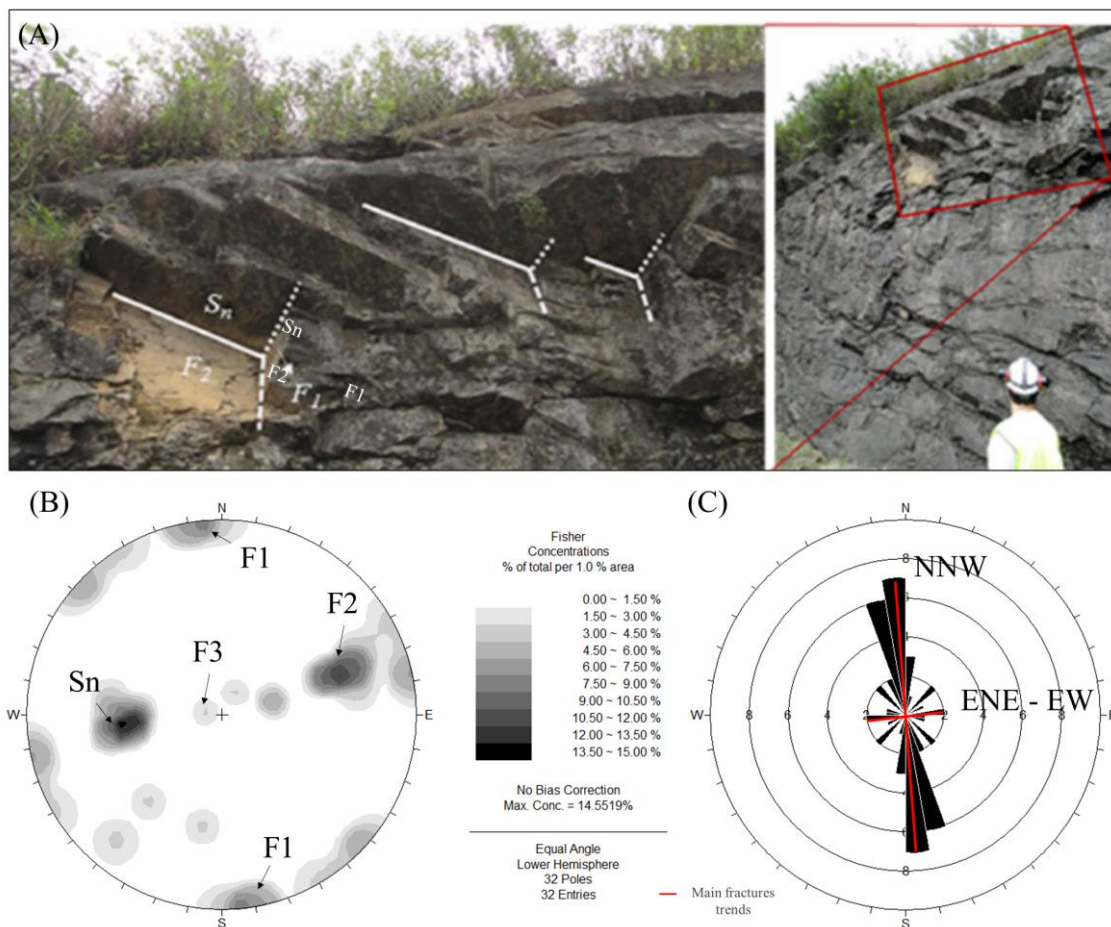


Figure 3.3 - Characterization of discontinuity sets by geological mapping (A) showing the contours of pole concentrations (B) and rose diagram (C) of the geological structures.

The geological structural characteristics formed a relief composed of hills and slopes with pronounced declivities along valleys structurally controlled by regional NNW lineament traces. The shape of the outcropping rock is that of a sugarloaf and has been affected by weathering and gravitational pluvial events, causing the valleys to be filled with varied materials from the hills. ENE-trending drainage leads superficial water

toward the valleys (Baltazar et al. 2010) (Figure 3.4).

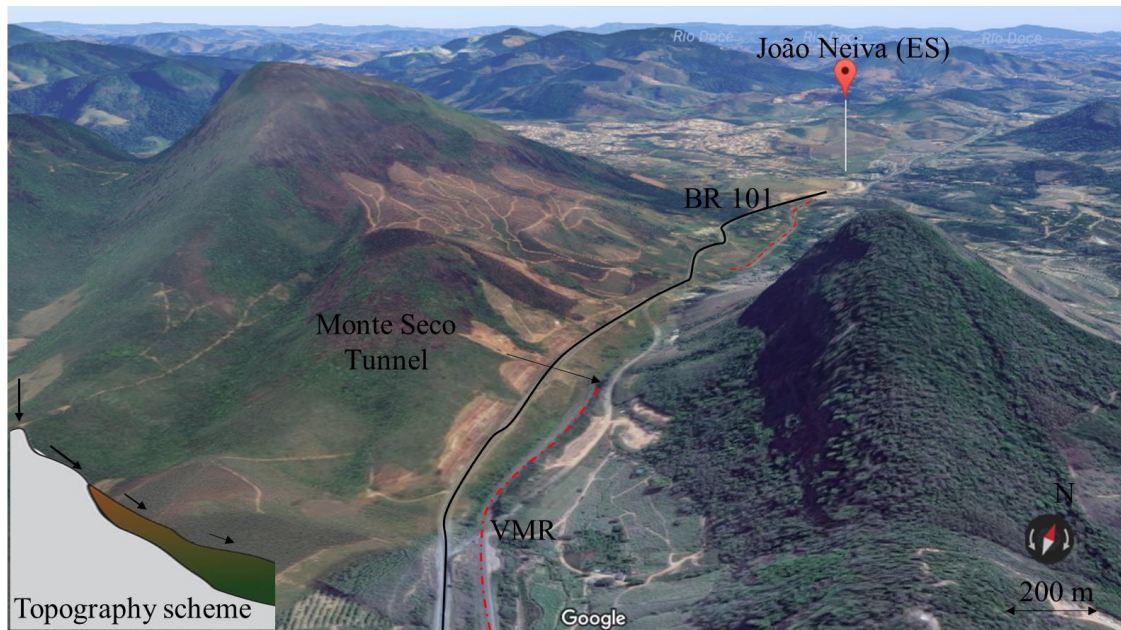


Figure 3.4 - Topographic features and their relationship with weathering, erosion and drainages in the Monte Seco site. The Vitória-Minas Railroad (VMR) and the local highway (BR 101) are represented by red and black lines, respectively.

Climatic conditions control the intensity of weathering on the surface. Disaggregation and decomposition of the rock mass are mainly influenced by temperature and rainfall. In the study area, seasonal rainfall varies from 100 to 120 cm in the summer and from 50 to 20 cm in the winter, and the average daily varies from 28 to 26 °C in the summer and 22 to 20 °C in the winter. According to Dearman et al. (1978), the climate is tropical, with clear contrasts between the dry and rainy seasons, characterizing a physical-chemical weathering intensity that varies from moderate to very slight (Figure 3.5).

It is important to consider the effect of the foliation of the gneissic rock mass according to two main factors: (i) the compositional variation in the lithology, which depends on the banding and the presence of micas in the foliation plane; and (ii) the orientation of the foliation, which controls the weathering advance in the subsurface (Dobereiner et al. 1993; Le Pera et al. 2001; Marques et al. 2010; Borreli et al. 2014; Regmi et al. 2014).

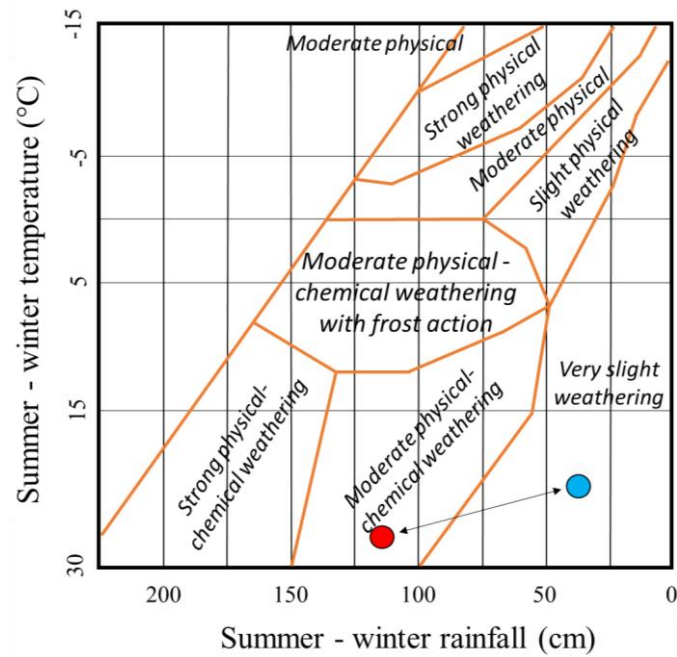


Figure 3.5 - Type and intensity of weathering in the Monte Seco Tunnel in the summer (red) and winter (blue) (modified after Dearman et al. 1978).

In relation to the alterability of the intact gneissic rock, this rock can be considered equivalent to an acidic (high SiO_2 content) igneous rock that is more resistant than intermediate and ultrabasic igneous rocks to weathering in tropical environments. However, the variation in composition of a gneissic rock caused by banding can create differences in alterability along the rock mass. The heterogeneity of the intact gneissic rock of the Monte Seco Tunnel region is shown in Figure 3.6.

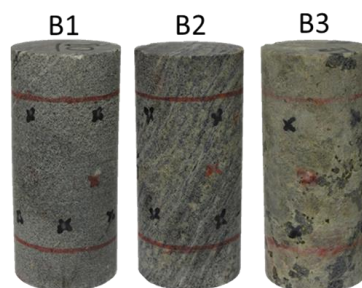


Figure 3.6 - Classification of heterogeneity in petrographic facies B1, B2 and B3 for the gneissic rock of the Monte Seco Tunnel.

The geological-geotechnical surveys, terrestrial laser scanning mapping, electrical resistivity investigations and rotary drilling took place during an intense rainy season that lasted from February to April. Therefore, the information obtained refers to conditions

under which the rock mass undergoes considerable water percolation and infiltration.

3.3 Terrestrial laser scanning analyses

TLS was used for discontinuity mapping and analysis along the Monte Seco tunnel, aiming to obtain the discontinuity geometrical parameters necessary for stability analyses (Cacciari and Futai 2016, 2017). Along the tunnel, 324 m was fully scanned, mapped and analyzed by Cacciari and Futai (2017). The authors were able to quantify the discontinuity volumetric intensity (P_{32}) continuously along the tunnel for each fracture set (F1, F2 and F3) by using automatic window sampling methods and discrete fracture networks (DFNs). P_{32} is defined as the total discontinuity area per unit volume of rock mass. Figure 3.7 shows the orientation data from TLS mapping and some examples of discontinuities that were apparent on the tunnel point cloud.

The scanner used was a Faro Focus 3D (Faro Technologies Inc.), which has a data acquisition rate of approximately 10^6 points/s. The output of TLS is a dense point cloud composed of the Cartesian coordinates and signal return intensity (SRI) of each point. The SRI varies with the color, texture and moisture of the scanned surfaces (tunnel surface).

During field and TLS inspections, water inflow and wet rock surfaces were identified in three different sectors of the tunnel, named A (0-15 m), B (60-90 m) and C (110-130 m). Figure 3.8A shows TLS point cloud cuts from these sections, in which the darkest regions highlighted are wet. In sectors A and C, the water inflow occurs via F1 and F2 discontinuity sets, respectively, while in sector B, the water inflow occurs via foliation Sn. Sector D, from 160 m forward, remains free from the action of weathering agents and is thus used comparatively to further guide the interpretations.

The distribution of the volumetric fracture intensity of the discontinuity sets in the rock mass of the Monte Seco Tunnel are shown in Figure 3.8B.

The values of P_{32} related to water inflow for F1 and F2 discontinuity sets are 1.3 and 0.9 1/m, respectively, in sector A and 1.5 1/m within the entire studied rock mass. Sector B, with P_{32} values slightly lower than those of sector A, presents water inflow conditioned by a specific plane of gneissic foliation that intercepts the tunnel over 30 m.

In sector C, the F2 P_{32} peaks on the order of 3.0 1/m, followed by that of F1, with peaks between 1.5 and 2.0 1/m. This sector can be treated as a singular region of the rock mass or a fault zone, where the water inflow is clearly structurally controlled by these discontinuity sets. Sector D presents high values of P_{32} that are lower than those of sector C; such high values could thus be related to water inflow, as in sector A. However, this sector (D) remains dry, free from weathering agents.

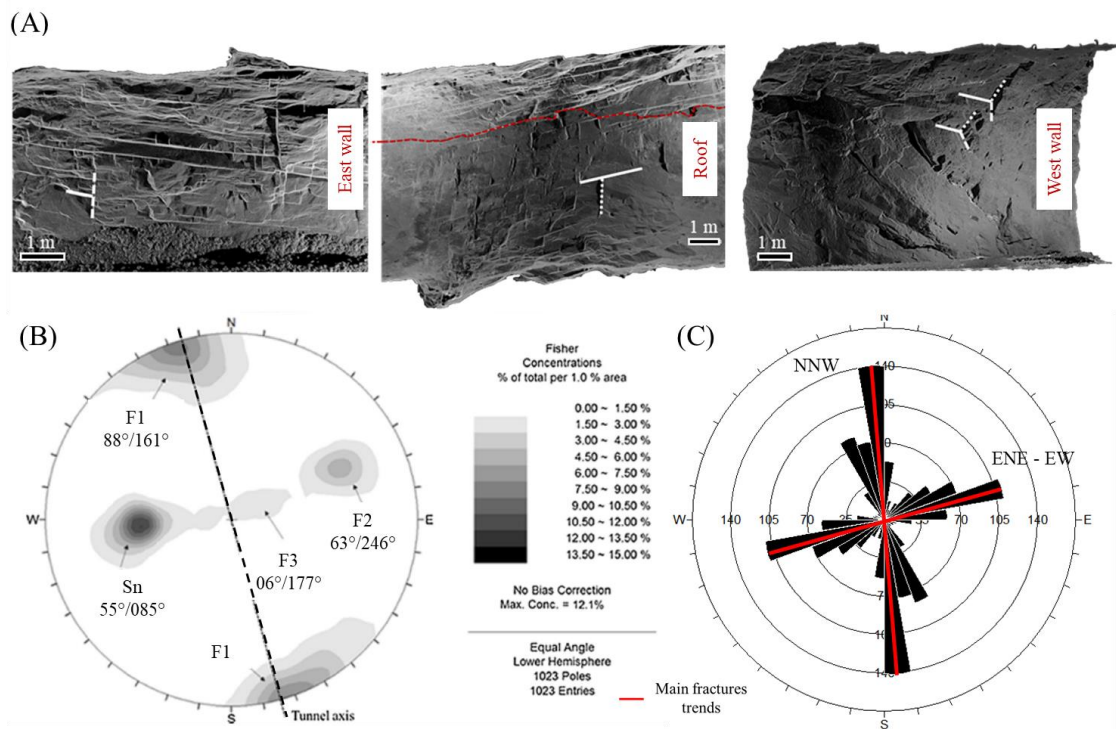


Figure 3.7 - Examples of discontinuities apparent on TLS point cloud (A), the contours of pole concentrations (B) and rose diagram obtained (C) of the geological structures (modified after Cacciari and Futai 2017).

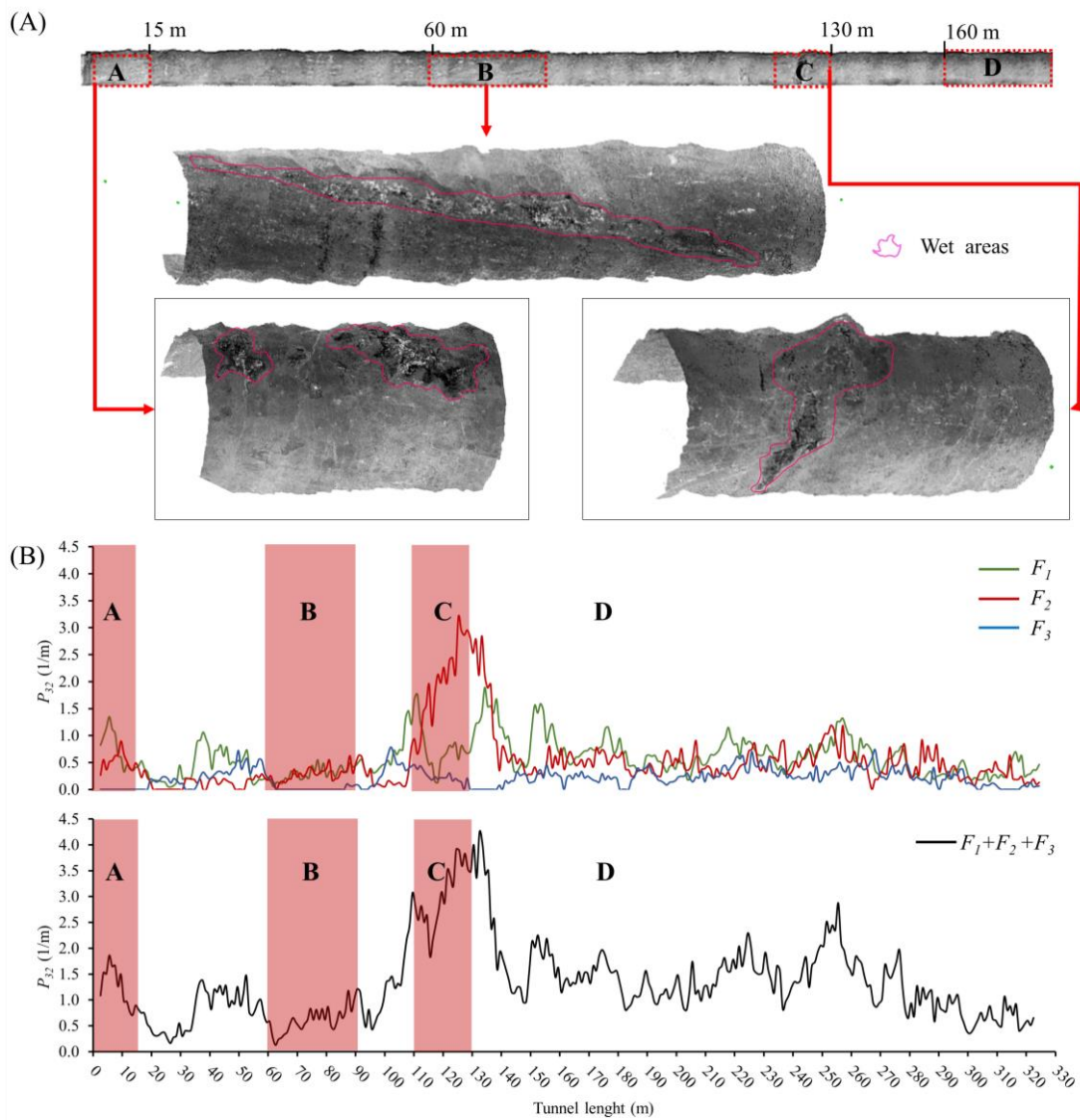


Figure 3.8 - Sectors A, B, C and D used for the analysis of the weathering conceptual model (A) and the distribution of the volumetric fracturing intensity for F_1 , F_2 and F_3 discontinuity sets, and for rock mass ($F_1+F_2+F_3$) (B) (modified after Cacciari et al. 2017).

3.4 Weathering profile

From the results of the indirect and direct investigations carried out at the study site, the weathering characterization of discontinuity walls and the conceptual model of weathering advance in the Monte Seco Tunnel region are presented below.

Indirect and direct investigations

The indirect and direct investigations at the Monte Seco Tunnel site consisted of eight geoelectrical profiles (GPs 1-8) and three drilling boreholes (SR-01, SR-02 and SR-03) (Figure 3.9). The weathering profile characterization was compared to the slope weathering profile of Deere and Patton (1971).

Geoelectrical imaging profile 1 was positioned above the drilling boreholes SR-02 and SR-03 to identify the electrical resistivities associated with the direct sampling of the weathering horizons. The interpreted geotechnical profile from SR-01, -02 and -03 and the corresponding geoelectrical resistivity of GP 1 are presented in Figure 3.10. GPs 2 to 7 were used to identify the geoelectrical anomalies related to fracture intensity, moisture presence and weathering profile pattern changes along the tunnel region and are presented in Figure 3.11. The steep valley on the tunnel site hindered positioning the geoelectrical imaging profiles perpendicular to the tunnel axis. Nevertheless, it was possible to include GP 8, which was positioned above an intensely fractured zone observed inside the tunnel (Figure 3.12).

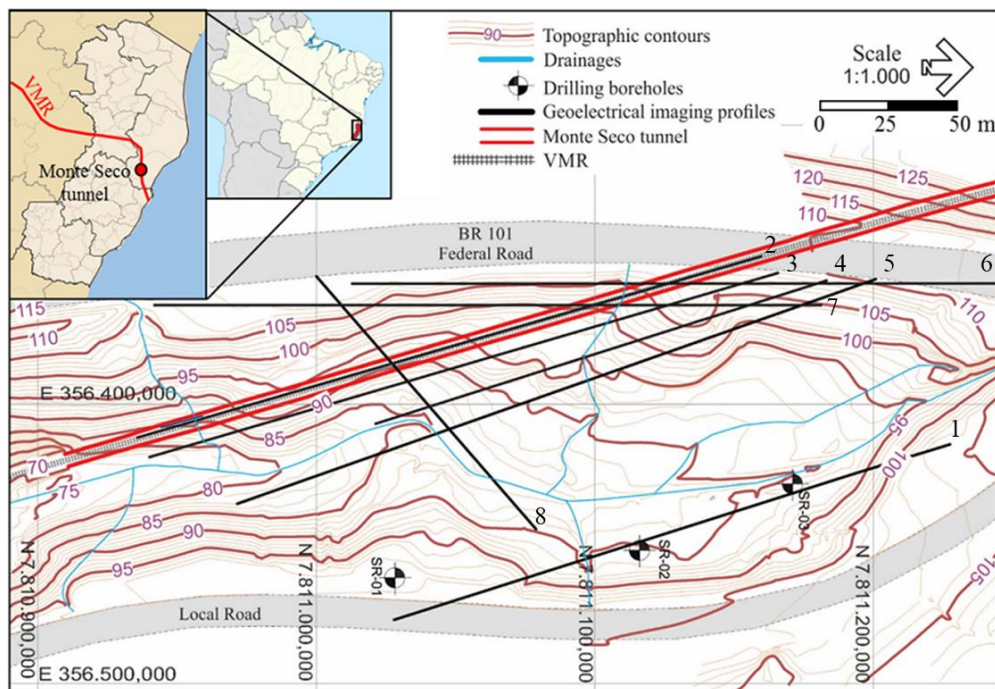


Figure 3.9 - Location of the first 340 m of the Monte Seco tunnel and geotechnical investigation performed at tunnel site (Cacciari and Futai 2016).

The local weathering profile consists of three weathering horizons: I – transported soil, II – very to moderately weathered rock, and III – weakly weathered rock (Figures 3.10 and 3.11).

Horizon I contains soil and various sizes of rock blocks that are partly weathered. The transported soil that covers the rock mass is characterized as an orange to reddish silty sand. In the electrical resistivity investigations, the soil is distinguished by its low resistivity, which is less than 750 Ohm.m, with respect to the higher resistivities interpreted as rock blocks with different weathering grades.

Horizon II is associated with an abrupt change in resistivity from 700 to 1700 Ohm.m; in the drilling boreholes, it is associated with fractured and weathered zones presenting mineral discoloration, iron oxide and hydroxide impregnation, and weakened structure, due to its relatively easy fracturing under hammer blows.

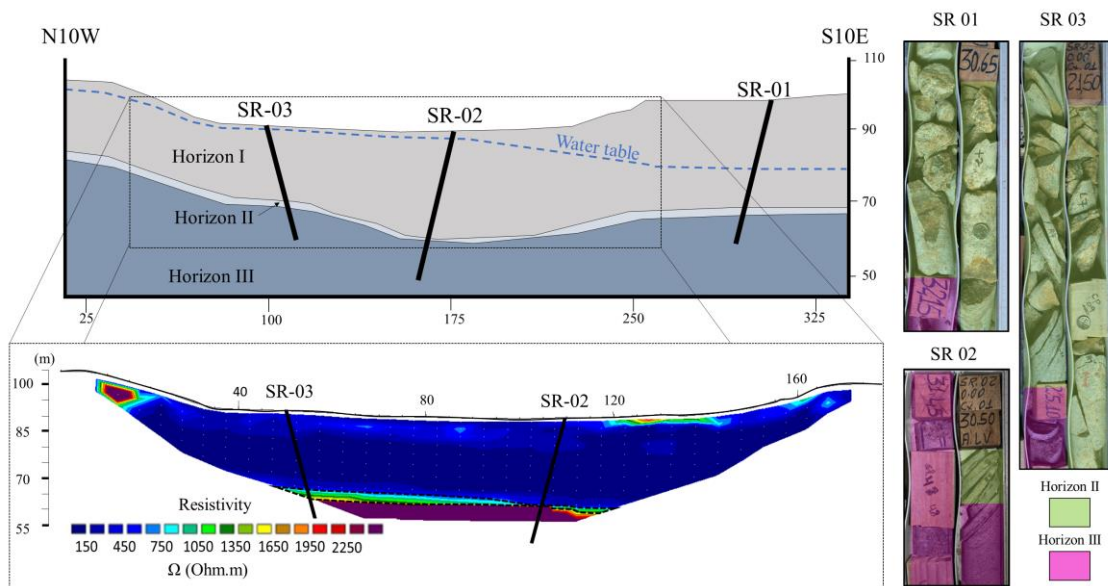


Figure 3.10 - Geotechnical profile from SR-01, 02 and 03, the correspondent geoelectrical profile 1 and the drilling boreholes illustrating the contrast between the weathering horizon along the valley.

Horizon III is defined by its high resistivity (higher than 1700 Ohm.m) and by the visual and tactile characteristics of a fresh to slightly weathered rock. In this horizon, only the discontinuity walls show significant weathering, as observed in the drilling boreholes.

The thickness of horizon I varies from 20 to 30 m in the valley and decreases

significantly with a higher incidence of rock blocks toward the slope face, where an abrupt contact between horizons I and III is found. This trend was also noticed in the outcrops close to the Monte Seco Tunnel site (Figure 3.13). The absence of intermediate horizons and the development of horizon II, whose thickness varies from a few centimeters to a few meters, is related to the environmental conditions, the presence of fractures and the orientation of the foliation.

The foliation dips subparallel to the slope of the hillside. Despite the downward flow of water, in a nonfractured portion of the rock mass, the weathering front cannot advance. However, an increase in the subvertical fracturing related to F1 and F2 increases the volume of rock in contact with weathering agents, consequently developing a very to moderately weathered rock mass.

The interpretation of the top of the bedrock, the contact between horizon I and horizons II-III, and the low-resistivity anomalies related to the fractured zones, inflow and weathering around the Monte Seco Tunnel were highlighted in the geoelectrical profiles (Figures 3.11 and 3.12). The low-resistivity anomaly identified in GP 2 is associated with the E-W drainage, leading to water inflow into sector A. The low-resistivity anomalies identified in GPs 4, 5 and 7 are associated with sector D and with the E-W drainage. In contrast the drainage in to sector A, that in sector D does not lead to water inflow into sector D, which indicates a lack of interconnection of the discontinuity sets from 160 m forward. The low-resistivity anomalies identified in GP 3 are related to sectors B and C, where the water inflow is controlled by the foliation and by the fault zone, respectively. This fault zone is more clearly identifiable in GP 8, where the geometry of the low-resistivity anomaly is structurally controlled by discontinuity set F2.

Notably, there is no drainage related to sectors B and C (Figure 3.9). In sector B, the direction of the water inflow follows the dip of the bedrock, whereas in sector C, it follows the dip of discontinuity set F2.

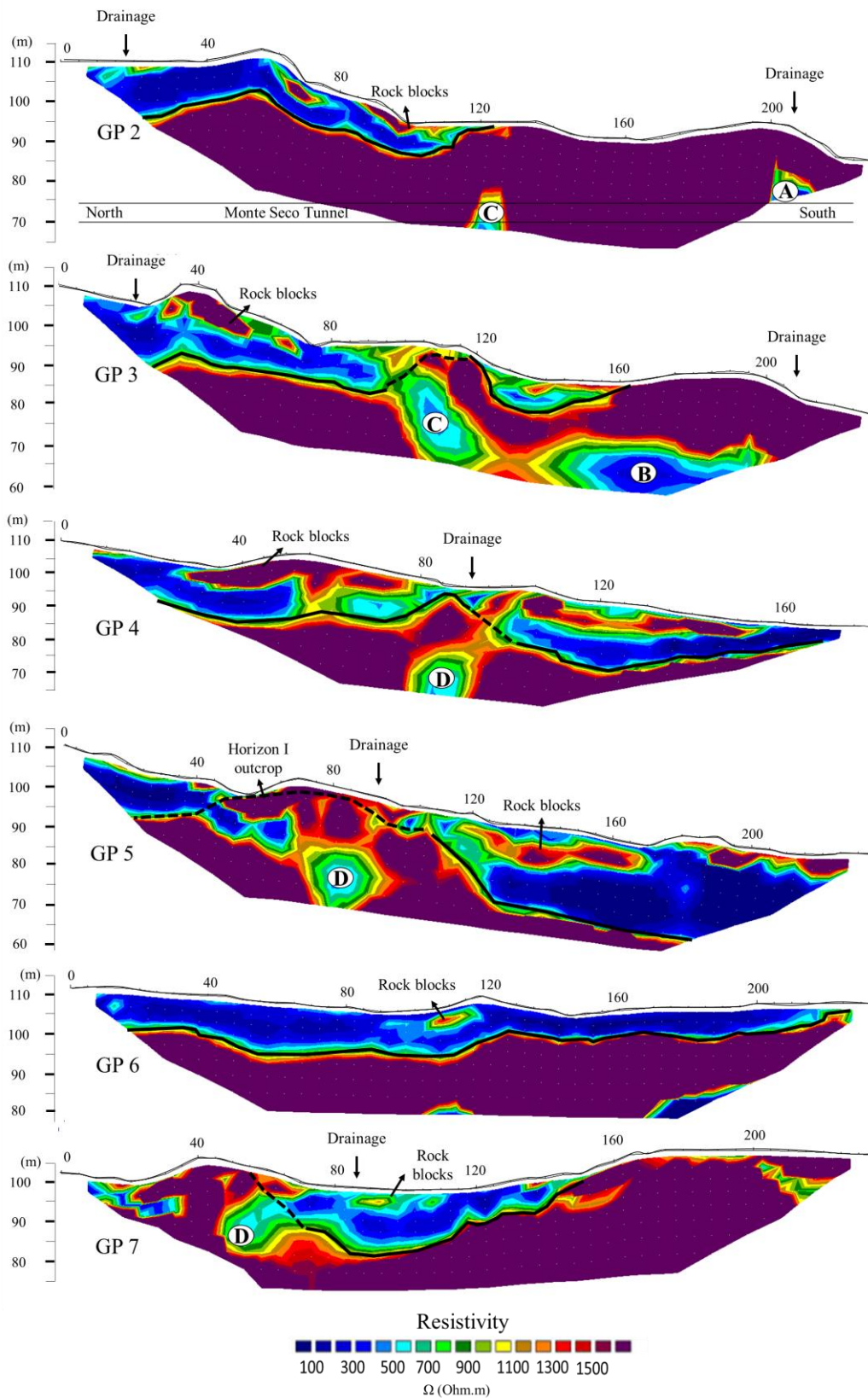


Figure 3.11 - Geoelectrical profiles illustrating the contrast between the weathering horizon along the valley (GP 2 to 7) and geoelectrical anomalies related to the sectors A, B, C and D of the TLS mapping.

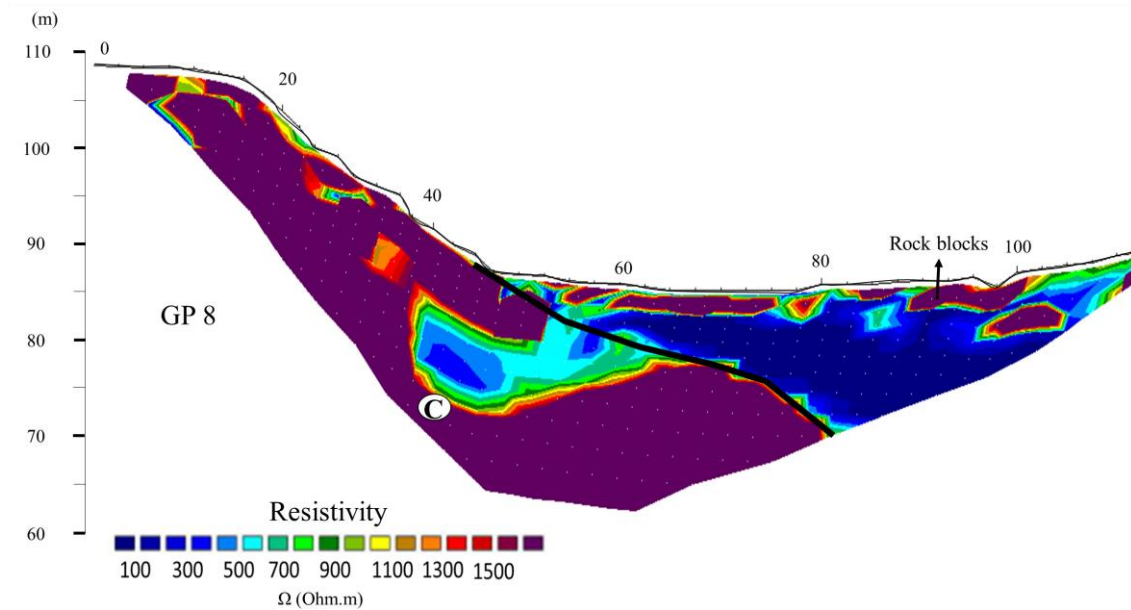


Figure 3.12 - Geoelectrical profile perpendicular to the tunnel axis (GP 8) and geoelectrical anomaly related to the sector C.

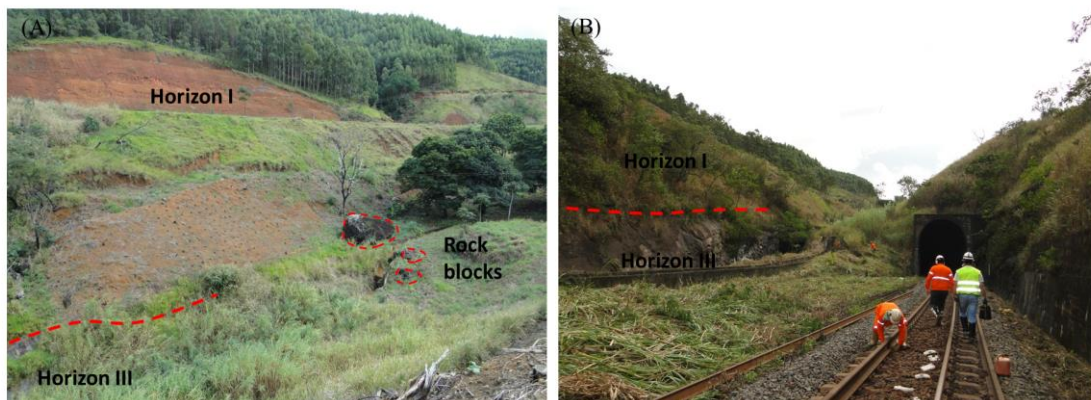


Figure 3.13 - Contact between weathering horizons I and III, close to the Monte Seco Tunnel site.

Weathering of discontinuity walls

The weathering condition of the discontinuity walls was characterized by tactile and visual features using drilling boreholes. Parameter J_a , the “joint weathering number”, defined in the geomechanical classification system of rock masses known as the Q System (Barton et al. 1974), is treated as a key parameter in this study because it allows for fast assessment of the relative aperture of discontinuities related to the changes induced by tectonic stresses and rock mass weathering.

Parameter J_a is subdivided into three categories according to the width of the

discontinuity, the relative degree of displacement between the walls, the tactile and visual features (Table 3.1). Additionally, thin sections were described to compare the mineral conditions at the surface of the discontinuity sets. The thin sections were collected parallel to the discontinuity wall. The discontinuity walls were sampled at the weathering front of the rock mass (horizon III) by cutting a thin layer of rock from the discontinuity plane. The information obtained was correlated with the apparent physical indexes, in accordance with International Society for Rock Mechanics (ISRM) procedures (ISRM, 1979).

The most representative samples showing the weathering along discontinuity walls and the differences in the petrographic characteristics are shown in Figure 3.14. The *Ja* classification and the physical properties of the samples, denoted D1 to D13, are presented in Table 3.2.

F1 and F3 discontinuity sets, as well as the foliation planes that split during core drilling, are characterized as rock-wall contacts with no relative displacement between the walls. The F1 samples showed higher residual friction angles than the foliation samples, which showed lower angles due to weathering increasing. The F2 discontinuity set also showed weathering aspects, such the thin fillings and rock-wall contacts with less than 10 cm of relative displacement (Table 3.2).

The walls of F1 discontinuity set are usually unaltered but slightly stained and present stretch marks. The petrographic analysis revealed a thin edge of intra- to transmineral unfilled fissures parallel to the discontinuity wall (Figure 3.14A). On the other hand, the walls of F2 discontinuity set (Figure 3.14B) and the foliation (Figure 3.14C) exhibit more advanced weathering grades, marked by coatings and stained and weakly weathered minerals: in the thin sections, a greater thickness of the fissure microsystem and stronger weathering of the wall minerals are observed. In these locations, the intra- to transmineral fissures are impregnated with iron oxides and hydroxides, and the original minerals are replaced with carbonate and clay minerals (pinite, chlorite and sericite).

F2 samples D5 and D7 and foliation sample D13 have notable weathering intensities (Table 3.2).

Sample D7 has well-consolidated fillings consisting of iron oxides and hydroxides and clay mineral coatings, indicating connections between discontinuities along the weathering profile. These connections can be related to the tectonic reactivation event that could have promoted an increase in fracture intensity and a significant displacement and dilation, increasing the discontinuity aperture and water flow, consequently weathering the walls and filling the apertures with secondary products.

The most susceptible minerals to weathering occur in bands through the intact rock; in this case, cordierite is replaced by pinite, chlorite and iron oxides and hydroxides (Figure 3.14).

This weathering path may reach significant distances, as shown in sample D13, where the presence of a weathered band composed of carbonate and clay minerals in the foliation plane caused fracturing when the rock was drilled from a previously intact portion of the rock mass. It is possible that a conductivity fracture is present nearby, providing water that weathered the rock, but was not sampled by drilling. Alternatively, the weathering may have occurred along specific planes of the foliation due to the complexity of the gneissic banding of the rock mass, constituting a significant subsurface weathering path that depends on the rock structure and composition.

Despite the limited number of discontinuity samples from the drilling cores, the foliation and discontinuity set F2 can be classified as advanced weathered, as observed by its tactile and visual features and the high apparent porosity and respective low average residual friction angle estimated by parameter Ja (Figure 3.15). In this interpretation, the high secondary porosity is assumed to be only related to the weathering of the thin layer of rock on the discontinuity wall. Among the physical properties, the residual friction angle against the porosity presented the highest coefficient of determination ($R^2 = 0.85$) (Figure 3.15).

This correlation may indicate unfavorable geological structures through the geomechanical classification applied to drilling boreholes and could be used as additional information to characterize the weathering of discontinuity sets.

Table 3.1 - Joint alteration number – J_a (Barton et al. 1974)

Joint weathering number – J_a (Barton et al. 1974)		ϕ_r approx.	J_a
a) Rock-wall contact (no mineral fillings, only coatings)			
A	Tightly healed, hard, nonsoftening, impermeable filling, i.e., quartz or epidote.	-	0.75
B	Unaltered joint walls, surface staining only.	25-35°	1
C	Slightly altered joint walls. Nonsoftening mineral coatings: sandy particles, clay-free disintegrated rock, etc.	25-35°	2
D	Silty or sandy clay coatings, small clay friction (nonsoftening).	20-25°	3
E	Softening or low-friction clay mineral coatings, i.e., kaolinite or mica. Additionally, chlorite, talc gypsum, graphite, etc., and small quantities of swelling clays.	8-16°	4
b) Rock-wall contact with less than 10 cm of shearing (thin mineral fillings)			
F	Sandy particles, clay-free disintegrated rock, etc.	25-30°	4
G	Strongly overconsolidated, nonsoftening, clay mineral fillings (continuous, but <5 mm thick).	16-24°	6
H	Moderate or low overconsolidation, softening, clay mineral fillings (continuous, but <5 mm thick).	12-16°	8
J	Swelling clay fillings, i.e., montmorillonite (continuous, but <6 mm thick). Value of J_a depends on the percentage of swelling clay-size particles.	6-12°	8-12
c) No rock-wall contact when sheared (thick mineral fillings)			
K	Zones or bands of disintegrated or crushed rock. Strongly overconsolidated.	16-24°	6
L	Zones or bands of clay, disintegrated or crushed rock. Moderate or low overconsolidation or softening fillings.	12-16°	8
M	Zones or bands of clay, disintegrated or crushed rock. Swelling clay. J_a depends on the percentage of swelling clay-sized particles.	6-12°	8-12
N	Thick continuous zones or bands of clay. Strongly overconsolidated.	12-16°	10
O	Thick, continuous zones or bands of clay. Moderate to low overconsolidation.	12-16°	13
P	Thick, continuous zones or bands of clay. Swelling clay. J_a depends on the percentage of swelling clay-size particles.	6-12°	13-20

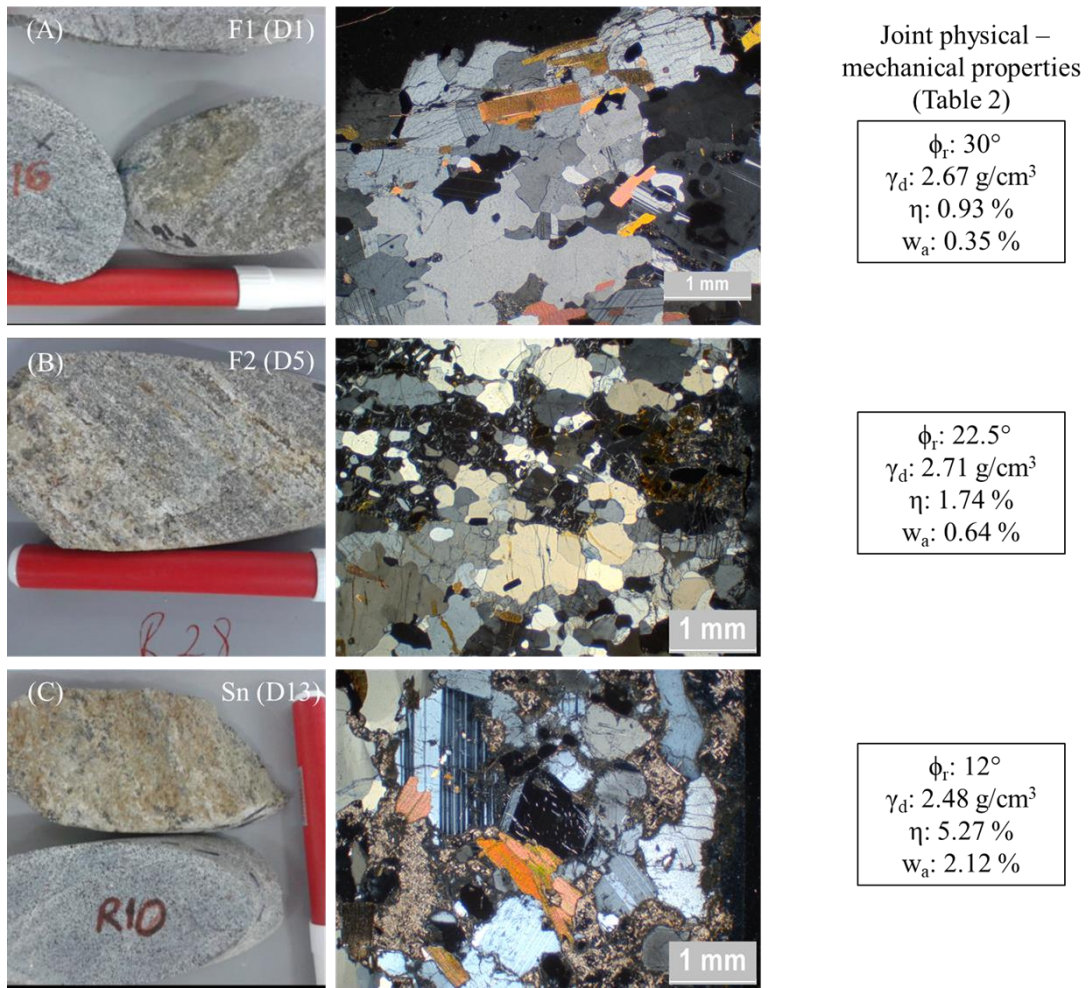


Figure 3.14 Representative weathering samples of F1 (A), F2 (B) discontinuity sets and foliation Sn (C) and photomicrographs illustrating mineral weathering. The discontinuity wall is positioned at the top of D1 (A) and to the right side of D5 (B) and D13 (C).

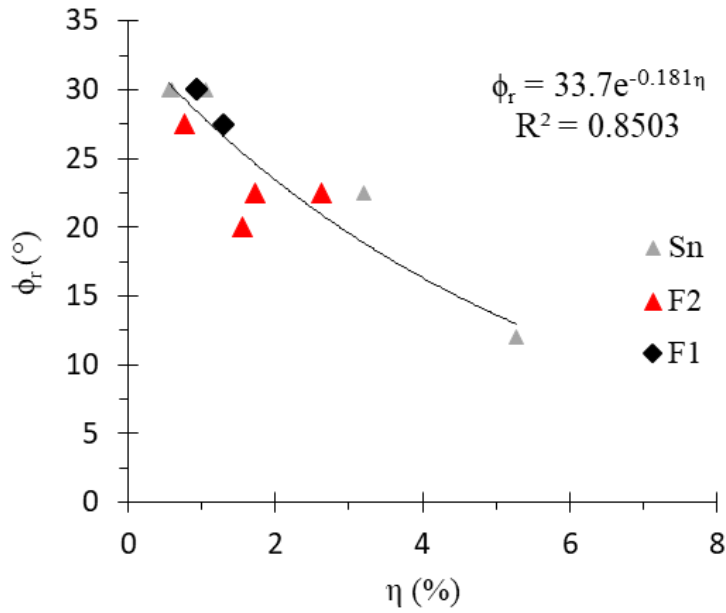


Figure 3.15 Relationship between average residual friction (ϕ_r) estimated by the Ja parameter and apparent porosity (η) of the discontinuity wall samples.

Table 3.2 - Joint weathering number and physical properties

Sample	Set	<i>Ja</i>	ϕ_r (°)			γ_d (g/cm ³)	η (%)	w_a (%)	
			Max.	Average	Min.				
D 1*	F1	a) B	1	35	30	25	2.671	0.934	0.350
D 2	F1	a) B	1	35	30	25	2.693	0.935	0.347
D 3	F1	a) C	2	30	27.5	25	2.735	1.291	0.472
D 4	F2	a) C	2	30	27.5	25	2.735	0.770	0.282
D 5*	F2	a) D	3	25	22.5	20	2.719	1.736	0.638
D 6	F2	a) D	3	25	22.5	20	2.689	2.627	0.977
D 7	F2	b) G	6	24	20	16	2.723	1.550	0.569
D 8	F3	a) B	1	35	30	25	2.720	0.817	0.290
D 9	Sn	a) B	1	35	30	25	2.693	0.552	0.205
D 10	Sn	a) B	1	35	30	25	2.683	0.590	0.230
D 11	Sn	a) C	2	30	30	25	2.692	1.054	0.391
D 12	Sn	a) D	3	25	22.5	20	2.660	3.200	1.230
D 13*	Sn	a) E	4	16	12	8	2.479	5.271	2.126

(*) Samples shown in Figure 3.14.

Conceptual model of weathering advance in the Monte Seco Tunnel region

The comparison of P_{32} (F1+F2+F3) between the tunnel, surface and bedrock topographies and the occurrence of water inflow and its probable flow direction are presented in Figure 3.16, in which sectors A, B, C and D are indicated. The data gathered indicate five conditioning agents: (i) water inflow via fractures and foliation; (ii) rock cover and (iii) P_{32} , which were correlated with the (iv) genesis of the geological structures and (v) weathering of discontinuity walls. The discrimination of these sectors and the following comments helped elucidate the conceptual model of weathering advance at this site, as presented in Figure 3.17.

The genesis of the foliation and the F2 discontinuity set is related to the Brasiliano orogenic cycle, the ductile-brittle regime active during the formation of the gneissic crystalline basement from the Neoproterozoic to the Paleozoic. F2 discontinuity set consists of fractures from the NNW-trending structural lineament set of the Colatina Lineament. At the regional scale, the most persistent fractures were reactivated as normal faults or were intruded by dikes in a distensional and brittle regime during Pangea fragmentation and opening of the South Atlantic Ocean in the beginning of the Cretaceous (Figures 3.1-3 and 3.7). Sector C may have been tectonically affected during this event, thus forming a fault zone, which is an intensely fractured region (Figures 3.16 and 3.17), where some structural planes were displaced in relation to others at different intensities. This movement is corroborated by the presence of thick weathering on the walls of F2 discontinuity set, as seen in the drill cores (Table 3.2 and Figure 3.14).

Among the stress states during the end of the Pleistocene and beginning of the Holocene (Cenozoic), the NW-SE-trending distensional regime is related to the emergence of F1 discontinuity set at the local scale (Figures 3.1-3 and 3.7). This trend is responsible for the formation of E-W- and ENE-trending normal faults, identified in the weathering soil of the Barreiras Formation and in superficial deposits.

In certain cases, F1 discontinuity set overlapped F2 discontinuity set, increasing the fracture intensity of the rock mass, as observed in sectors A and D and more intensely in sector C (Figure 3.8). In the weathering profile, the presence of these discontinuities (F1 and F2) is correlated with the development of horizon II, which promotes the connection between weathering horizons I and III, transporting the weathering agents to the intact rock mass (Horizon III) (Figures 3.10 and 3.17). In sectors A and C, which have

less rock cover than sector D, this connection could be identified by the geoelectrical anomalies and TLS analysis results (Figures 3.8, 3.16 and 3.17) inside the tunnel. Moreover, the last in situ stress state related to the genesis of F1 discontinuity set influenced the preferential water flow direction driving the weathering agents through this fracture system. The unusual degree of weathering of the F1 walls highlights that this weathering event was younger and less intense than that evidenced along F2 discontinuity set, which is intensely weathered (Table 3.2 and Figure 3.14).

F3 discontinuity set, related to denudation and uplift of the rock mass, formed following the topography and the gneissic foliation (Figures 3.3, 3.4 and 3.7). The foliation, parallel to the hillside, influenced the genesis of these discontinuities, which are structurally related to the anisotropy of the rock mass. In sector B, which is only slightly fractured, the water infiltration along 30 m of a specific foliation plane (S_n) may be related to overlapping of the relief fractures (F3) (Figure 3.8).

In sector D, there is no interference of weathering in the tunnel, probably because it is thicker than other sectors and has a lack of connections between fractures (Figures 3.8, 3.11, 3.16 and 3.17). The conditioning agents of the weathering advance in the Monte Seco Tunnel are briefly summarized in Table 3.3, in which sector C is indicated as the highest susceptibility to weathering and, consequently, to tunnel instability.

Table 3.3 – Weathering agents affecting the tunnel

Conditioning agents	Water infiltration	Rock cover	Fracture intensity P_{32} (F1 – F2) (1/m)		Interference in the tunnel
Sector A	Via fractures F1, followed by F2	Low	1.3	0.9	Medium - Roof
Sector B	Via foliation (S_n)	Medium	0.5	0.5	Low – Walls and roof
Sector C	Via fractures F1, followed by F2	Low	< 2	> 2	High – Roof and walls
Sector D	No infiltration	Medium / High	1	1	None

Obs.: Rock cover – Low (up to 1x the tunnel diameter), Medium (up to 2x) and High (more than 2x the tunnel diameter).

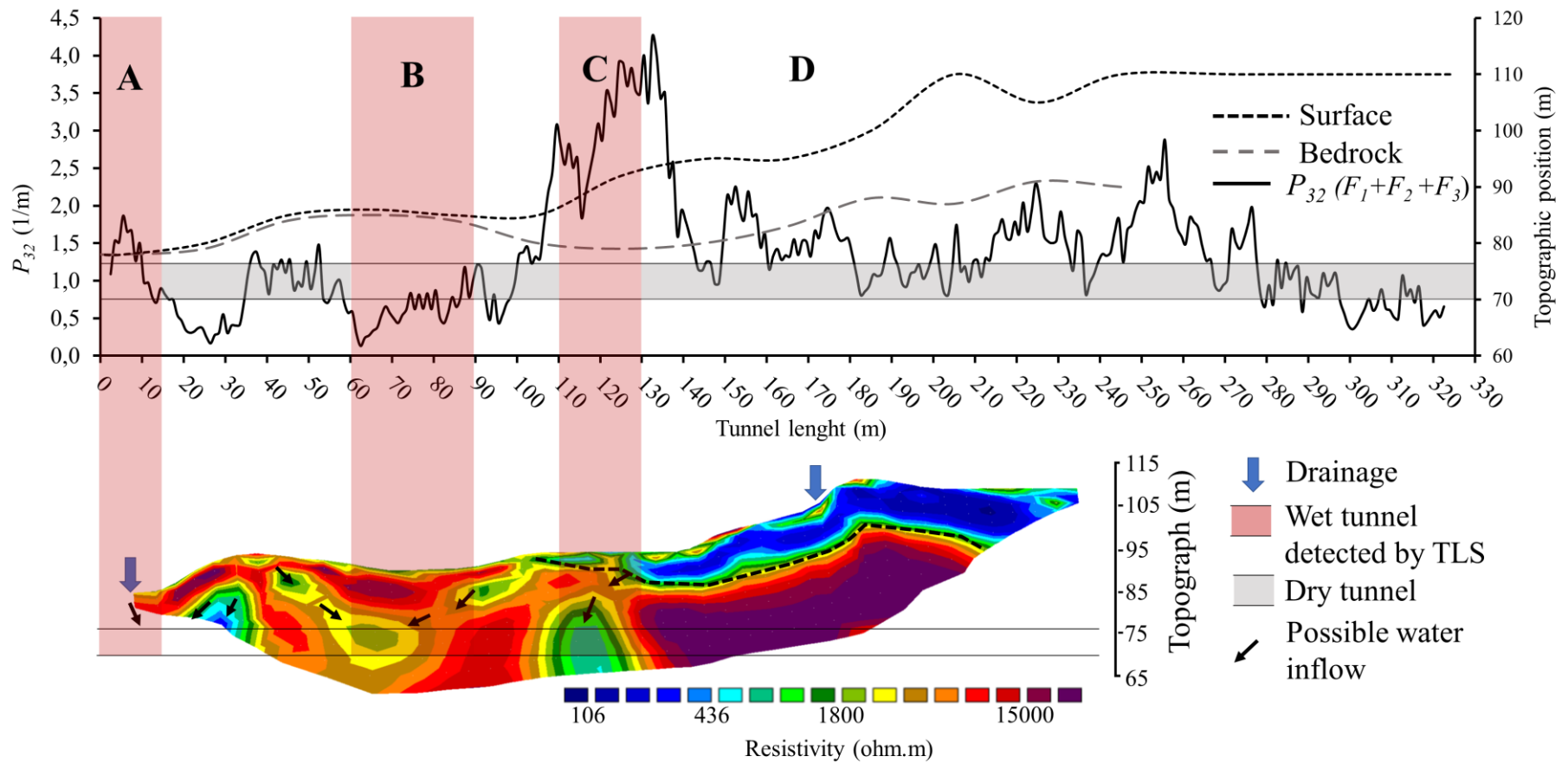


Figure 3.16 Distribution of the volumetric fracturing intensity ($F_1+F_2+F_3$) (modified after Cacciari et al., 2017) and indication of the sectors A, B, C and D used for analyzing the conceptual weathering model.

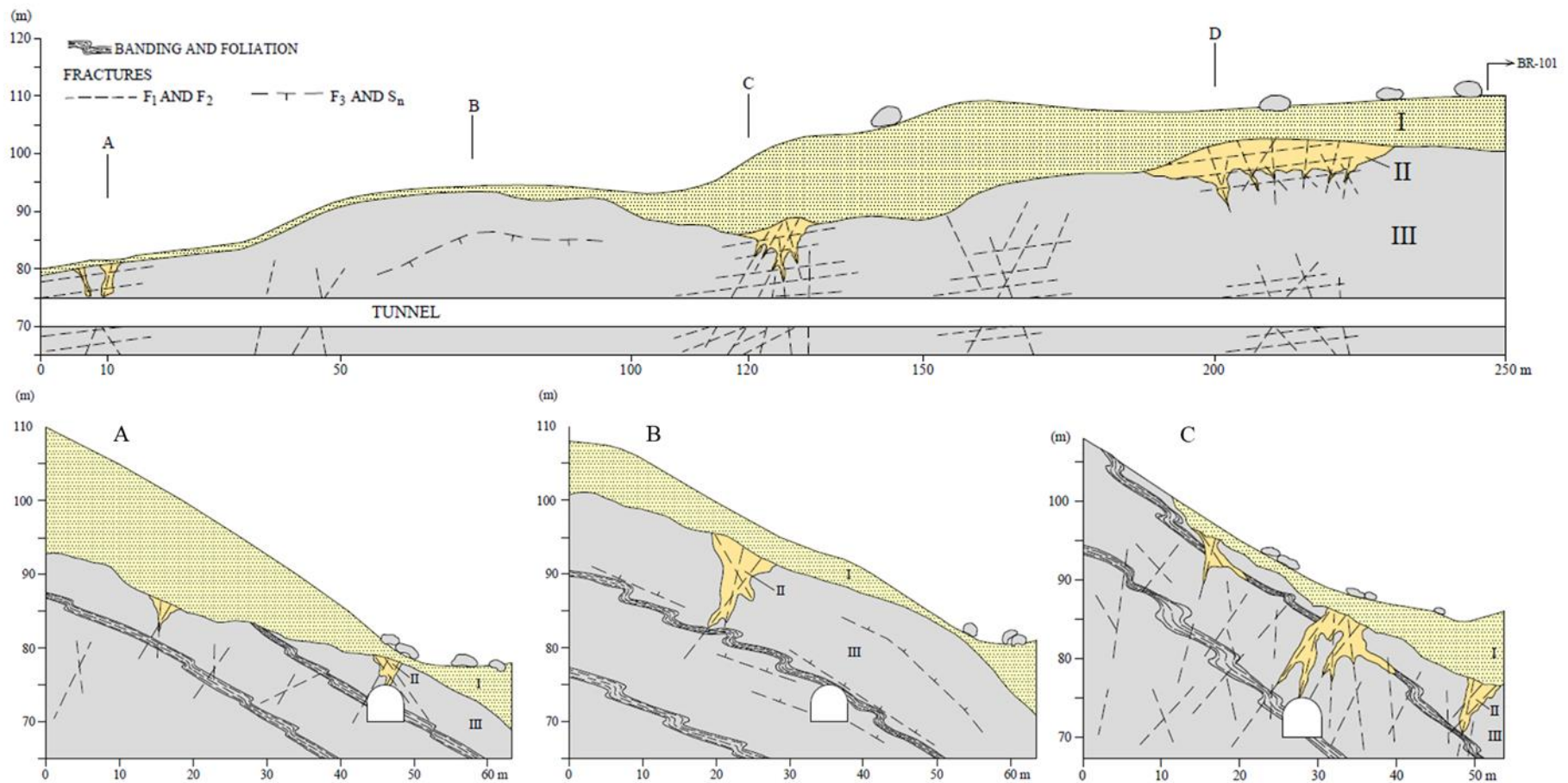


Figure 3.17 Weathering profile indicating sectors A, B, C and D. Illustration of the formation of Horizon II (very to intermediately weathered rock mass) and advance of weathering via F1 and F2 discontinuity sets, and sheet fractures related to foliation opening (F3 - Sn). Horizon I – Transported Soil, and Horizon III – Weakly weathered rock mass.

3.5 Conclusions

The overall geology and structural framework of the Monte Seco Tunnel site is related to the Brasiliano orogenic cycle (Proterozoic to Paleozoic), which is characterized by a succession of accretionary and collisional episodes. Locally, these deformational events generated the structural fabric of the gneissic rock mass, resulting in four discontinuity sets: F1, F2, F3 and Sn.

Foliation and F2 discontinuity set show the same trend as the regional NNW lineaments, which corresponds to the regional-scale trend from the Neoproterozoic to the Paleozoic. F1 discontinuity set shows the same trend of regional ENE and E-W lineaments, which corresponds to the initial phase of the intraplate neotectonic activity in Brazil (started in the Paleogene and continued during the Neogene and the Holocene).

F1, F2, F3 and Sn were mapped both by manual fieldwork and by TLS point clouds (in detail), and the results are similar between these methods. The reactivation of F2 during the Cretaceous created the fault zone in sector C, clearly observed from the TLS mapping due to the abrupt P_{32} increase in this portion of the tunnel. This fracture set, associated with F1, controls the water inflow in sectors A and C, as confirmed by the high electrical conductivity of these sections observed on the geoelectrical profiles. In sector B, a persistent and permeable foliation plane is responsible for the water inflow and, consequently, the high conductivity, as F1 and F2 showed low intensity in this section.

Because of the aforementioned water inflow, the weathering advanced via F1 and F2 discontinuity sets in sectors A and C and via foliation Sn in sector B, while no weathering agents were observed in sector D. However, the watering grade of F2 and Sn is much higher than that of F1. As identified by the J_a parameter, the residual friction is considerably reduced by weathering, compromising the strength of these discontinuities and the overall quality of the rock mass.

From the conceptual weathering model presented herein, sectors A and C should be studied in detail for different reasons: Sector C represents the lowest rock mass quality due to its high fracture intensity (F2 fault zone), presence of water (TLS images and geoelectrical profiles) and, consequently, high weathering potential. Sector A shows a much lower fracture intensity than that of sector C but also shows the presence of water

and is extremely shallow (close to horizons II and I); thus, it also has a high weathering potential.

3.6 References

- Alkmim F., Marshak S., Pedrosa-Soares A., Peres G., Cruz S. 2006. Kinematic evolution of the Araçuaí-West Congo orogen in Brazil and Africa: Nutcracker tectonics during the Neoproterozoic assembly of Gondwana. *Precambrian Research*, 149: 43–64.
- Baltazar O.F., Zucchetti M., Oliveira S.A.M., Scandalara J., Silva L. 2010. Report of the São Gabriel da Palha and Linhares Project. Belo Horizonte, CPRM (Geological Survey of Brazil), 144 p.(in Portuguese)
- Barton C.A., Zoback M.D., Moos D. 1995. Fluid flow along potentially active faults in crystalline rock. *Geology*, 23: 683–686. doi:10.1130/0091-7613(1995)023<0683
- Barton N., Lien R., Lunde J. 1974. Engineering classification of rock masses for the design of tunnel support. *Rock Mechanics*, 6: 189–236. doi:10.1007/BF01239496
- Borrelli L., Perri F., Critelli S., Gullà G. 2014. Characterization of granitoid and gneissic weathering profiles of the Mucone River basin (Calabria, southern Italy). *Catena*, 113: 325–340. doi:10.1016/j.catena.2013.08.014
- Braum O.P.G. 1982. A structural synthesis of Brazil, based on the study of major lineaments derived from remote sensing imagery interpretation. *Photogrammetria*, 37: 77-108.
- Cacciari, P.P. and Futai, M.M. 2017. Modeling a Shallow Rock Tunnel Using Terrestrial Laser Scanning and Discrete Fracture Networks. *Rock Mechanics and Rock Engineering*, 50: 1217–1242. doi:10.1007/s00603-017-1166-6
- Cacciari, P.P. and Futai, M.M. 2016. Mapping and characterization of rock discontinuities in a tunnel using 3D terrestrial laser scanning. *Bulleting of Engineering Geology and Environment*, 75: 223–237. doi:10.1007/s10064-015-0748-3
- Calegari S.S., Neves M.A., Guadagnin F., França G.S., Vincentelli M.G.C. 2016. The Alegre Lineament and its role over the tectonic evolution of the Campos Basin and

- adjacent continental margin, Southeastern Brazilian. *Journal of South American Earth Sciences*, 69: 226–242. doi:10.1016/j.jsames.2016.04.005
- Almeida F.F.M., Hasui Y., de Brito Neves B.B., Fuck R.A. 1981. Brazilian structural provinces: An introduction. *Earth-Science Review*, 17: 1–29. doi:10.1016/0012-8252(81)90003-9
- Brito Neves, B.B. and Fuck, R.A. 2013. Neoproterozoic evolution of the basement of the South-American platform. *Journal of South American Earth Sciences*, 47: 72–89. doi:10.1016/j.jsames.2013.04.005
- Dearman W.R., Baynes F.J., Irfan T.Y. 1978. Engineering grading of weathered granite. *Engineering Geology*, 12: 345–374. doi:10.1016/0013-7952(78)90018-2
- Deere, D.U. and Patton, F.D. 1971. Slope Stability in Residual Soils. 4th Panamerican Conference of Soil Mechec. Found. Eng. States art Paper, 525: 87–170. doi:10.1016/0267-7261(96)00001-2
- Delvigne J.E. 1998. Atlas of Micromorphology of Mineral Weathering and Weathering. The Canadian Mineralogist, Ottawa, Ontario, Canada. 516 p.
- Dewandel B., Alazard M., Lachassagne P., Bailly-Comte V., Couëffé R., Grataloup S., Ladouche B., Lanini S., Maréchal J.C., Wyns R. 2017. Respective roles of the weathering profile and the tectonic fractures in the structure and functioning of crystalline thermo-mineral carbo-gaseous aquifers. *Journal of Hydrology*, 547: 690–707. doi:10.1016/j.jhydrol.2017.02.028
- Dobereiner L., Durville J. L., Restitutito J. 1993. Weathering of the massiac gneiss (massif central, France). *Bulleting of Engineering Geology and Environment*, 47: 79–96. doi:10.1007/BF02639596
- Ehlen J. 2005. Above the weathering front: Contrasting approaches to the study and classification of weathered mantle. *Geomorphology*, 67: 7–21. doi:10.1016/j.geomorph.2004.09.026
- Ferrill D.A., Winterle J., Wittmeyer G., Sims D., Colton S., Armstrong A., Morris A.P. 1999. Stressed rock strains groundwater at Yucca Mountain, Nevada. *GSA Today* 9, 1–8. doi:10.1038/scientificamerican0688-18a

- Hasui, Y., 1990. Neotectonics and fundamental aspects of resurgent tectonics in Brazil. In: Brazilian Symposium on Geology - Workshop on Neotectonic and Cenozoic Continental Sedimentation of the Brazilian Southeast. Belo Horizonte, 31 p. (in Portuguese)
- Mello C. L., Rodrigues H. B., Hatushika R.S. 2005. Quaternary tectonics and drainage anomalies in the north central region of Espírito Santo. In: Proceedings of the 10th ABEQUA Congress. Rio de Janeiro, Brazil, 6 p. (in Portuguese)
- Hatushika R. S., Mello C. L., Silva C. G. 2005. Evidence of neotectonic performance in the formation of Juparanã-Linhares Lake (ES). In: 10th Congress of the Brazilian Association of Quaternary Studies. Guarapari, Espírito Santo, Extended Abstracts, CD-ROM. (in Portuguese)
- ISRM. 1979. Suggested Method for Determination of Water Content, Porosity, Density, Absorption and Related Properties and Swelling, Slake Durability Index Properties. International Journal of Rock Mechanics and Mining Sciences, 16: 141–156.
- Freeze R. A. & Cherry J. A. (eds.). 1979. Groundwater. Prentice-Hall, Englewood Cliffs, NJ, 604 p.
- Konzuk, J.S. and Kueper, B.H. 2004. Evaluation of cubic law based models describing single-phase flow through a rough-walled fracture. Water Resources Research, 40. doi:10.1029/2003WR002356
- Lachassagne, P. and Wyns, R. 2011. The fracture permeability of Hard Rock Aquifers is due neither to tectonics, nor to unloading, but to weathering processes (Review article). Terra Nova, 23: 145-161. doi:10.1111/j.1365-3121.2011.00998.x
- Le Pera E., Critelli S., Sorriso-Valvo M. 2001. Weathering of gneiss in Calabria, southern Italy. Catena 42: 1–15. doi:10.1016/S0341-8162(00)00117-X
- Marques E.A.G., Barroso E. V., Menezes Filho A.P., Vargas E. do A. 2010. Weathering zones on metamorphic rocks from Rio de Janeiro-Physical, mineralogical and geomechanical characterization. Engineering Geology, 111: 1–18. doi:10.1016/j.enggeo.2009.11.001
- Modenesi-Gauttieri M.C., Takashi Hiruma S., Riccomini C. 2002. Morphotectonics of a

- high plateau on the Northwestern flank of the continental rift of Southeastern Brazil. *Geomorphology*, 43: 257–271. doi:10.1016/S0169-555X(01)00137-4
- Monticeli J.P., Cantarella V.P., Cacciari P.P., Futai M.M. 2015. Roughness characterization of discontinuity sets by profilometer scanner images. In: 15° Pan American Conference on Soil Mechanics and Geotechnical Engineering. Buenos Aires, Argentina, 7 p.
- Morin, R.H. and Savage, W.Z. 2003. Effects of crustal stresses on fluid transport in fractured rock: Case studies from northeastern and southwestern USA. *Hydrogeology Journal*, 11: 100–112. doi:10.1007/s10040-002-0235-3
- Novais L.C.C., Teixeira L. B., Neves M.T., Rodarte J.B.M., Almeida J. C. H., Valeriano C.M. 2004. New occurrences of diabase dikes in the Colatina-ES belt: brittle structures associated and tectonic implications for the Campos and Espírito Santo basins. *Petrobras Geosciences Bulletin*, 12: 191–194. (in Portuguese)
- Pedrosa-Soares A. C., Noce C. M., Wiedemann C., Pinto C.P. 2001. The Araçuaí-West-Congo Orogen in Brazil: an overview of a confined orogen formed during Gondwanaland assembly. *Precambrian Research*, 110: 307-323.
- Place J., Géraud Y., Diraison M., Herquel G., Edel J.B., Bano M., Le Garzic E., Walter B. 2016. Structural control of weathering processes within exhumed granitoids: Sectorialisation of geophysical properties by faults and fractures. *Journal of Structural Geology*, 84: 102–119. doi:10.1016/j.jsg.2015.11.011
- Regmi A.D., Yoshida K., Dhital M.R., Pradhan B. 2014. Weathering and mineralogical variation in gneissic rocks and their effect in Sangrumba Landslide, East Nepal. *Environment Earth Sciences*, 71: 2711–2727. doi:10.1007/s12665-013-2649-8
- Riccomini, C. and Assumpção, M. 1999. Quaternary tectonics in Brazil. *Episodes*, 22: 221–225. doi:citeulike-article-id:8858421
- Riccomini C., Peloggia A.U.G., Saloni J.C.L., Kohnke M.W., Figueira R.M. 1989. Neotectonic activity in the Serra do Mar rift system (southeastern Brazil). *Journal of South American Earth Sciences*, 2: 191–197. doi:10.1016/0895-9811(89)90046-1
- Saunders, M.K. and Fookes, P.G. 1970. A review of the relationship of rock weathering and climate and its significance to foundation engineering. *Engineering Geology*, 4:

289–325. doi:10.1016/0013-7952(70)90021-9

Sial A.N., Oliveira E.P., Choudhuri A. 1987. Mafic dyke swarms of Brazil. *Mafic Dyke Swarms Brazil*. *Geol. Assoc. Can. Spec. Papers*, 34: 467–481.

Turkington A. V., Phillips J.D., Campbell S.W. 2005. Weathering and landscape evolution. *Geomorphology*, 67: 1–6. doi:10.1016/j.geomorph.2004.08.013

Valente S.C., Dutra T., Heilbron M., Corval A., Szatmari P. 2012. Lithogeochemistry of dykes of the diabases of the Colatine Belt, ES. *Geochimica Brasilienses*, 23: 177–192.(in Portuguese)

Vieira V.S., Novais L.C.C., Kahwage M.A. 2013. The probable volcanic arch of Vitória-Ecoporanga, an analogy with the arch of Ponta Grossa. In: 14^o National Symposium of Tectonic Studies. Chapada dos Guimaraes, Mato Grosso, Brazil. 14 p. (in Portuguese)

Vieira V.S., Silva M.A., Corrêa T.R., Lopes, M.H.B. 2014. Geological Map of Espírito Santo, scale 1: 400.000. Belo Horizonte, CPRM (Geological Survey of Brazil). In: 6^o Brazilian Symposium on Mineral Exploration. Ouro Preto, Minas Gerais, Brazil.

4. RELANTIONSHIP BETWEEN DURABILITY INDEX AND THE UNIAXIAL COMPRESSIVE STRENGTH IN DIFFERENT WEATHERING GRADES OF A GNEISSIC ROCK MASS²

Abstract

This article presents a study of the durability indexes obtained in the Slake Durability Test (SDT) and the uniaxial compressive strength (UCS) of three petrographic facies from a gneissic rock mass excavated for a railway tunnel without lining, which has presented problems of instability of blocks due to long term exposition to weathering. The characterization of the gneissic rock matrix was made tactile visually and by means of microscopical petrography, combining the tests of physical properties, SDT, UCS with weathering indexes. It is argued, particularly, for the importance of describing the heterogeneity of the gneissic rock to interpret its influence in geotechnical parameters. The interpretation of the results indicates that the rock being studied presents one facies with greater susceptibility to weathering, loss of strength and durability. This study also proposes an equation to access the alterability parameter, recently added in the 2014 update of the Rock Mass Rating (RMR), which may be overvalued to crystalline rocks, as observed in the analysis.

Keywords: Slake Durability Index, Gneissic Rocks, Weathering Grades, Alterability Parameter, RMR Update.

² Authors: Monticelli J.P., Ribeiro R. P., Futai M. M.

4.1 Introduction

The Monte Seco Tunnel, pertaining to the Vitória-Minas Railroad (VMR), responsible for the transportation of ore from the region of Belo Horizonte (BH) to Vitória (VT), southeast Brazil, was excavated in a gneissic rock of the Nova Venécia Complex (Vieira et al. 2014) (Figure 4.1). Given the very favorable stability conditions of the rock at the time (decade of 1950), neither shotcrete nor bolts were used to treat the rock, but, in the last years, as reported by the railroad maintenance team, problems of instability of blocks in this and other tunnels of the VMR have been noticed. Although they do not indicate a generalized risk, these problems can cause severe logistic damages in cargo transport. This theme has recently motivated researchers from the GeoInfraUSP of the Department of Geotechnical Engineering of the EPUSP to develop several studies to evaluate the geomechanical behavior of the Monte Seco Tunnel (Cacciari et al. 2013; Monticeli et al. 2015; Monticeli et al. 2016; Cacciari and Futai, 2017).

The block instability observed in the Monte Seco Tunnel results from several factors associated with the tropical climate that, through the years, caused the degradation of geological-geotechnical parameters of the rock mass, causing blocks to loosen from the tunnel roof and walls, particularly in fractured and weathered zones, turning excavation unsafe through the years. In this manner, the detailed study of modifications in the characteristics of heterogeneous rocks, such as gneissic rocks, in different weathering grades, has proved to be fundamental for reevaluating rock mass behavior.

In the present article information is collected regarding the durability of the gneissic rock matrix, aiming at a better comprehension of the intact rock disaggregation in the Monte Seco Tunnel. The effect of the heterogeneity of the rock, classified according to petrographic facies, is analyzed in terms of the petrographic analysis, physical properties, uniaxial compressive strength (UCS) and durability along weathering grades, indicating in which cases the rock matrix would be more susceptible to disaggregation and loss of strength. In general, the classification of gneissic rocks in terms of their heterogeneity and their geotechnical behavior when affected by weathering, which are the motivation of this study, are themes not usually seen in the literature. Despite of the influence of the foliation in the UCS tests and the strength

of rock wedges and blocks, this study does not address it directly in its relation to the heterogeneity of the gneissic rocks.

This study also proposes an equation to quantify the alterability parameter as an alternative to the procedures presented in the recent update of the RMR system (Celada et al. 2014). The necessity of RMR adaptations in engineering is a common practice to manage specific geological conditions, particularly in tropical environments such as Southeast Brazil (Santos et al. 2012; Amaral Junior et al. 2016).

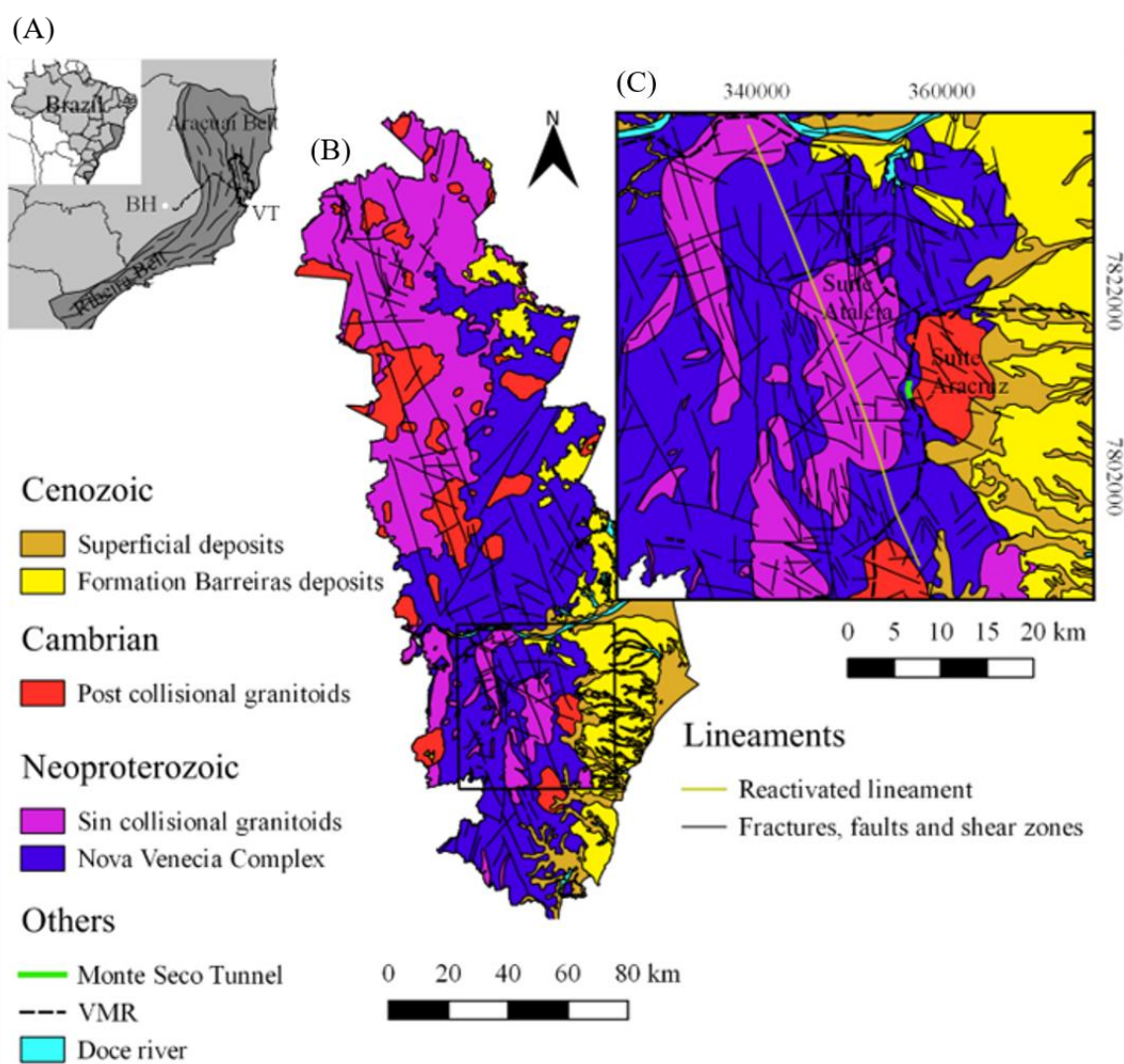


Figure 4.1 - Site of the Monte Seco Tunnel. Southeast Brazil (A), Colatina Lineament Domain (B) and in detail, the local geological map (C) (modified from Vieira et al. 2014).

4.2 UCS and SDT in RMR 2014 update

The uniaxial compressive strength (UCS) is widely used in rock mechanics and is considered a major parameter in the RMR classification system (Bieniawski, 1989) and was kept essentially in the same way in the RMR 2014 update (Celada et al. 2014). On the other hand, the slake durability test (SDT) has been used with great success in the study of tunnels, seeking the prediction of the mechanical behavior of the substrate in certain geological conditions, in which the rock is prone to disaggregation and expansion when absorbing water or being exposed in the excavation front (Franklin and Chandra, 1972). Recently, because of its relevance to the understanding of the geomechanical behavior of rock masses, the durability index (Id_2) has been incorporated as a classification criterion in the RMR 2014 system update (Celada et al. 2014).

Bieniawski, in the World Tunnel Congress, Foz do Iguaçu (Brazil), presented the study of Celada et al. (2014), which introduces three modifications related to the number of fractures per meter instead of RQD and joint spacing, rearranging the values of joint conditions and incorporating the alterability parameter, accessed by the Id_2 and obtained by the SDT. According to that study, which is based on results obtained from 2,298 cases in Spain, RMR 89 concentrates the values in their third part and the alterability parameter was chosen to distribute the RMR values along the third and second geomechanical classes. The Monte Seco Tunnel rock mass concentrates the RMR 89 values between 56 to 62 (III – II) (Cacciari, 2014) and has an instability problem related to long term exposition of the surrounding rock to weathering. For this reason, the use of the RMR update in the geomechanical reevaluation of the Monte Seco Tunnel, performed with a view to characterize the heterogeneity of the gneissic rock matrix, may identify areas related to the rock falls currently observed by the GeoInfraUSP researchers. This study will focus on the estimate of the newly incorporated parameter – alterability, regarding intact rocks.

4.3 Characterization of weathering grades

The SDT was originally performed in soft and weak rocks prone to expansion and disaggregation when absorbing water. It has also been also applied in the study of weathering

and alterability of igneous and medium- to high-grade metamorphic rocks, basically because of the need to predict the behavior of the rock submitted to tropical environments (Arel and Tugrul, 2001; Gupta and Rao, 2001; Gupta and Ahmed, 2007; Marques et al. 2010; Moradizadeh et al. 2016; Ahmad et al. 2017; Momeni et al. 2017).

The durability index presents a favorable relationship with the strength ratio (R_s) in the assessment of weathering grades, as shown in Figure 4.2. The strength ratio proposed by Gupta and Rao (2001) correlates the UCS values of weathered rocks with the UCS value of the fresh rock. It was obtained for different igneous and metamorphic rocks, being correlated with the Id_2 of the SDT (Arel and Tugrul, 2001; Gupta and Rao, 2001; Ceryan et al. 2008; Marques et al. 2010; Khanlari et al. 2012), according to the ISRM (2015) subdivision of weathering grades.

It can be observed that for fresh to slightly weathered grades the Id_2 hardly discriminates the rock crystalline behavior as R_s ($R_s > 85\%$ and $85\% > R_s > 60\%$, respectively) in a general weathering classification. On the other hand, starting from a moderately weathered grade there is a clear influence in the variation of the durability behavior ($95\% > Id_2 > 80\%$) due to weathering intensity, which can be also noticed in strength ratio values ($60\% > R_s > 20\%$). For highly and completely weathered grades the variation of the durability index increases (respectively, $80 > Id_2 > 50\%$ and $Id_2 < 50\%$) in relation to strength ratio values (respectively, $20\% > R_s > 5\%$ and $5\% > R_s$) (Figure 4.2).

As specific types of secondary products form and their respective quantities vary throughout the weathering of each kind of rock, the durability index reflects the relative strength reduction and can be used to compare or distinguish disaggregation degrees of crystalline rocks caused by water absorption, drying and SDT abrasion cycles, which are roughly compared to weathering in tropical environments. In the geotechnical practice, the use of SDT combined with the UCS test can characterize the most important rock modifications and can be used as an important additional information for the characterization of weathering grades of igneous and metamorphic rocks.

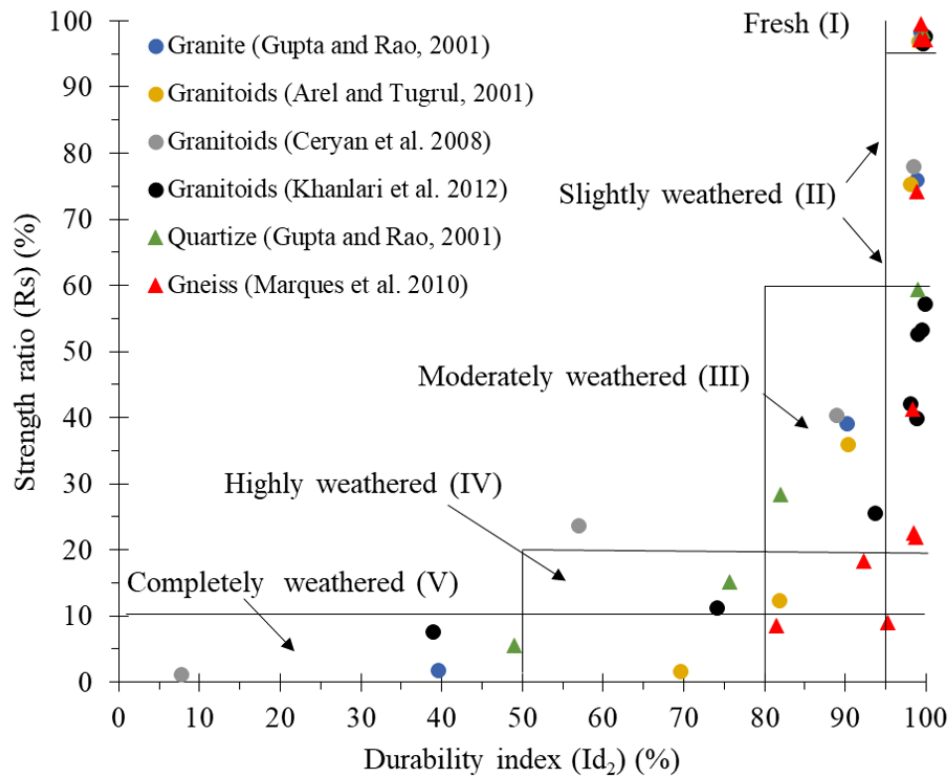


Figure 4.2 - Relationship between strength ratio and durability index for some igneous and metamorphic rocks in accordance with a general classificatory approach of weathering grades.

Rock characteristics, such as mineral composition, grain size, structural and textural properties (Gupta and Rao, 2000), the geometry of pores and fissures (Arel and Tugrul, 2001), and the appearance and types of secondary minerals and increasing fissures (Momeni et al. 2017), are the main factors influencing rock strength and durability with weathering. For example, the increase in the average crystal size is inversely proportional to the uniaxial compression and tensile strength of crystalline rocks in fresh to slightly weathered rocks (Sajid et al. 2016). Moreover, the mineralogical characteristics are responsible for the different alteration potentials of a rock (Delvigne, 1998) and are closely related to the durability values of the material (Dhakal et al. 2002). Therefore each kind of rock (igneous or metamorphic) has a mineral composition that influences rock strength and durability with weathering and that must be investigated thoroughly.

Petrographic analyses are necessary for a better understanding of the mineral characteristics, their conditions and transformations. When it comes to weathered material, indices are usually used to characterize the weathered rock, such as the micropetrographic index

(I_p) of Irfan and Dearman (1978), which has been compared to other indices to check its applicability to the characterization of different rock weathering grades (Gupta and Rao, 2001). These authors indicate that, despite the wide range of values of this index (0-100), it is best applied to granites of varied compositions, but not to quartzites and basalts.

Many authors have used the micropetrographic index, showing that it is reliable to estimate the weathering stages of different kind of rocks, including heterogenous rocks. In fact, I_p can better estimate rock weathering, helping interpret correlations between weathering and mechanical degradation for geological and engineering aims (Le Pera et al. 2001; Khanlari et al. 2012; Borrelli et al. 2014; Ahmad et al. 2017).

4.4 Materials and methods

The fresh gneissic rock of the study area is composed of quartz, plagioclase, alkaline feldspar, biotite, cordierite, hypersthene, and garnet. Other minerals (sillimanite, hercynite and opaque minerals) occur subordinately and are not responsible for the loss of rock strength (Monticeli et al. 2016).

The samples were carefully collected from drilling cores and outcropping rock blocks in the vicinity of the southern part of the Monte Seco tunnel in order to represent the three alteration horizons of the rock mass (Figures 3.10 and 3.17). The weathering grades of the samples were characterized according to the proposal presented in Table 4.1, which was based on Hoek and Brown (1997), BS 5930 (1999) and ISRM (2015) weathering classification.

To consider the abrupt weathering behavior observed in field investigations and the hardly distinguishable durability of a crystalline and heterogeneous rock, the fresh (I) and slightly weathered (II) grades were grouped in grade W1. The moderately (III) and highly weathered grade (IV) were maintained in W2 and W3 respectively. In this proposal, the highly weathered grade (IV), in its tactile features, could be distinguished into highly and completely (V) weathered grades, depending upon results of laboratory tests. Unfortunately, it was not possible to assess weathering grade W2 in one of the gneiss facies for the SDT. Petrographic analysis and physical-mechanical tests (physical properties, UCS and SDT) were carried out in




laboratories of the Institute of Geosciences, EPUSP and the Engineering School of São Carlos – University of São Paulo.

Initially, the characterization of the gneissic matrix was carried out by means of tactile and visual inspection and petrography. Mineral composition, structure, texture and grain-size of the rock were described, as well as an accurate description of grades, types of weathering and mineral cracking. The modal composition of primary minerals and secondary products was obtained by counting points for each facies, totalizing fifteen thin sections. The micropetrographic index (I_p), following the recommendations of Irfan and Dearman (1978), was obtained to investigate the mineralogical characteristics and the transformations due to weathering. This index is the ratio between the number of sound minerals (SM) and unsound constituents (UC) that include unsound or weathered minerals (UM), fissures (F) and voids (V).

The representative specimens of each weathering grade (Table 4.1) and petrographic facies were submitted to physical tests. Porosity, density and apparent absorption were obtained following the ISRM (1979a) guidelines. The UCS of the 53 samples were obtained following the ISRM (1979b) guidelines. The angle (β) between foliation and load direction obtained for weathering grade W1 fell around 60° and 0° and 90° for grades W2 and W3.

With the use of equipment and procedures recommended by ASTM D4644-16 (2016) the I_d were obtained during SDT. The I_d values were categorized according to Table 4.2 presented in Gamble (1971) and suggested for the classification of rock durability (ISRM, 1979a). The I_d values were also classified according to the alterability parameter from RMR 2014 update (Celada et al. 2014). The criterion is the fifth parameter of classification and is accessed by the I_{d2} of the SDT. Table 4.2 shows that ten points are grouped in classes Very High (VH), High (H) and Medium High (MH); for the other three classes – Medium (M), Low (L) and Very Low (VL), a significant drop in material durability and longer grading intervals occur, as the value decreases to zero.

Table 4.1 - Intact rock weathering grades (Modified after Hoek and Brown, 1997; BS 5930 1999, ISRM, 2015)

Grades	Visual Tactile Features	UCS by simple means (MPa)
W1 (I - II)	<p>Fresh to incipient weathered. Macroscopically there is no evidence of weathering of minerals. Minerals have luster. Slabs with difficulty at various hammer blows, resisting the cut of the steel knife and the finger pressure.</p>	 <p>100 - 200 (> 200)</p>
W2 (III)	<p>Shows signs of mineral weathering. Minerals show lack glare and noticeable discoloration, sometimes occurs with a film of yellow material (iron oxides and hydroxides). Breaking with some difficulty from hammer blow. Steel knife scratches the surface and removes crystals, resisting finger and nail pressure.</p>	 <p>50 - 100</p>
W3 (IV/V)	<p>Rock and minerals significantly weathered, being found friable. Minerals lacking luster and are strongly discolored; iron oxides and hydroxides impregnate the sample. Breaks easily with a hammer blow*. Minerals are removed by finger and nail pressure; steel knife easily causes grooves in the sample**.</p>	 <p>12.5 - 50 (*) 1.25 - 12.5 (**)</p>

Obs: W1 - fresh to slightly weathered, W2 - moderately weathered and W3 – highly to completely weathered.

Images sizes 54.5 mm

Table 4.2 - Durability classifications

Id ₂ (%)	a) Slake Durability Index (Gamble, 1971)	b) Alterability (Celada et al., 2014)	
Values	Classification	Symbol	Value
100-98	Very High	VH	10
98-95	High	H	10
95-85	Medium High	MH	10
85-60	Medium	M	8
60-30	Low	L	4
30-0	Very Low	VL	0




4.5 Results and discussion

4.5.1 Petrographic and physical characterization of the gneissic rock

The lithotype, referred to simply as gneissic rock, is light gray to bluish dark gray, fine- to medium-grained, secondarily coarse-grained. Centimeter- to meter-sized bands that correspond to the mesosome are characterized by a lepidogranoblastic texture and a biotite-rich gneiss foliation, interspersed with millimeter-sized light (felsic) and centimeter-sized quartz-feldspathic lenses. Well-formed bands of granoblastic texture correspond to the medium- to coarse-grained leucosome composed of feldspar, quartz, cordierite, garnet and opaque minerals.

The presence of these features, closely related to metamorphism of a sedimentary prototype, leads to the heterogeneity of the rock matrix. These variations, which represent the gneissic banding, were classified as petrographic facies B1, B2 and B3, according to mineral composition, structure, texture and grain size (Table 4.3). The most representative photomicrographs are presented in Figure 4.3. The micropetrographic indexes for each thin section numbered 1 to 15, with the respective test of apparent physical properties, are shown in Table 4.4 and the correlation between I_p and porosity is presented in Figure 4.4.

Table 4.3 - Description of the petrographic facies of the gneissic rock

Facies	Structure	Texture	Grain size	Mineralogical assembly (%)					
				Mineral	Average	Ranged	Mineral	Average	Ranged
B1		Equigranular – inequigranular	Fine-grained	Qz	36.26	30-40	Cr	15.30	10-30
				Fk	14.73	5-25	Hp	0.98	0-3
		Lepidogranoblastic	0.1-3 mm	Pl	12.50	5-20	Gr	0.39	0-2
				Bt	16.01	10-25	Ot	3.90	0-5
B2		Inequigranular	Fine- to medium- grained	Qz	38.23	30-40	Cr	19.49	10-35
				Fk	12.85	5-20	Hp	1.15	0-3
		Lepidogranoblastic to granoblastic	(L) 1-5 mm (D) 0.1-3 mm	Pl	14.20	10-20	Gr	0.45	0-2
				Bt	11.98	5-20	Ot	1.65	0-5
B3		Inequigranular porphyroblastic	Coarse-grained	Qz	34.96	10-55	Cr	13.70	5-30
				Fk	25.42	5-50	Hp	1.24	0-5
		Granoblastic	5-20 mm	Pl	19.24	5-25	Gr	0.17	0-2
				Bt	4.07	0-15	Ot	1.20	0-5

Obs: Minerals: quartz (Qz), orthoclase (Fk), plagioclase (Pl), biotite (Bt), cordierite (Cr), hypersthene (Hp), garnet (Gr) and other minerals (Ot).

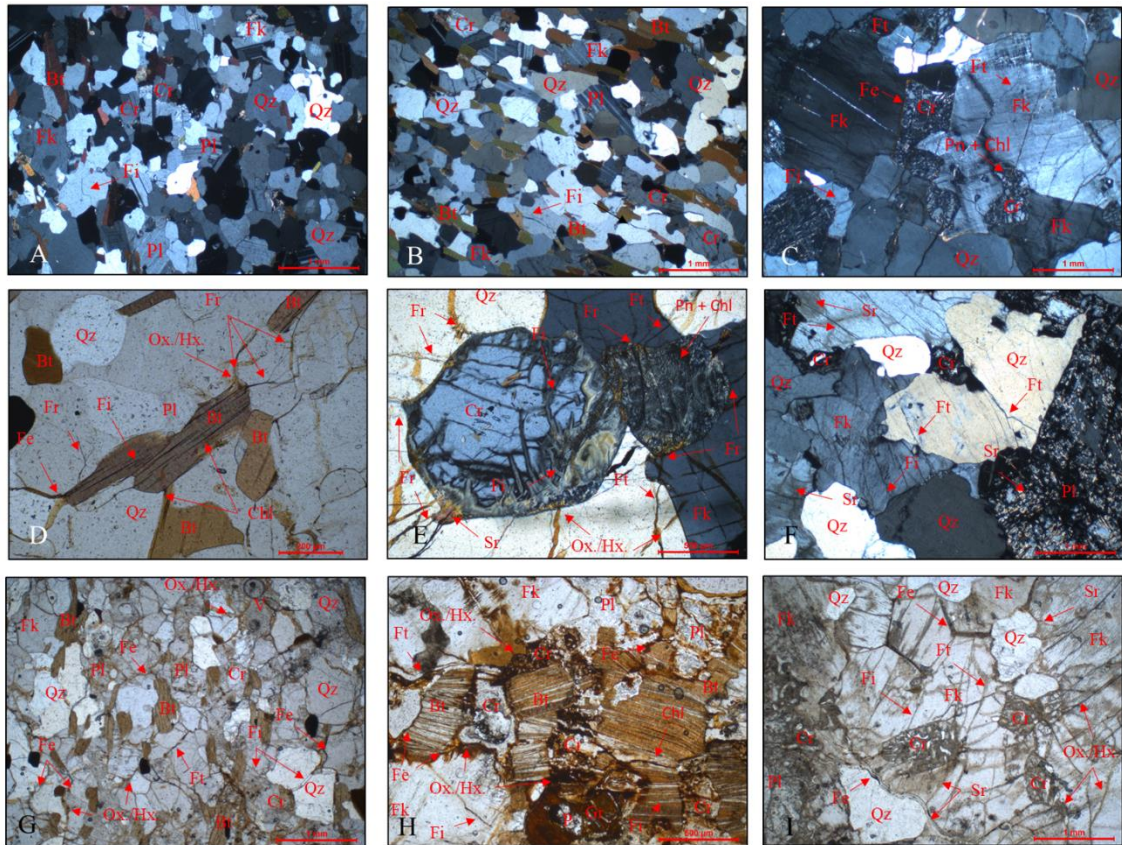


Figure 4.3 - Photomicrographs illustrating: A) facies B1; B) facies B2; C) facies B3; D) biotite altered to chlorite and iron oxides and hydroxides; E) cordierite altered to pinites, chlorite, sericite and iron oxides and hydroxides; F) plagioclase and orthoclase altered to sericite; G) intermineral fissures in facies B1; H) fissured weathered matrix of facies B2 impregnated with iron oxides and hydroxides, and I) fissured weathered matrix of facies B3, fissures currently found empty. Abbreviations: Fi – intramineral fissure, Fe – intermineral fissure, Ft – transmineral fissure and Fr – radial fissure; V- voids; Qz – quartz, Cr – cordierite, Fk – orthoclase, Pl – plagioclase, Bt – biotite, Pn – pinites, Chl – chlorite, Sr – sericite and Ox./Hx. – iron oxides and hydroxides.

Fresh to slightly weathered gneissic rock

In thin sections 1-2, 6-7 and 11-12 from the facies B1, B2 and B3 respectively, a clear change of the microsystem contact among the minerals of the rock matrix is observed, which translates into the structure, from foliate to incipient massive with loss of foliation given by the planes of aligned micas, and into the texture, initially equigranular and lepidogranoblastic to inequigranular and granoblastic. This modification is accompanied mainly by the increase in grain-size of the rock matrix that varies significantly for facies B3, rich in quartz, feldspar, and cordierite porphyroblasts (Tables 4.3 – 4.4).

Intramineral microcracks are absent or incipient in facies B1, leading to a more evolved fissure microsystem in facies B3, marked by a significant quantity of intramineral fissures (Fi) that reach the quartz, feldspars and cordierite rims, being sometimes connected with other Fi, forming intermineral (Fe) and transmineral fissures (Ft) (Figure 4.3A - C). Some minerals only show signs of alteration in some more weatherable minerals such as cordierite in fissured portions of the rock matrix. The difference in the degree of microcracking of facies B3 of the gneissic rock matrix showing incipient weathering causes a great difference in Ip obtained in weathering grade W1 (Figure 4.4).

Table 4.4 - Physical and petrographic properties observed in thin sections

Samples		γ_d	η	w_a	SM	UM	Fi	Fe	Ft	V	
n°	WG	PF	(g/cm ³)	(%)	(%)	(%)	(%)	(%)	(%)	(%)	
1	W1		2.69	0.55	0.20	98.87	1.13	1.13	0.00	0.00	0.00
2			2.72	1.55	0.57	98.21	2.56	1.79	0.00	0.00	0.00
3	W2	B1	2.66	3.59	1.24	88.71	11.69	2.84	0.51	0.28	0.00
4			2.55	4.37	1.70	78.17	21.83	5.21	2.13	0.47	0.00
5	W3		2.38	10.61	4.46	60.51	39.49	4.52	1.75	1.51	0.00
6	W1		2.74	0.77	0.28	98.60	1.40	1.40	0.00	0.00	0.00
7			2.69	1.65	0.60	91.46	8.54	2.05	0.49	0.00	0.00
8	W2	B2	2.69	2.63	0.98	83.05	16.95	3.41	0.65	1.38	0.00
9			2.53	6.35	2.43	69.79	30.21	5.23	1.00	1.99	0.00
10	W3		2.30	16.31	7.09	25.82	74.93	8.29	5.77	5.30	0.41
11	W1		2.71	0.80	0.24	73.59	26.41	6.08	0.42	0.68	0.00
12			2.70	1.63	0.61	70.82	29.18	6.52	1.91	1.69	0.00
13	W2	B3	2.68	3.36	1.28	56.44	43.92	7.58	2.86	2.72	0.00
14			2.53	5.79	2.03	31.87	69.44	9.49	2.88	3.93	0.59
15	W3		2.17	13.38	6.12	21.73	78.27	5.38	3.60	8.12	1.29

Obs: WG: weathering grade, PF: petrographic facies, γ_d : density, η : porosity, w_a : water absorption, SM: sound minerals, UM: unsound minerals, Fi, Fe and Ft: intra, inter and transmineral fissures and V: voids.

Moderately weathered gneissic rock

Weathering begins in fact with the emergence of physical-chemical alteration in minerals (quartz – cracks; cordierite, biotite, plagioclase, orthoclase, and hypersthene – decomposition and disintegration), with the generation of secondary minerals where a

network of fissures (intra to transmineral) is under development, as seen in the samples 3, 8, and 13, respectively from the facies B1 to B3 (Table 4.4). Hypersthene and garnet are weathered to iron and aluminum oxides and hydroxides along intra, inter and transmineral fissures. Biotite is weathered along the open cleavage planes with the production of chlorite and iron oxides and hydroxides (Figure 4.3D). Cordierite is altered to pinite, chlorite, sericite and iron oxides and hydroxides (Figure 4.3E). Orthoclase and plagioclase are altered to sericite along the intra to transmineral fissures (Figure 4.3F).

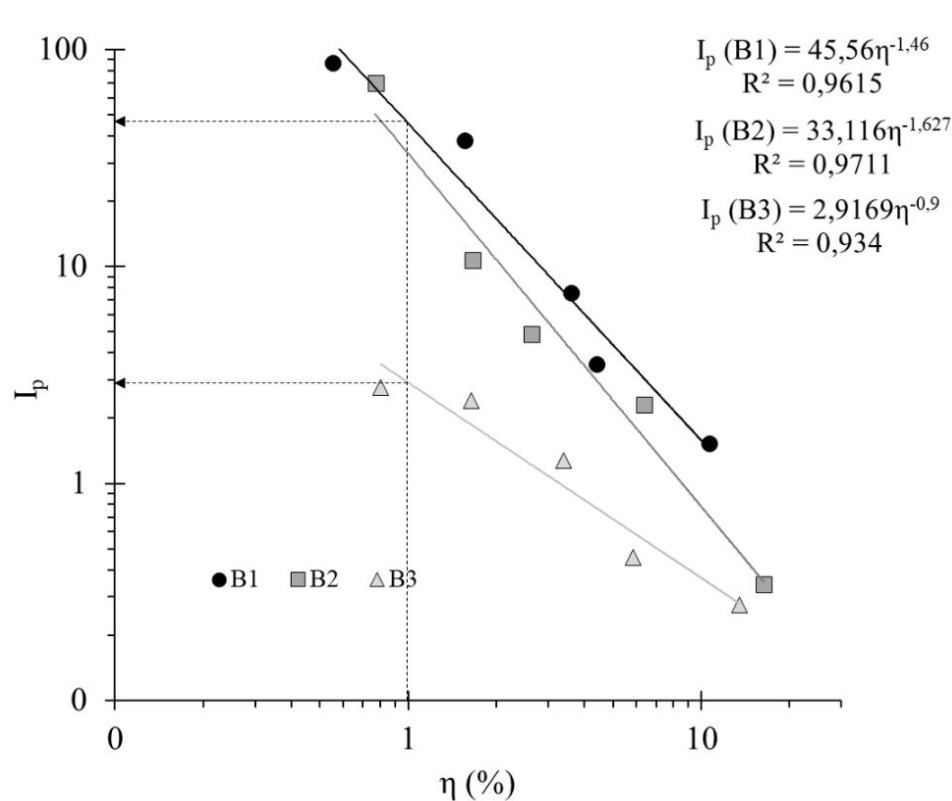


Figure 4.4 - Relationship between micropetrography index (I_p) and porosity (η) for the gneissic rock facies B1, B2 and B3.

Cordierite and the biotite lead to the impregnation of iron oxides and hydroxides in the matrix, causing, when weathered, changes in texture by the appearance of radial fissures (Fr) in the minerals adjacent to them (Monticeli et al. 2016). These changes act as a weakening factor, increasing the coalescence of fissures into intermineral and transmineral fissures by the physicochemical weathering of the microsystem formed by them (Delvigne, 1998). This process weakens the bonds between adjacent minerals and favors the advance of the weathering agents to other minerals, increasing the alteration of

the whole rock matrix (Figure 4.3 D and E). The whole of mineralogical transformations increases the porosity of the rock in about 3%, while I_p values are significantly decreased for the rock matrix classified in facies B1 and B2, following the order of the scale to facies B3 (Figure 4.4).

Highly (to completely) weathered gneissic rock

Weathering had an intense effect upon the primary minerals, often causing their total transformation into secondary minerals, now in high quantity in the fissured weathered matrix, as seen in samples 4-5, 9-10 and 14-15, respectively facies B1, B2 and B3. The set of mineral transformations decreases I_p values to the lowest of each facies, as the porosity of the samples drastically increases (Table 4.4 and Figure 4.4). The petrographic analyses showed that each matrix presents some particularities regarding the development of secondary minerals, types of fissures and fillings.

It can be noticed in facies B1 that intra and intermineral fissures are more common. The intermineral fissures (F_e) can be seen only because they are filled with iron oxides and hydroxides (Figure 4.3G), while facies B2 and B3 show all kinds of fissures (intra, inter and transmineral) particularly filled with iron oxides and hydroxides in high quantities and secondly by pinite, chlorite and sericite in the foliation plane in facies B2 (Figure 4.3H). In facies B3, fissures are filled in great quantity with sericite, secondly with iron oxides and hydroxides only close to cordierite (Figure 4.3I). The fissure microsystem of each facies controls particularly the intensity of the weathering of minerals in each matrix, as observed by differences in the percentage of sound and unsound minerals in facies B1 in relation to facies B2 and B3. The micropetrographic index and porosity were sensitive to these mineralogical aspects, showing higher I_p and lower porosity values for facies B1 in relation to B2 and B3 of grade W3 (Table 4.4 and Figure 4.4).

The correlation between I_p and the physical properties of the petrographic facies defines a trend along the weathering evolution that may help outline distinctions or similarities between samples, weathering stages and mechanical behavior. Among them, preference was given to porosity, because it presents a higher coefficient of determination

than density and absorption. Facies B1 and B2 clearly present the same trend at earlier stages of weathering but, when weathering intensifies, facies B2 approaches the trend of facies B3, which presents a completely distinct behavior in respect to weathering.

The thin sections of facies B3 of grade W1 (Table 4.4) show petrographic aspects that result in a lower I_p value in relation to facies B1 and B2, despite the close values of porosity around one per cent, as indicated by the dotted line (Figure 4.4). The I_p values of facies B3 of grade W1 are those of grade W2 – facies B1 and B2. In this sense, the petrographic index is a good additional information on the rock matrix condition in face of weathering, thus permitting us to predict certain mechanical behavior of the rocks being studied.

4.5.2 Durability and strength characterization of the gneissic rock

Figure 4.6 shows the photos of the sample assemblies after all the SDT cycles. Figure 4.7 shows the I_d values according to the cycle number (n) for all facies of weathering grades W1 and W3; for facies B1 and B3 of grade W2, as it was not possible to obtain enough representative pieces of rock to define sample B2. Durability classifications (Gamble, 1971) and the value of the alterability parameter (Celada et al. 2014) taken from Table 4.2 are also shown in Figure 4.6.

In Figure 4.7, UCS and R_s were correlated with porosity, I_p and I_d . To investigate the influence of heterogeneity in the variation of the results, all data were plotted *versus* the porosity of the samples (Figure 4.7A and D). To analyze the difference between the I_p values for petrographic facies B1 and B2 in relation to B3, especially in the earlier stages of weathering as observed previously in Figure 4.4, the average I_p values of the thin sections of each weathering grade calculated from Table 4.4 were correlated to the mean UCS and R_s (Figure 4.7B and E).

The relationship between the mean UCS value and I_d along the SDT cycles is presented in Figure 4.7C, and the best correlation (4th cycle) was used to guide a general weathering grade classification (I, II, III, IV and V) based on R_s and I_{d4} (Figure 4.7F). The data from Gupta and Rao (2001) and Khanlari et al. (2012) were also plotted to calibrate the range of values. The maximum UCS obtained for facies B1 was 164 MPa

and this result was used for the R_s calculations. The average values of UCS and I_d along the SDT cycles are presented in Table 4.5. The weathering grade classification of the gneissic rock from the Monte Seco tunnel is displayed in Table 4.6.

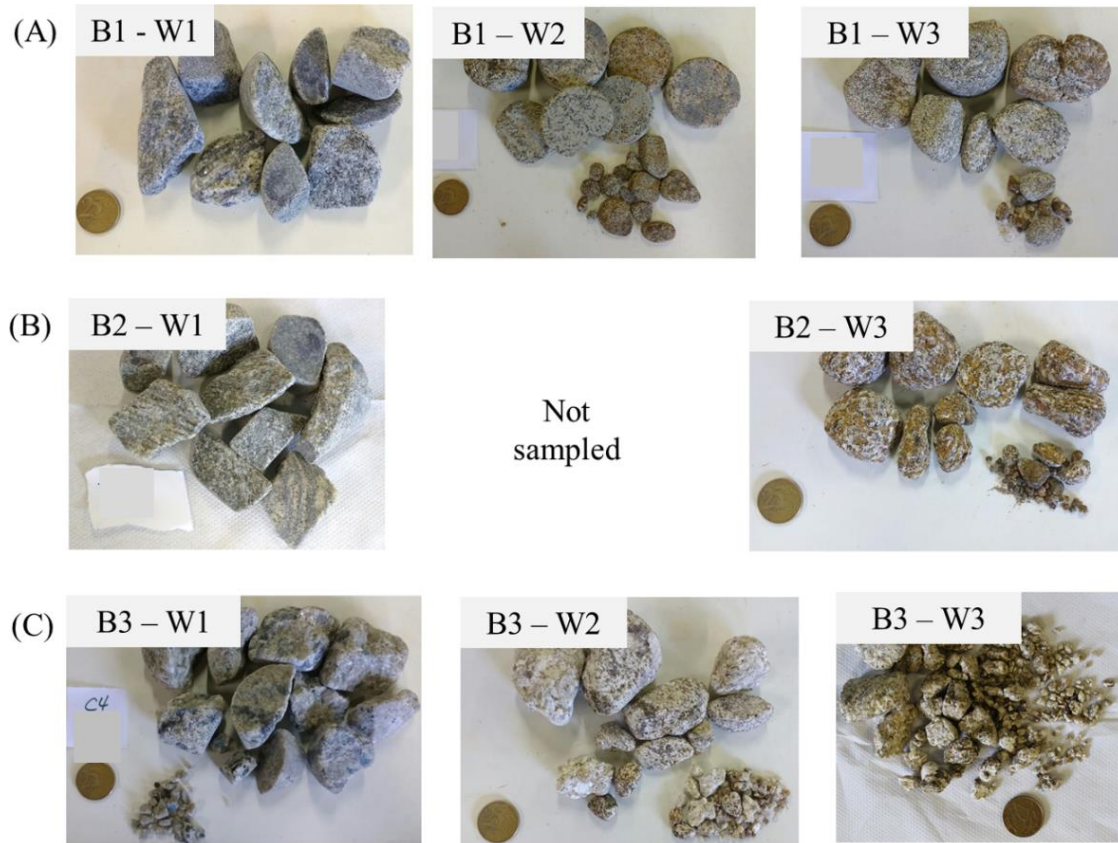


Figure 4.5 - Photos after all the SDT cycles for each petrographic facies and weathering grade. Petrographic facies: (A) B1, (B) B2 and (C) B3. Weathering grades: W1 (fresh to slightly weathered), W2 (moderately weathered) and W3 (highly to completely weathered).

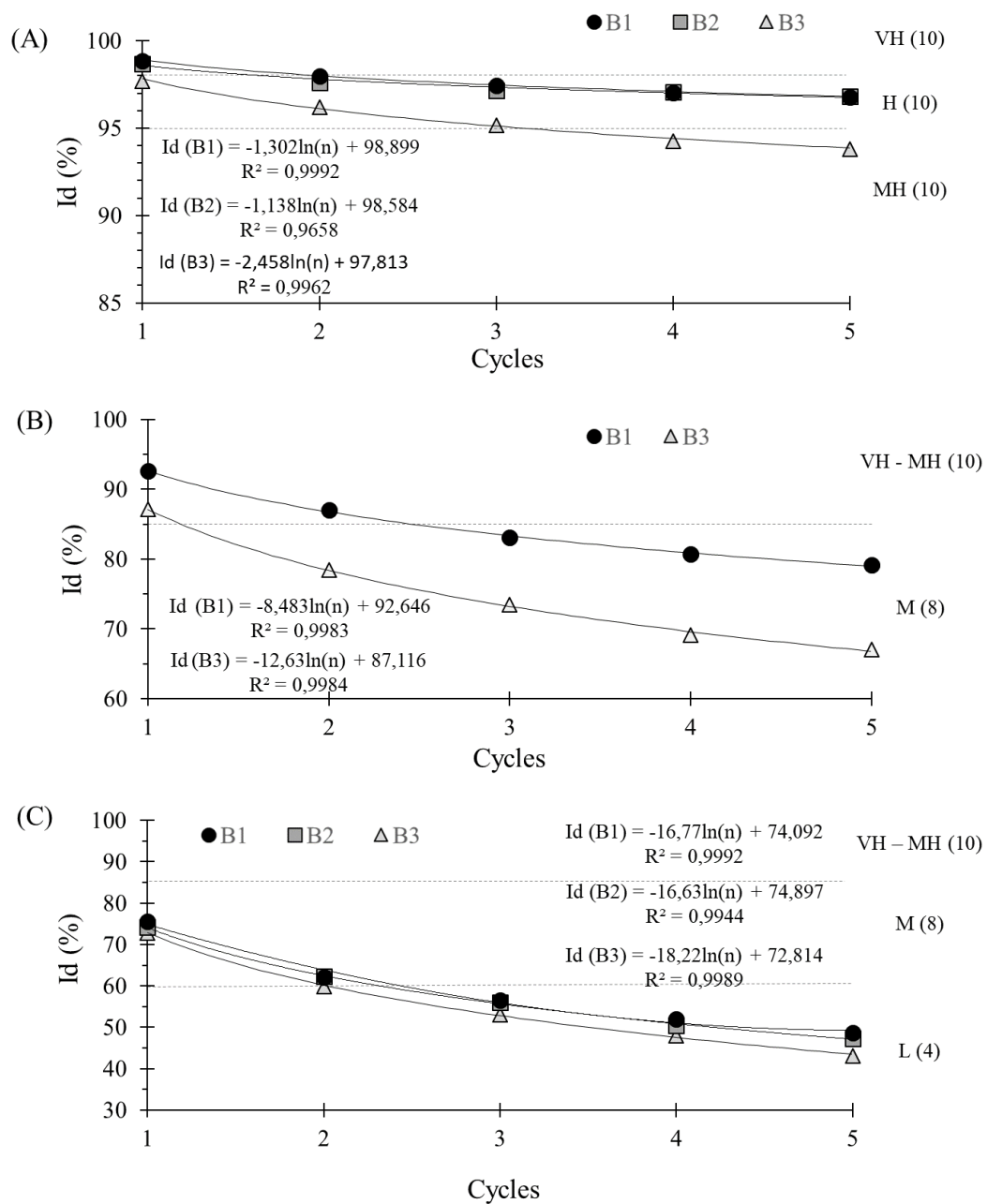


Figure 4.6 - The behavior of Id according to the weathering grade of each petrographic facies along the five SDT cycles. It is shown in detail the mutual behavior of the facies for weathering grades (A) W1 (fresh to slightly weathered), (B) W2 (moderately weathered) and (C) W3 (highly to completely weathered). Slake durability classes (Gamble, 1971): VH (very high); H (high), MH (medium high), M (medium), L (low), VL (very low) with the value of the alterability parameter (10 – 4) (Celada et al. 2014).

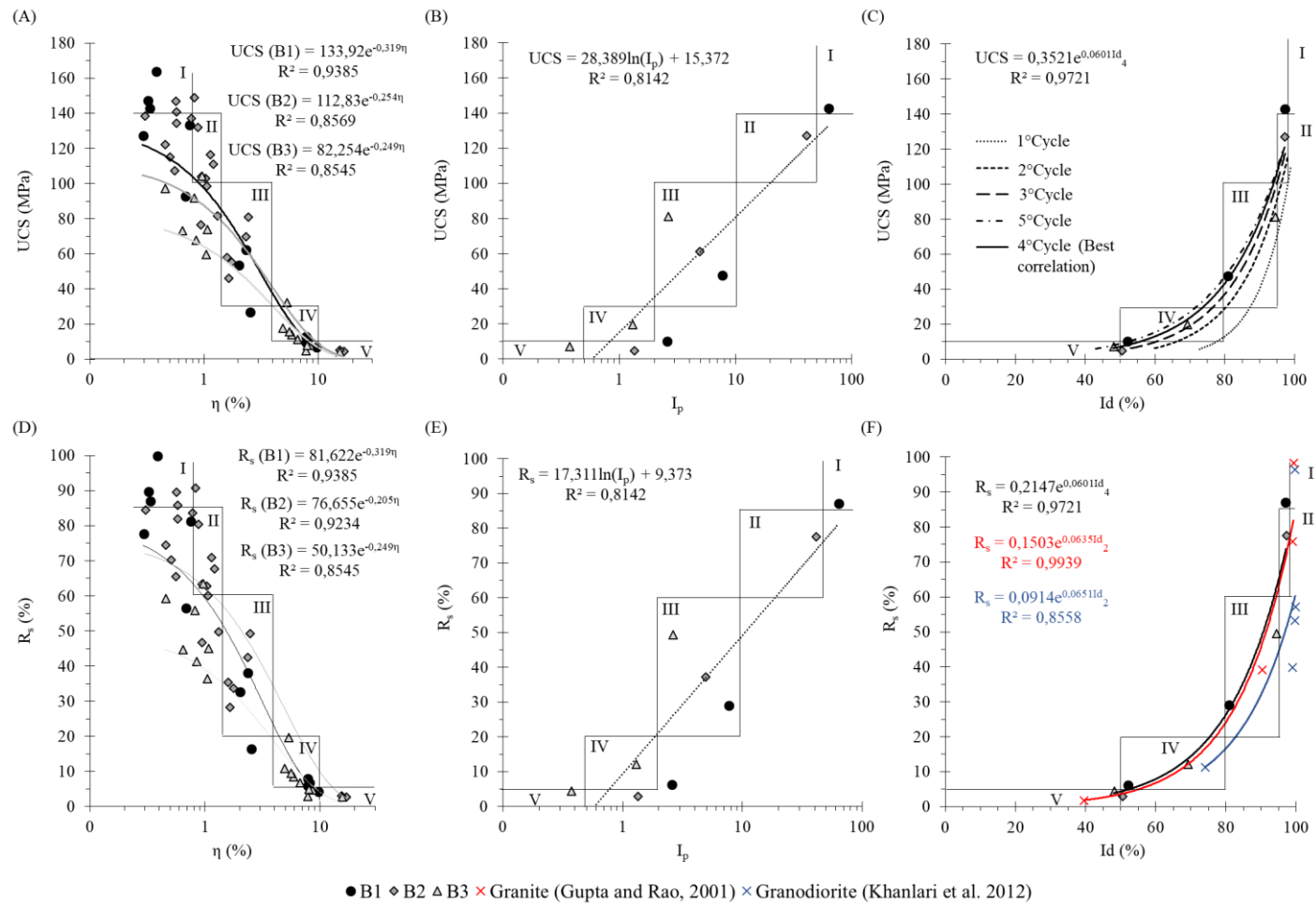


Figure 4.7 - Relationships between the uniaxial compressive strength (UCS) and strength ratio (R_s) with porosity (η) (A and D), micropetrographic index (I_p) (B and E) and durability index (Id) (C and F), presenting the general weathering grades classification for the intact rock of the Monte Seco Tunnel. Weathering grades: I: fresh, II: slightly weathered, III: moderately weathered, IV: highly weathered and V: completely weathered.

It can be observed in the SDT that the edges and corners of weathering grade W1 samples are generally comminuted for all facies characterized as Type I (ASTM, 2016), but the formation of non-passing fragments in the mesh only for facies B3 reflects the influence of the grain-size of the minerals in the defragmentation process. For all the facies of weathering grades W2 and W3 an intense comminution of the specimens is observed with the formation of non-through fragments in the mesh, characterized as Type II (ASTM, 2016) (Figure 4.5). It is observed in the B3 – W3 facies that this process is more intense with a larger number of fragments than in original samples. It was noticed that the through-material of facies B1 and B2 is fine to medium grained and that it is clearly fine to coarse grained for B3.

Table 4.5 - Durability and strength of the gneissic rock from the Nova Venécia Complex

n	WG	Petrographic facies	Durability index (%)					Uniaxial compressive strength (MPa)			
			SDT Cycles					Max	Min	Mean	SD
			1	2	3	4	5				
1	W1		98.9	98.0	97.5	97.1	96.8	164.0	127.7	143.2	14.0
2	W2	B1	92.6	87.0	83.1	80.7	79.2	62.6	27.2	47.9	18.5
3	W3		75.6	62.1	56.5	52.0	48.7	13.2	7.1	10.5	2.6
4	W1		98.7	97.7	97.2	97.1	96.8	149.2	103.3	127.5	15.5
5	W2	B2			*			76.9	46.3	61.4	12.0
6	W3		74.2	62.2	56.0	50.4	47.3	5.4	4.7	5.0	0.5
7	W1		97.7	96.2	95.2	94.3	93.8	104.4	59.9	81.4	16.6
8	W2	B3	87.1	78.4	73.5	69.1	67.1	32.5	14.1	20.1	8.4
9	W3		72.8	59.9	53.1	48.0	43.0	11.5	4.6	7.5	2.8

Obs: WG: weathering grade, Max: maximum, Min: minimum, SD: standard deviation. *Not sampled.

Concerning the second SDT cycle, the petrographic facies B1 and B2 of grade W1 yield higher Id_2 values, respectively, 98.89% and 98.72% and are classified in the same category Very High, while B3, with a slightly lower value of 97.73% falls in a lower category (High) (Figure 4.6). In all of them, the durability of the material decreases as the weathering intensity increases, as shown in grades W2 and W3. The durability indexes of

the petrographic facies are classified in equal categories, respectively, Medium High, for facies B1 and B3, respectively 92.61% and 87.09% and Medium, for all facies B1, B2 and B3, respectively 75.64%, 79.29% and 72.81%. As for the results along the SDT cycles, it is observed a noticeable decrease in the durability indexes and the categories of classification. The I_d values for facies B1 and B2 overlap the subsequent numbers of cycles in weathering grade W1 and almost in grade W3. In contrast to that, facies B3 shows a slightly different behavior, the drop-in durability class occurring many cycles before B1 and B2. This behavior translates into the durability classification of facies B3 normally in a lower category than the others depending on the SDT cycle (Figure 4.6).

The gneissic rock heterogeneity has a clear effect in UCS and R_s in weathering grade W1 (I and II), where the porosity is lower than 1.5% (Figure 4.7A and D). As commented by Sajid et al. (2016), the increasing grain size is inversely proportional to UCS in the earlier stages of weathering and, in parts, controls the difference noticed between petrographic facies B1 to B3. However, as observed in the petrographic analysis, this strength variation is also related to the characteristics of the rock, structure and texture modification (Table 4.3), followed by the increasing degree of microcracking triggered by the incipient process of weathering of cordierite from facies B1 to B3. These aspects were highlighted by I_p (Figure 4.7B and E) and I_d (Figure 4.7C and F), whose correlations point out that facies B3 samples previously characterized by visual tactile features of weathering grade W1 (Table 4.1) present the behavior of petrographic facies B1 and B2 of weathering grade W2 (III), in accordance with laboratory tests.

UCS and R_s values of the gneissic rock facies B1, B2 and B3 decrease with weathering, following exponential functions in relation to porosity and I_d , and a logarithmic function in relation to I_p . The influence of heterogeneity in the variation of UCS and R_s values decreases while the porosity increases drastically (Figure 4.7A and D). Again, as with facies B3, the previously weathering grade characterized as W2 (III) shows, in fact, more signs of alteration, being classified in grade IV by all the properties studied here (Figure 4.7). It is worth mentioning that I_p and the degradation of I_d with the SDT cycles were crucial to the interpretation above, once these aspects noticed in facies B3 were not observed in facies B1 and B2, whose samples, previously characterized using Table 4.1, are in accordance with the general classification based on laboratory tests (Figure 4.7 and Table 4.6).

In spite of the decreasing strength variation among petrographic facies with weathering, the characteristic transformations of the rock and the kind of secondary products produced in each petrographic facies are continually heterogeneous, which is slightly reflected in the increasing difference of durability between B1 and B3 along the SDT cycles employed (Figure 4.6 and Table 4.5). Facies B1 of these samples, previously characterized in the advanced weathering grade W3 as highly weathered (IV), was kept in this category, whereas facies B3, with lower UCS and durability values, was comparably placed in the category completely weathered (V). Facies B2 remains in-between, based on UCS and R_s and Id_4 (4th cycle) values (Figure 4.7F). Previously, I_p values in Figure 4.4 also indicated these aspects.

As expected, the combination of UCS and R_s with I_p and Id is sensitive to the differences and transformations in the rock matrix, presenting a significant reduction with weathering (Figure 4.7). The combination of weathering grades (Table 4.1), in order to provide a brief characterization of the rock mass condition, can be applied to the tunneling practice by means of laboratory tests, considering whether weathering indexes, such as R_s , I_p and Id_4 , are adequate to investigate the influence of heterogeneities in the gneissic rock on its physical-mechanical properties, especially those related to loss of strength and disaggregation (Figures 4.6 and 4.7). In fact, this procedure helped differentiate the behavior of the petrographic facies and then correct their comparative positioning in the general weathering grade classification and subdivision (Table 4.6).

Recently, Kahraman et al. (2017) found a strong correlation between UCS and Id_4 and pyroclastic rocks (extrusive igneous rocks), and Momeni et al. (2017) indicates two cycles or more to distinguish weathering grades and capture the durability aspects of crystalline rocks. Indeed, the correlations of Id values along the cycles with UCS was a good procedure for weathering grade characterization and strength estimate, making possible the identification of Id_4 as the best correlation. This trend ($Id_{4th\ cycle}$) comparatively correlated with data collected from Gupta and Rao (2001) and Khanlari et al. (2012), both using Id_2 , to guide the arrangement of the scale of values of the general weathering grade classification of gneissic rock of the Monte Seco tunnel (Figure 4.7C and F, Table 4.6).

The trend line for loss of strength and durability of the gneissic rock from the first to the second SDT cycle resembles that of a granodiorite, whereas that from the fourth to

the fifth cycle resembles that of a granite, whose weathering grades are better defined by these properties. Comparing the number of cycles needed to access the best fit line from a gneissic rock to a granite, it can be remarked that the granite has a relative intensity of disaggregation four to fifth times superior than the gneissic rock under such SDT conditions. This comparison could be used as additional information in the study of the behavior of crystalline rocks during the process of durability degradation.

Table 4.6 - General weathering grade classification of the gneissic rock of the Monte Seco tunnel

PF	Table 1	WG	I_p	η (%)	UCS (MPa)	R_s (%)	Id (%)		Durability class	
							(1°cycle)	(4°cycle)		
B1 + B2	W1	I	> 50	< 0.8	> 140	> 85	> 98	> 95	VH	
		II	50-10	0.8-1.5	140-100	85-60	98-95		H	
	W2	III	10-2	1.5-4	100-30	60-20	95-80	95-80	MH	
	B3	W3	IV	2-0.5	4-10	30-10	20-5	80-50	80-50	M
			V	< 0.5	> 10	< 10	< 5	< 50	< 50	L – VL

Obs: petrographic facies (PF), weathering grades (WG), micropetrographic index (I_p), porosity (η), uniaxial compressive strength (UCS), strength ratio (R_s) and durability index (Id).

4.5.3 RMR ratings of Id and UCS

The alterability parameter (Celada et al. 2014) was previously shown together with the durability classification (Gamble, 1971) in Figure 4.6. The alterability of the gneissic rock is maximum throughout the cycles from fresh to moderately weathered grades. When weathering intensifies from moderately to completely weathered grades, the categories of its durability fall, consequently decreasing the scores of the geomechanical parameter. The value drops from ten to eight from weathering grades III to IV, and subsequently from eight to four from grades IV to V, this being the total number of cycles employed in SDT. In this manner, the alterability criterion indicates that the rock can only be driven to a decrease in geomechanical quality if it is in advanced weathered condition.

Aiming at a detailed characterization and classification of the Monte Seco tunnel, especially considering intact rock parameters and degradation due to weathering, the UCS and alterability RMR parameters are correlated in Figure 4.8, considering the Id values along the cycles. The number of cycles plays an important role in determining r^2 ,

especially in Id_2 , the Id suggested to parameter estimative. The coefficient is 0.76 in the first cycle (Figure 4.8A), decreases to 0.59 in the second cycle (Figure 4.8B) and reaches the best value (0.91) from the third cycle onwards (Figure 4.8C).

As seen in Figure 4.8B, it is not possible to distribute the alterability values adequately among the weathering grades using the alterability parameter (Table 4.2) and Id_2 only, as recommended by Celada et al. (2014). Furthermore, the Monte Seco tunnel classification would not properly discriminate the geomechanical behavior of the rock facies, as may be later revealed in field investigations.

The increase of the number of cycles to more than three in order to better estimate the alterability parameter clearly distributes the scores as weathering intensifies and UCS decreases (Figure 4.8C). However, the value of the alterability parameter obtained with Table 4.2 may be, in general, overvalued for the gneissic rock along the weathering grades. For instance, the alterability value for grades IV and V, which show characteristics like a residual soil, is 4 (Id_4). Values around 0 would be expected, as observed for UCS, which achieved scores around 1.5, a value much closer to the extreme 0.

In this manner, as Id reflects the relative strength degradation and rock disaggregation, showing well established relationships with UCS and R_s (Figures 4.2, 4.7C and F), it can be assumed that the value of the alterability parameter could be equivalent to the strength ratio in the weathering grade characterization.

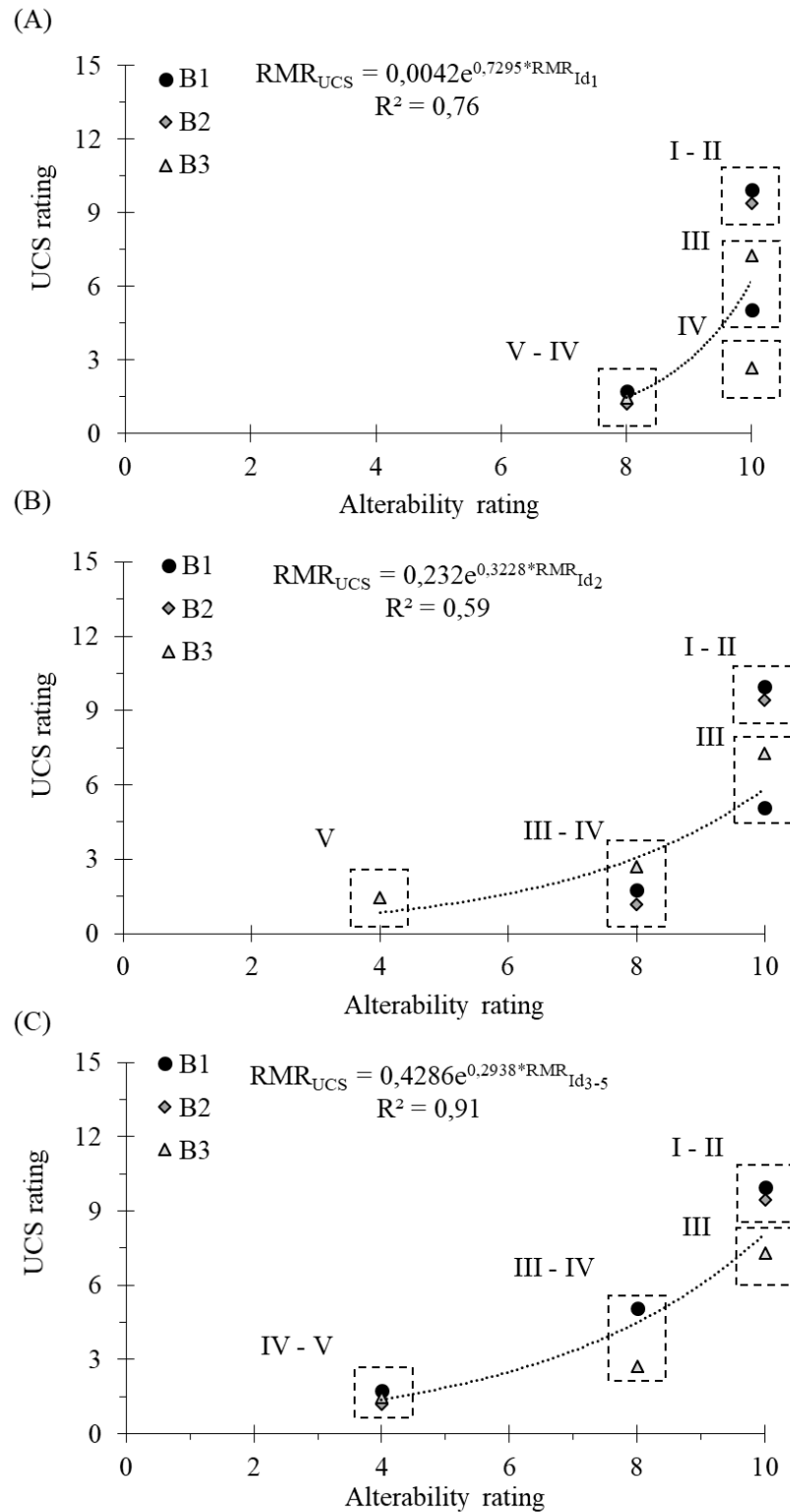


Figure 4.8 - Relationship between UCS and Id RMR rating values along the 1st cycle (A), 2nd cycle (B) and 3rd to 5th cycle (C). Weathering grades: fresh (I), slightly weathered (II), moderately weathered (III), highly weathered (IV) and completely weathered (V).

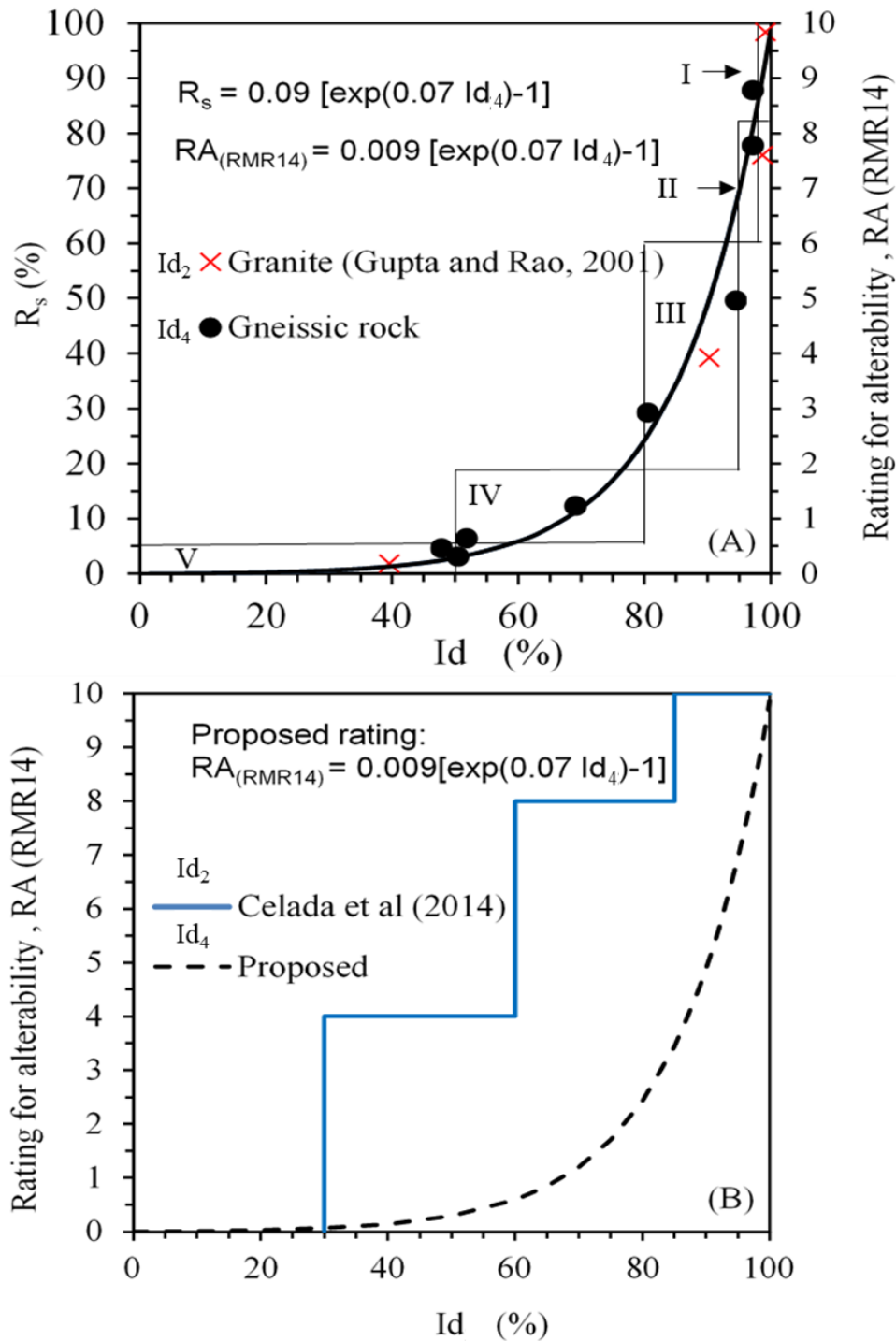


Figure 4.9 - Relationship between the R_s and Id along the weathering grades with the alterability equation proposed for granite and gneissic rocks, Id_4 (A) and compared with Celada et al. (2014) (B).

In this case, an adjusted equation is proposed, based on the granite Id_2 and the gneissic rock, Id_4 , in order to access the alterability parameter along the weathering grade classification (Figure 4.9A). The proposed equation (1), when compared to Celada et al.

(2014) (Figure 4.9B), fulfills the values of the alterability parameter along the weathering grades, improving the initial idea mentioned by these authors, namely that of using Id to distribute the RMR values (Table 4.7).

$$RA_{(RMR14)} = 0.009[\exp(0.07 Id_4) - 1] \quad (4.1)$$

Table 4.7 - The alterability parameter for a granite and gneissic rocks

Petrographic facies	Weathering grades	Alterability (Id_2)	Alterability (Id_4)
		Celada et al. (2014)	(proposal)
B1 + B2 B3	Fresh (I)	10	10-8
	Slightly weathered (II)	10	8-6
	Moderately weathered (III)	10	6-1.5
	Highly weathered (IV)	10-8	1.5-0
	Completely weathered (V)	8	0

4.6 Conclusion

In the study of the relationship between durability and strength of an intact gneissic rock along weathering grades, it was fundamental to characterize its heterogeneity, since it clearly affects the variation of these properties, as in the related estimate of parameters.

The gneissic rock presents three petrographic facies B1, B2 and B3, which characterize the heterogeneity of the lithotype banding. Among these facies structural changes can be noticed, from foliated to massive, and also textural, from lepidogranoblastic to granoblastic, accompanied by increasing grain size, fissures and disappearance of the micas that define the anisotropy plane of the rock (Table 4.3). These mineral characteristics generate different alterability conditions, which, in turn, influence the specific appearance of secondary products, creating a unique mineralogical microsystem for each facies along weathering (Figure 4.3).

The visual and petrographic analysis and the physical-mechanical tests (SDT and UCS) resulting in weathering indexes (I_p , Id and R_s) were able to qualify, quantify and

distinguish this mineralogical information (Figures 4.4 to 4.7), improving the weathering grade classification for the revaluation of the Monte Seco tunnel (Table 4.6). Comparatively to facies B1 and B2, facies B3 was placed at the start of the moderately weathered grade (III), because it presents greater potential to weathering, loss of strength and durability, is subject to disaggregation and therefore more susceptible to produce fragments. This aspect was highlighted by relationships between weathering indexes (I_p , Id_4 and R_s), which proved to be a good procedure for weathering grade characterization and strength estimate. Moreover, Id_4 proved to be the best durability index to the relationship with UCS and R_s in the gneissic rock studied.

The assessment of the alterability parameter needs to be further investigated by the geological engineering community for a better understanding of its applicability and influences in tunneling in different kinds of rocks and weathering conditions. For now, when it comes to the gneissic rock of the Monte Seco tunnel, submitted to a tropical environment, the use of Id_2 and the respective parameter value, following the procedures in the RMR update (Celada et al. 2014), is not adequate to express strength and durability degradation noticed for this lithotype along the weathering grades (Figures 4.8 – 4.9). Moreover, it appears to be overvalued for granite and gneissic rocks.

For this reason, an equation has been proposed, which is based on the relationship between strength ratio and Id_4 assessed through the alterability parameter. The proposed equation contributes to a better distribution of values (10 – 0) than that obtained by following the procedures of Celada et al. (2014) (10 – 8) (Table 4.7) as to the gneissic rock under consideration, indeed improving the initial idea these authors had of using Id to indicate differences in RMR classes. In tropical climates, such as in the southern part of Brazil, the study of adaptations in geomechanical classifications is a topic of great importance and has been considered by several authors (Santos et al. 2012; Amaral Junior et al. 2016).

The procedure developed to characterize the intact rock heterogeneity and its influence on related parameters (UCS and alterability) could be tested in this tunnel as well as in other VMR tunnels in which problems of instability have been noticed and were excavated in different igneous and low- to high-grade metamorphic rock masses, that undoubtedly have different strength and durability behaviors according to the time of exposition to weathering. The use of the RMR 2014 update may be a significant

alternative to differentiate these tunnels, once two of five parameters can be related to the characteristics of intact rocks.

4.7 References

- Ahmad, M., Ansari, M.K., Singh, R., Sharma, L.K., Singh, T.N., 2017. Assessment of Durability and Weathering State of Some Igneous and Metamorphic Rocks Using Micropetrographic Index and Rock Durability Indicators: A Case Study. *Geotech. Geol. Eng.* 35, 827–842. doi:10.1007/s10706-016-0146-z
- Amaral Junior, A.F., Santos, Y.L.O.P., Chaves, S.S., Paredes, J.P., Zenóbio, A.A., 2016. Proposição de adequação da equação de correlação RMR-Q para o quadrilátero ferrífero., in: *Simpósio Brasileiro de Mecânica Das Rochas - Conferência Especializada ISRM-2016*. Belo Horizonte.
- Arel, E., Tugrul, A., 2001. Weathering and its relation to geomechanical properties of Cavusbasi granitic rocks in Northwestern Turkey. *Bull. Eng. Geol. Environ.* 60, 123–133. doi:10.1007/s100640000091
- ASTM D4644-16, 2016. Standard Test Method for Slake Durability of Shales and Other Similar Weak Rocks. ASTM Int. West Conshohocken, PA.
- Bieniawski, Z.T., 1989. Engineering rock mass classifications : a complete manual for engineers and geologists in mining, civil, and petroleum engineering. *Eng. rock mass Classif. a Complet. Man. Eng. Geol. mining, civil, Pet. Eng.*
- Borrelli, L., Perri, F., Critelli, S., Gullà, G., 2014. Characterization of granitoid and gneissic weathering profiles of the Mucone River basin (Calabria, southern Italy). *Catena* 113, 325–340. doi:10.1016/j.catena.2013.08.014
- BS 5930, 1999. Code of Practice for Site Investigations, British Standard. British Standards Institution, London.
- Cacciari, P.P., 2014. Estudo de um túnel em maciço rochoso fraturado por investigação geológico-geotécnica e análises pelo método dos elementos distintos Estudo de um túnel em maciço rochoso fraturado por investigação geológico-geotécnica e análises pelo método dos elementos d. Universidade de São Paulo.

- Cacciari, P.P., Futai, M.M., 2017. Modeling a Shallow Rock Tunnel Using Terrestrial Laser Scanning and Discrete Fracture Networks. *Rock Mech. Rock Eng.* 50, 1217–1242. doi:10.1007/s00603-017-1166-6
- Cacciari, P.P., Pereira, R.V.B., Monticeli, J.P., Suzuki, S., Ribeiro, F.S., Futai, M.M., 2013. Análise comparativa entre inspeções de “bate choco” e formação de blocos chave controlados por descontinuidades, in: 14° Congresso Brasileiro de Geologia de Engenharia E Ambiental. ABGE, Rio de Janeiro, pp. 1–10.
- Celada, B., Tardáguila, I., Varona, P., Bieniawski, Z.T., 2014. Innovating Tunnel Design by an Improved Experience-based RMR System, in: *World Tunnel Congress 2014 – Tunnels for a Better Life*. Foz do Iguaçu, pp. 1–9.
- Ceryan, S., Tudes, S., Ceryan, N., 2008. Influence of weathering on the engineering properties of Harsit granitic rocks (NE Turkey). *Bull. Eng. Geol. Environ.* 67, 97–104. doi:10.1007/s10064-007-0115-0
- Delvigne, J.E., 1998. *Atlas of Micromorphology of Mineral Alteration and Weathering*, The Canadian Mineralogist. Ontario, Canada.
- Dhakal, G., Yoneda, T., Kato, M., Kaneko, K., 2002. Slake durability and mineralogical properties of some pyroclastic and sedimentary rocks. *Eng. Geol.* 65, 31–45. doi:10.1016/S0013-7952(01)00101-6
- Franklin, J.A., Chandra, R., 1972. The slake-durability test. *Int. J. Rock Mech. Min. Sci.* 9, 325–328. doi:10.1016/0148-9062(72)90001-0
- Gamble, J., 1971. *Durability-Plasticity Classification of Shales and Other Argillaceous Rocks*. PhD Dissertation, University of Illinois.
- Gupta, A.S., Rao, K.S., 2001. Weathering indices and their applicability for crystalline rocks. *Bull. Eng. Geol. Environ.* 60, 201–221. doi:10.1007/s100640100113
- Gupta, A.S., Rao, K.S., 2000. Weathering effects on the strength and deformational behaviour of crystalline rocks under uniaxial compression state. *Eng. Geol.* 56, 257–274. doi:10.1016/S0013-7952(99)00090-3

- Gupta, V., Ahmed, I., 2007. The effect of pH of water and mineralogical properties on the slake durability (degradability) of different rocks from the Lesser Himalaya, India. *Eng. Geol.* 95, 79–87. doi:10.1016/j.enggeo.2007.09.004
- Hoek, E., Brown, E., 1997. Practical estimates of rock mass strength. *Int. J. Rock Mech. Min. Sci.* 34, 1165–1186. doi:10.1016/S1365-1609(97)80069-X
- Irfan, T.Y., Dearman, W.R., 1978. The engineering petrography of a weathered granite in Cornwall, England. *Q. J. Eng. Geol. Hydrogeol.* 11, 233–244. doi:10.1144/GSL.QJEG.1978.011.03.03
- ISRM, 2015. *The ISRM Suggested Methods for Rock Characterization, Testing and Monitoring: 2007-2014*. Springer International Publishing, Cham. doi:10.1007/978-3-319-07713-0
- ISRM, 1979a. Suggested Method for Determination of Water Content, Porosity, Density, Absorption and Related Properties and Swelling, Slake Durability Index Properties. *Int. J. Rock Mech. Min. Sci.* 16, 141–156.
- ISRM, 1979b. Suggested methods for determining the uniaxial compressive strength and deformability of rock materials. *Int. J. Rock Mech. Min. Sci. Geomech.* 16.
- Kahraman, S., Fener, M., Gunaydin, O., 2017. Estimating the uniaxial compressive strength of pyroclastic rocks from the slake durability index. *Bull. Eng. Geol. Environ.* 76, 1107–1115. doi:10.1007/s10064-016-0893-3
- Khanlari, G.R., Heidari, M., Momeni, A.A., 2012. Assessment of weathering processes effect on engineering properties of Alvand granitic rocks (west of Iran), based on weathering indices. *Environ. Earth Sci.* 67, 713–725. doi:10.1007/s12665-011-1518-6
- Le Pera, E., Critelli, S., Sorriso-Valvo, M., 2001. Weathering of gneiss in Calabria, southern Italy. *Catena* 42, 1–15. doi:10.1016/S0341-8162(00)00117-X
- Marques, E.A.G., Barroso, E. V., Menezes Filho, A.P., Vargas, E. do A., 2010. Weathering zones on metamorphic rocks from Rio de Janeiro-Physical, mineralogical and geomechanical characterization. *Eng. Geol.* 111, 1–18. doi:10.1016/j.enggeo.2009.11.001

- Momeni, A., Hashemi, S.S., Khanlari, G.R., Heidari, M., 2017. The effect of weathering on durability and deformability properties of granitoid rocks. *Bull. Eng. Geol. Environ.* 1–13. doi:10.1007/s10064-016-0999-7
- Monticeli, J.P., Cantarella, V.P., Cacciari, P.P., Futai, M.M., 2015. Roughness characterization of discontinuity sets by profilometer scanner images, in: XV Pan American Conference on Soil Mechanics and Geotechnical Engineering. SAIG, Buenos Aires, pp. 85–92.
- Monticeli, J.P., Sígolo, J.B., Futai, M.M., 2016. O uso da Análise Petrográfica e Micromorfológica na Determinação dos Graus de Alteração de um Maciço Rochoso Gnáissico, in: VII Simposio Brasileiro de Mecânica Das Rochas (SBMR). p. 8.
- Moradzadeh, M., Cheshomi, A., Ghafoori, M., TrighAzali, S., 2016. Correlation of equivalent quartz content, Slake durability index and Is50 with Cerchar abrasiveness index for different types of rock. *Int. J. Rock Mech. Min. Sci.* 86, 42–47. doi:10.1016/j.ijrmms.2016.04.003
- Sajid, M., Coggan, J., Arif, M., Andersen, J., Rollinson, G., 2016. Petrographic features as an effective indicator for the variation in strength of granites. *Eng. Geol.* 202, 44–54. doi:10.1016/j.enggeo.2016.01.001
- Santos, Y.L.O.P., Chaves, S.S., Paredes, J.P., Zenobio, A.A., 2012. Proposta de índice de ajuste (Aw) utilizando o grau de intemperismo no sistema RMR (Rock Mass Rating) de classificação do maciço rochoso., in: Congresso Brasileiro de Mina a Céu Aberto E Mina Subterrânea. Belo Horizonte.
- Vieira, V.S., Silva, M.A., Corrêa, T.R., Lopes, M.H.B., 2014. Mapa Geológico do Espírito Santo - Escala 1:400.000., in: Simpósio Brasileiro de Exploração Mineral, Ouro Preto.

5. TEXTURAL AND MICROMORPHOLOGICAL CHARACTERIZATION OF TROPICAL WEATHERING EFFECTS ON CORDIERITE IN GNEISSIC ROCK³

Abstract

This paper evaluates the tropical weathering of cordierite in the gneissic rock mass surrounding the Monte Seco Tunnel, an in-situ laboratory. This tunnel was excavated in the 1950s and, except for the entrance and exit, does not include the use of either only concrete liners or both liners and bolts. The weathering, rock matrix deterioration and arenization, promoted the edge effect of biotite alteromorphs due to its meso-alteromorphic texture. The microsystem of the foliation formed by the biotite and cordierite alteromorphs produced secondary minerals, such as chlorite and smectite, that contributed to the fissuring and weathering. The cordierite distributed in the rock mass (intact rock), concentrated along the foliation, was destroyed by pinitization, chloritization and replaced by pinitite, chlorite, sericite, smectite, kaolinite and goethite along cleavage planes, intramineral fissures and the alteromorph rims. The corresponding weathering pattern is characterized by the generation of secondary crystalline products that interfere in the intramineral fissuring of the adjacent minerals that form the rock microsystem, leading to a textural change characterized as meso- and halo-alteromorphic. These weathered minerals contribute to the generation of a secondary fissural porosity, and the resulting textural change reflects the fragility mechanism of the crystalline fabric or the lepidogranoblastic texture. The tropical environment intensifies the effects of this type of fragility because wetting and drying cycles allow the secondary materials that fill the fissures to leach or expand and contract, further loosening the bonds between the minerals and compromising cohesion. When the minerals present in the foliation, such as biotite and cordierite, undergo weathering, they promote fissuring of the crystalline fabric and the subsequent loosening of mineral bonds.

Keywords: gneissic alteromorphs, cordierite, weathering, texture, petrographic indexes.

³ Authors: Monticelli J. P., Sígolo J.B., Futai M. M.

5.1 Introduction

The complex behavior of a rock mass is strongly influenced by geological structures such as joints, faults, and foliations and by weathering stages. This paper elucidates the weathering and degradation stages of gneissic rock in an old tunnel associated with block instability.

The Monte Seco Tunnel is the in-situ laboratory and is located close to Vitória, the capital city of the state of Espírito Santo, Brazil, and is a segment of the Vitória–Minas Railway (EFVM, *Estrada de Ferro Vitória–Minas*). As the majority of the tunnels constructed along this railway in the 1950s, it was excavated in gneissic rock, and except for the entrance and exit, does not include the use of either only concrete liners or both liners and bolts. Due to the long-term exposure of the rock to weathering, the initial mechanical characteristics of these EFVM tunnels have been degraded, resulting in rock falls from the ceiling and walls. EFVM is responsible for the transport of iron ore from the Iron Quadrangle (*Quadrilátero Ferrífero*) in the state of Minas Gerais: its full operation is important because any delay in ore supply can cause logistical losses.

The detailed assessment of the present geological-geotechnical conditions of the Monte Seco Tunnel and of the other tunnels along this railway, to determine the risks associated with rock instability, constitutes a fundamental part of several studies from the GeoInfraUSP (*University of Sao Paulo*) research group (Cantarelli et al., 2016, Cacciari and Futai, 2016, 2017, 2018). Among the parameters being investigated, the weathering grades of a rock mass (intact rock and discontinuity-bearing rock) have been characterized based on petrographic analyses and destructive and nondestructive tests, such as the sclerometer test, the slake durability test, and the uniaxial compression test.

Regarding petrographic analyses aiming at the definition of petrographic weathering indexes at the microscale (Lumb 1962, Mendes et al. 1966, Onodera et al. 1974, Irfan and Dearman 1978, Cole and Sandy 1980, Gupta and Rao 2000, Arel and Tugrul 2001, Gupta and Rao 2001, Ceryan et al. 2008), we observe that mineral textures and micromorphology are seldom correlated with patterns and evolutionary stages of weathering. For a certain weathering grade, the variation in strength of a rock is basically related to its texture (Sajid et al. 2016). However, when texture is described by petrographic indexes, such as the textural coefficient (TC), these indexes are neither

sensitive to the mineralogical transformations related to weathering nor correlate well with the geotechnical properties (Azzoni et al. 1996, Gupta and Rao 2001). Notably, mineral composition and textural properties, such as fissures and voids, are the most important factors in the determination of the strength of a rock (Gupta and Rao 2000).

Therefore, to understand the physical-mechanical degradation of a rock, it is fundamental to describe the weathering processes and the textural modifications in a standard way. The classification presented by Delvigne (1998) is an alternative to the analysis of the textural modifications of the crystalline fabric of a rock that underwent weathering and can improve the interpretations of the petrographic weathering indexes and their relationship with the physical-mechanical behavior of the rock.

Delvigne (1998) proposed a classification of weathering patterns for individual minerals of a rock based on their micromorphological and textural description. The weathered minerals are called alteromorphs and can be dealt with either individually or in groups constituting three main types of microsystems: (i) Contact: contacts between unweathered minerals. (ii) Plasmic: minerals undergoing weathering. (iii) Fissures: intra-, inter- and transmineral fissures. The identification of the microsystem, extent of the weathering and proportions of the primary and secondary minerals and pores and fissures, as well as the way that the weathering affects the minerals, are the basis of the classification system. According to the extent of the preservation, size and shape of the primary minerals that underwent weathering, three weathering texture types can be distinguished: iso-alteromorph, meso-alteromorph and kata-alteromorph (Figure 5.1). Depending on the intrinsic properties of a mineral, such as its cleavage, twinning, structural integrity, and grain size, weathering takes place in a specific way, which determines the mineral weathering pattern and evolutionary stages (0, unweathered, to 4, completely weathered), as presented in more detail in Delvigne (1998).

The objective of this study is the textural and micromorphological characterization of weathered minerals from a gneissic rock from the Monte Seco Tunnel, which has experienced tropical climate conditions, and the roles of texture and micromorphology in rock degradation along the weathering grades. Petrographic analyses and X-ray diffraction tests were conducted to characterize the primary and secondary products along the weathering grades. The gneissic rock-forming minerals were characterized according to the textural classification presented in Delvigne (1998). However, we do not address

cordierite alteromorphs, which are one of the main constituents of the gneissic rock where the tunnel was excavated, and consequently its micromorphological modifications with weathering. Moreover, the description of cordierite in the literature is usually limited to its mineralogical and crystallographic properties (Prider 1945, Vogel 1975, Klein 2007, Nesse 2012). In this sense, cordierite alteromorph characterization according to textural and micromorphological classification and by means of petrographic intramineral weathering indexes that are proposed here, namely, extent of weathering (E_a) and intramineral fissures (I_f), is pioneering work in the study of cordierite.

In contrast to the orthoclase, plagioclase, hypersthene and garnet alteromorphs that showed textural modifications in the petrographic analyses, the cordierite and biotite alteromorphs showed an edge effect, producing intra- to transmineral fissures in the adjacent minerals and increasing the bond loss of the foliation plane, consequently causing instability of the rock blocks in tropical conditions. It is expected that this study can aid in the textural and micromorphological classification of minerals undergoing weathering in general, as well as in the study of the modifications of the gneissic crystalline fabric caused by such a process in engineering geology applications.

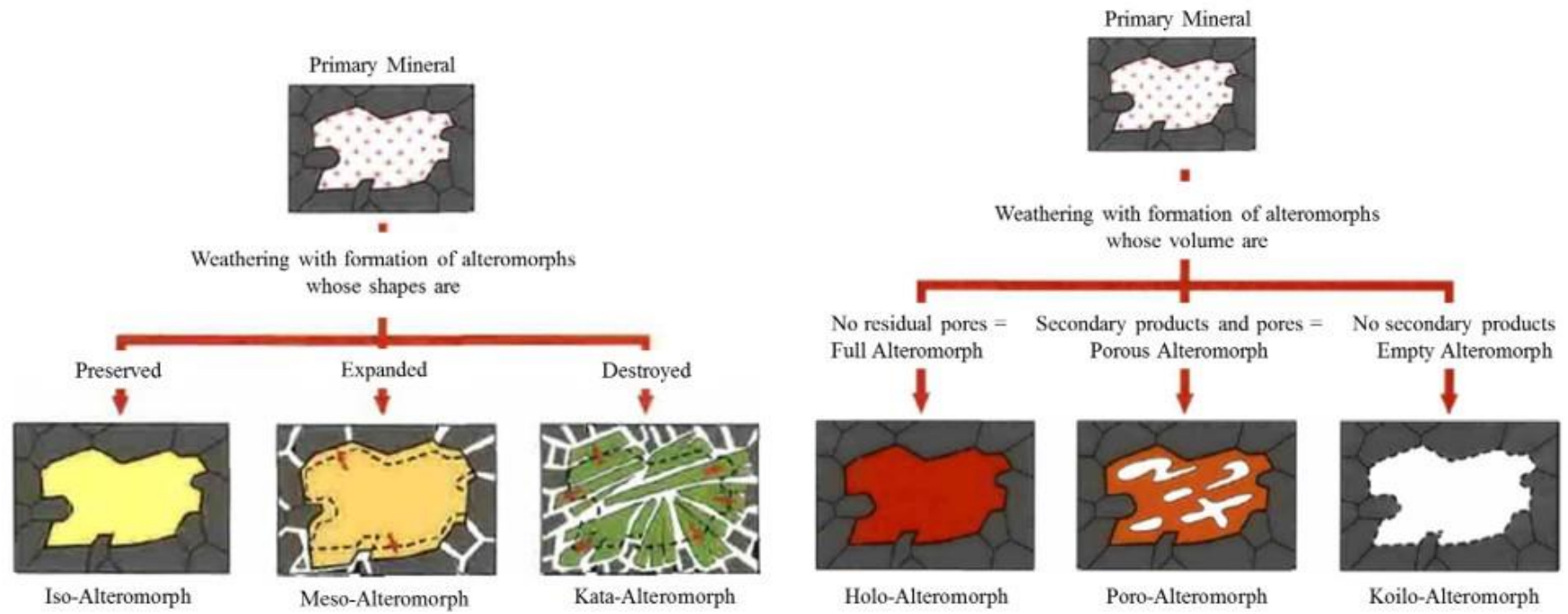


Figure 5.1 - Micromorphological and textural description of weathered minerals based on the shape and volume of the alteromorphs (Modified from Delvigne 1998).

5.2 Geological and weathering conditions

The geological setting of the region where the Monte Seco Tunnel was excavated is the Nova Venécia Complex, located in the Paraíba do Sul Domain of the Araçuaí Orogenic Belt of Mantiqueira Province. The rock analyzed in this study is a migmatitic sillimanite-garnet-cordierite-biotite gneiss (Baltazar et al. 2010), herein referred to as gneiss.

Climatic conditions control the intensity of weathering mechanisms such as disaggregation and decomposition of the rock, which are basically influenced by temperature and rainfall. In the study area, the rainfall varies from 100 to 120 cm in the summer and from 50 to 20 cm in the winter, and the temperature varies from 28 to 26 °C in the summer and 22 to 20 °C in the winter. According to Dearman et al. (1978), the climate is tropical with clear contrasts between the dry and rainy seasons, characterizing a physical-chemical weathering of moderate intensity, varying from strong to very weak.

The geological and environmental conditions led to the modeling of a relief composed of hills and slopes with pronounced declivity: the outcropping rock has a sugarloaf shape. Underground investigations via geoelectrical profiles and rotatory drillings were conducted and used to determine the geological profile. The local weathering profile was created by a continuous geomorphologic evolution and therefore is compared to the slope weathering profile of Deere and Patton (1971); the profile is constituted by three weathering horizons (Figure 5.2): I – transported Soil, II – very to moderately weathered rock mass, and III – weakly weathered rock mass. Horizon I contains soil and rock blocks of various sizes, which are in part very weathered.

Abrupt or weakly evolved contacts between the weathering horizons are common in slopes developed in gneissic regions, especially in Southeastern Brazil, where the study area is located (Barroso et al. 1996, Pimentel and Barroso 1996, Marques et al. 2010).

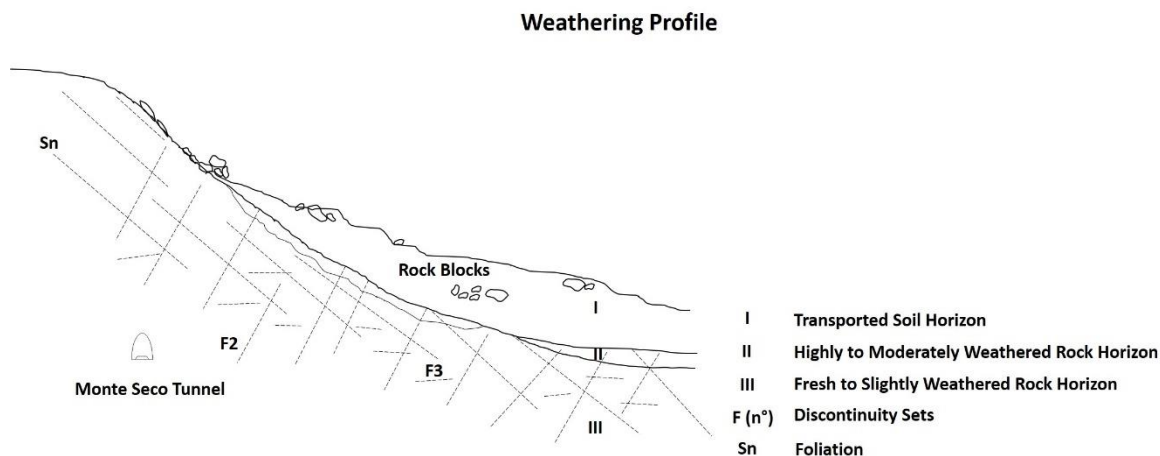


Figure 5.2 - Weathering profile adopted to study the Monte Seco Tunnel rock mass

5.2 Materials and methods

The gneissic rock samples were carefully collected from drilling cores and outcropping rock blocks in the vicinity of the Monte Seco Tunnel to represent all three weathering horizons (Figure 5.2). The weathering grades of the samples were characterized by visual and tactile procedures according to the descriptions presented in Table 5.1.

Due to their fragility, samples representing grades W2 and W3 were impregnated with an epoxy resin inside a vacuum heater; then, thin sections were carefully prepared from those samples at the Geoscience Institute of São Paulo University (IGc-USP). This procedure helped maintain the sample in a more compact form, preserving textural and micromorphological features that could be disturbed during preparation of the sections. The petrographic analyses were conducted with the Leica Zeiss Axioplan optical microscope of the Laboratory of Sedimentology of the IGc. The images were captured using the Leica Application Suite (LAS) V4.7 software. Duplicate samples were submitted to for X-ray diffraction testing to characterize the weathering products not usually identifiable in petrographic analyses. These two sets of tests were conducted separately at the IGc and the Engineering School of the University of São Paulo (EPUSP) laboratories. The weathering grade characterization and the additional work carried out on the thin sections are described in Table 5.2.

The initial procedure was to characterize the dominant weathering processes acting to transform the primary mineralogy into secondary minerals and the type of secondary

mineralogy produced. The information obtained helped in the identification, characterization and classification of the microsystems, the mineral weathering pattern and the textural and micromorphological aspects of the weathered minerals. The gneissic rock-forming minerals and their alteromorphs were described in terms of the weathering grades according to Delvigne (1998). Additionally, the cordierite alteromorphs were characterized by intramineral weathering petrographic indexes, the extent of weathering index (E_a) and the intramineral microfissure index (I_f), which were used to quantify the disaggregation and decomposition processes. The methodology applied in this study and the literature consulted to characterize the weathering process are summarized in the flowchart shown in Figure 5.3.

In the additional step, the cordierite alteromorphs were first identified and compared to the weathering stages of the Delvigne (1998) classification. Approximately sixty alteromorphs were sampled for the analyses. The E_a index of an alteromorph, expressed as a percentage, is the relationship between the area occupied by the secondary products and the total area of the original cordierite. The I_f index, expressed in fissures per millimeter (f/mm), is the number of fissures of any type (intra- to transmineral), counted on a scanline drawn inside the alteromorph. The scanline was drawn perpendicular to the most pronounced orientation of the observed fissures. The measurement and treatment of data were performed using ImageJ software. The image treatment consisted of transforming the photomicrograph (taken with crossed nicols) and extracting the background using the software tool *extract background*. By applying this tool, the fissures and the relief of the unweathered mineral are enhanced, whereas the weathered portion is not. This additional step is described in detail in the flowchart shown in Figure 5.4.

Table 5.1 - Intact rock weathering grades (Modified after Hoek and Brown, 1997; BS 5930, 1999, ISRM, 2015)

Grades	Visual Tactile Features	UCS by simple means (MPa)
W1 (I - II)	<p>Fresh to incipient weathered. Macroscopically there is no evidence of weathering of minerals. Minerals have luster. Slabs with difficulty at various hammer blows, resisting the cut of the steel knife and the finger pressure.</p>	<p>100 - 200 (> 200)</p>
W2 (III)	<p>Shows signs of mineral weathering. Minerals show lack glare and noticeable discoloration, sometimes occurs with a film of yellow material (iron oxides and hydroxides). Breaking with some difficulty from hammer blow. Steel knife scratches the surface and removes crystals, resisting finger and nail pressure.</p>	<p>50 - 100</p>
W3 (IV/V)	<p>Rock and minerals significantly weathered, being found friable. Minerals lacking luster and are strongly discolored; iron oxides and hydroxides impregnate the sample. Breaks easily with a hammer blow*. Minerals are removed by finger and nail pressure; steel knife easily causes grooves in the sample**.</p>	<p>12.5 - 50 (*) 1.25 - 12.5 (**)</p>

W1 - fresh to slightly weathered, W2 - moderately weathered and W3 - highly to completely weathered. Images sizes 54.5 mm

Table 5.2 - Weathering grade characterization and additional thin section work.

N°	Weathering Profile	Weathering Grades	Epoxy resin impregnation	X-ray diffraction test
1	III	W1		
2	III	W1		
3	II	W2	x	x
4	I	W2	x	x
5	I	W3	x	x
6	III	W1		
7	III	W1		
8	II	W2	x	x
9	II	W3	x	x
10	I	W3	x	x
11	III	W2		
12	II	W2		
13	II	W3	x	x
14	I	W3	x	x
15	I	W3	x	x

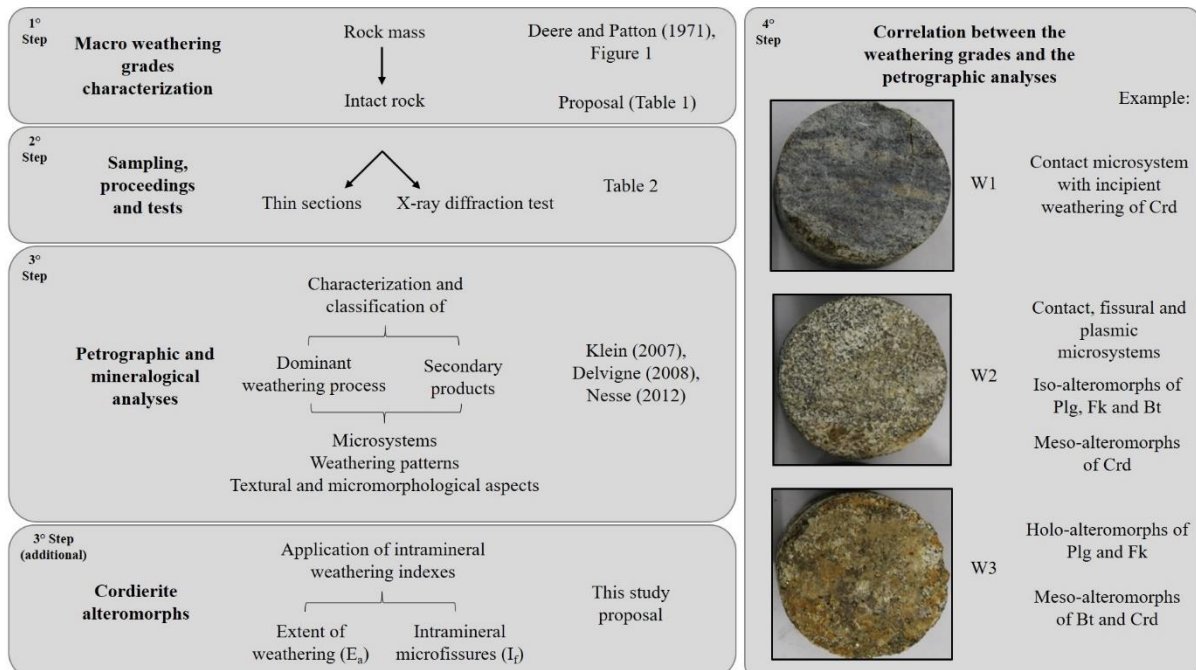


Figure 5.3 - Flowchart of the methodology.

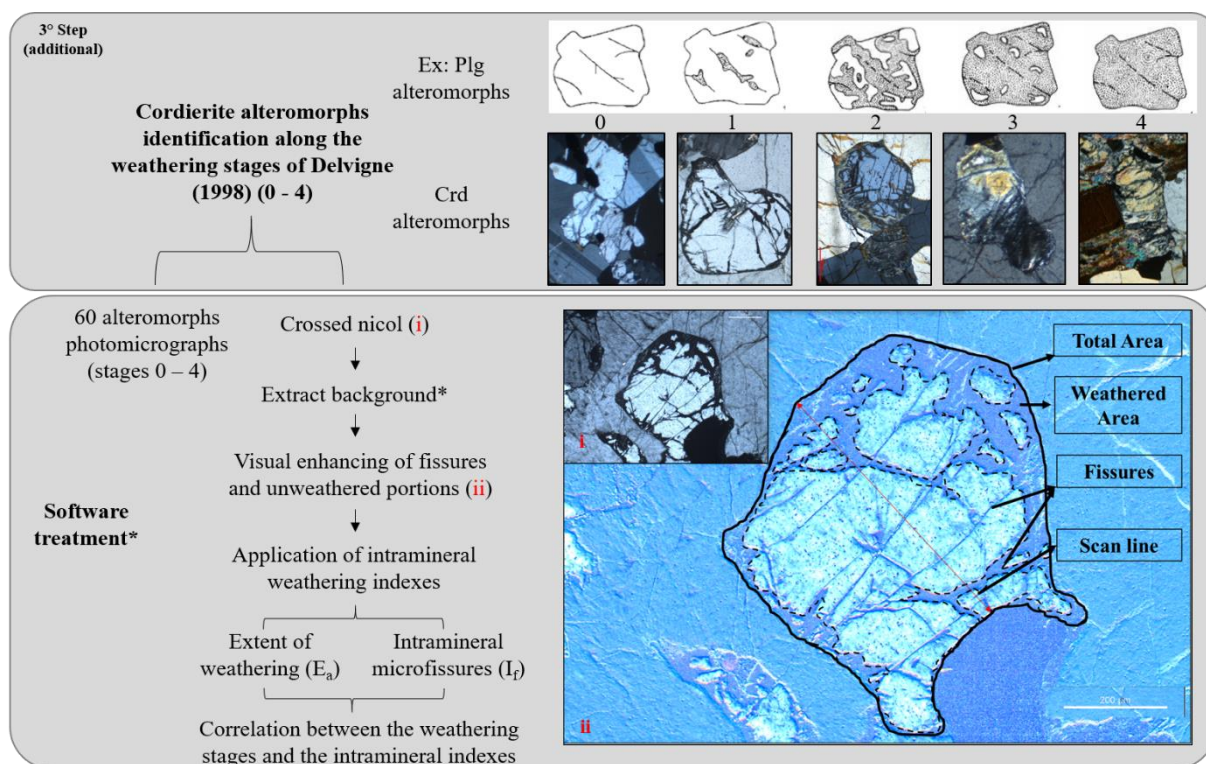


Figure 5.4 - Flowchart of the methodology of the additional step: cordierite alteromorph characterization.

5.4 Results

The results for the gneissic rock characterization will be presented considering the cordierite alteromorphs, which are described in detail below.

5.4.1 Gneissic textural and micromorphological characterization

The gneissic rock is composed of quartz (Qz), orthoclase (Fk), plagioclase (Pl), cordierite (Cr), biotite (Bt), hypersthene (Hp) and garnet (Gr). Sillimanite and other minerals, including opaque minerals, are subordinate. Figure 5.5 shows the most representative photomicrographs for the textural and micromorphological characterization and classification developed for the mineralogical assemblage of the gneissic rock. Figure 5.6 shows an example of the X-ray diffraction test result (sample n°5) used to identify the final weathering product. The dominant weathering processes acting to transform the primary minerals to secondary minerals are

presented in Figure 5.7. The classification of the microsystems, weathering patterns and textural modifications of the alteromorphs are organized schematically in Figure 5.8.

The quartz, resistant to decomposition, suffers preferential disaggregation processes due to the occurrence of intra- to transmineral fissures in the microsystems formed with the biotite and the cordierite alteromorphs (Figures 5.5 G and 5.7).

The feldspars (orthoclase and plagioclase - andesine), felsic minerals, undergo a partial hydrolysis process with various intermediate minerals throughout their weathering stages, 0 to 3 and 0 to 4, respectively. The mineralogical transformation of these alteromorphs is triggered by sericitization with the formation of sericite (illite), kaolinite and gibbsite.

The weathering in the orthoclase begins from the edges and cleavages, following a regular pattern, whereas in the plagioclase, it starts from the irregular intramineral fissures, following an irregular pattern, speckled and patchy. These alteromorphs present secondary products with low crystallinity and cavernous residues, with primary mineral nuclei fissuring. These minerals present a textural modification characterized by iso-alteromorphs and halo-alteromorphs and contribute to an intramineral secondary porosity, which is linked to the secondary mineral porosity, and fissural porosity, related to the opening of cleavage planes in the orthoclase (Figures 5.5 B - C, 5.7 and 5.8).

Cordierite and biotite, intermediate mafic minerals, also undergo a partial hydrolysis process, producing various intermediate minerals throughout their weathering stages, 0 to 4 and 0 to 3, respectively. The mineralogical transformation is triggered by pinitization followed by chloritization in the cordierite and chloritization in the biotite, with the formation of pinite, chlorite, sericite (illite), smectite, kaolinite, gibbsite and goethite. The weathering in the cordierite starts from the borders and intramineral fissures in a regular banded pelicular pattern.

The weathering in the biotite starts from the cleavages, opening them in a regular linear parallel pattern. These alteromorphs present secondary products, such as chlorite and smectite, that influence the intramineral fissuring process of these alteromorphs as well as of the adjacent minerals, forming the microsystems of the gneissic rock matrix. Through weathering stages 1 to 2, due to crystallization of these secondary products, the modification of the volume of the cordierite and biotite alteromorphs is noticeable in at least one crystallographic direction. These minerals present a textural modification characterized by meso-alteromorphs and halo-alteromorphs and contribute to a secondary intramineral porosity, linked to the secondary

products formed, and fissural porosity, clearly related to the development of fissures and the coalescence of intra- and intermineral fissures, forming transmineral fissures (Figures 5.5 F-G, 5.5 D-E, 5.7 and 5.8).

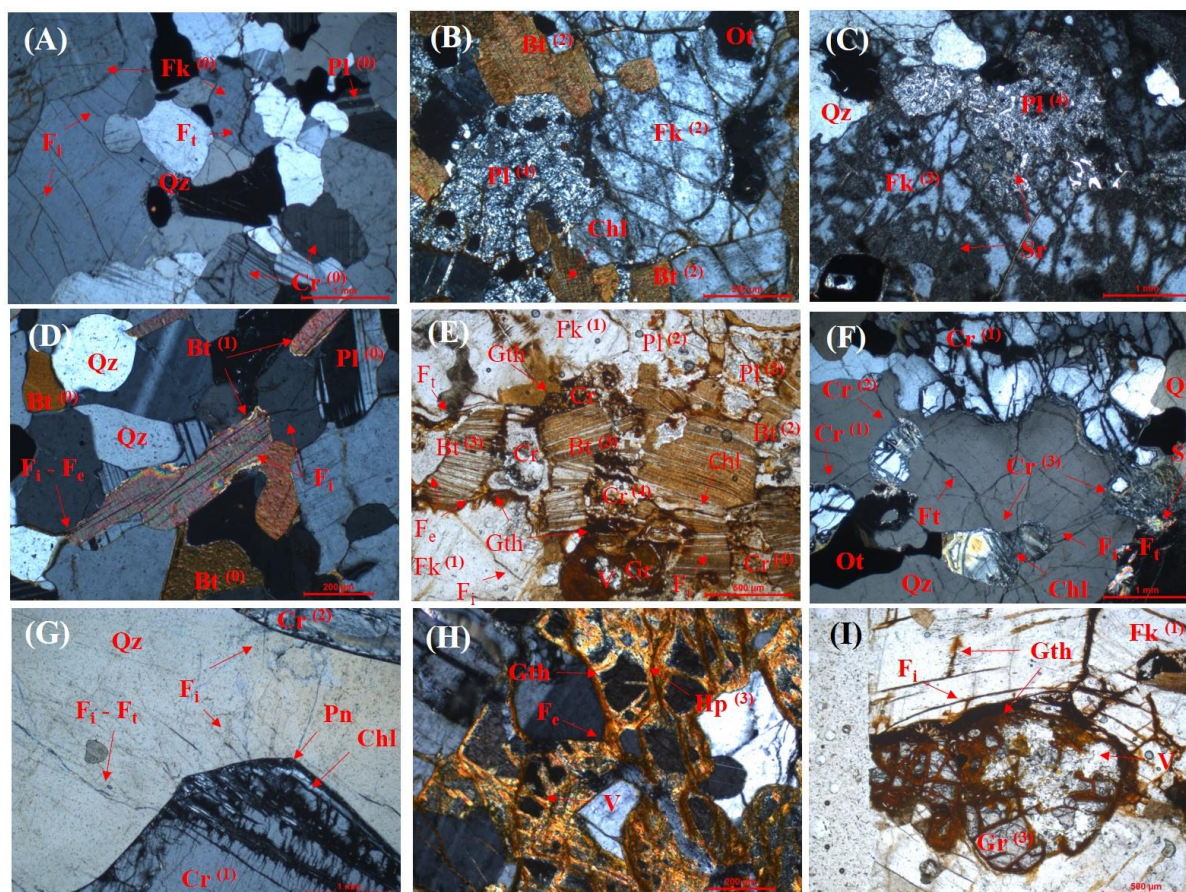


Figure 5.5 - Photomicrographs of the mineral weathering stages and weathering process in fissured quartz (Qz), orthoclase (Fk) and plagioclase (Pl) (A – C). Biotite (Bt) undergoing incipient weathering, producing goethite (Gth) along some cleavages (D) and interlayered chlorite (Chl) and probably smectite in an advanced weathering stage (E). Cordierite (Cr) undergoing weathering, producing pinite (Pn) and chlorite with an incipient wedge effect (G) in an advanced weathering condition or producing interlayered pinite, chlorite and probably smectite, with sericite (Sr) with an extreme wedge effect (F). Hypersthene (Hp) (H) and garnet (Gr) (I) producing high quantities of goethite. In the images, (D – G) depict the fissuring process due to the textural modification of the biotite and cordierite alteromorphs. The voids are represented by the letter V, while the mineral weathering stages (0 – 4) are denoted inside the brackets.

Hypersthene and garnet, mafic minerals with a small amount of silicon in their composition, tend to undergo a very intense alteration process of total hydrolysis plus oxidation despite their completely different alterabilities. Hypersthene weathers up to stage 4 in slightly

to moderately weathered samples, whereas the garnet weathers to stage 3 in completely weathered samples. The weathering of these minerals generates large amounts of goethite; in particular, weathering of the garnet generates abundant gibbsite.

The weathering in the hypersthene starts from the edges and cleavages in a regular, pelicular to linear pattern. The weathering in the garnet starts from the borders and intramineral fissures in an irregular, crossed and linear pattern. These alteromorphs present residual primary mineral nuclei that are fissured and in contact with intramineral voids in a skeleton formed by goethite. These minerals present a textural modification characterized by iso-alteromorphs and poro-alteromorphs, specifically septo-poro-alteromorphs, and contribute to secondary porosity related to intramineral pores and fissures (Figures 5.5 H-I, 5.7 and 5.8).

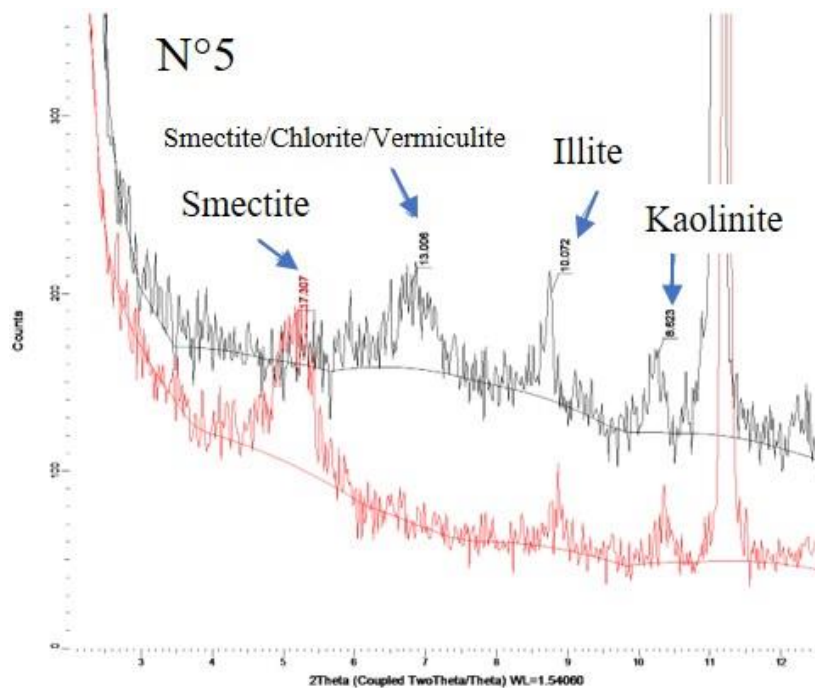


Figure 5.6 - Illustration of a X-ray diffraction test showing some of the final weathering products, in this case, smectite, illite and kaolinite.

The mafic minerals, when weathered, release Fe^{2+} ions, which, due to their low mobility, soon oxidize and precipitate in the form of goethite, iron oxide and hydroxide, usually filling and cementing the intra-, inter- and transmineral fissures, generally increasing the iron content in the rock matrix. This aspect can also characterize the texture of the echino-alteromorphs

microsystems in the rock matrix, helping to describe the mineral boundaries and the evolution of the fissure microsystem in accordance with each mineral weathering stage (Figure 5.8).

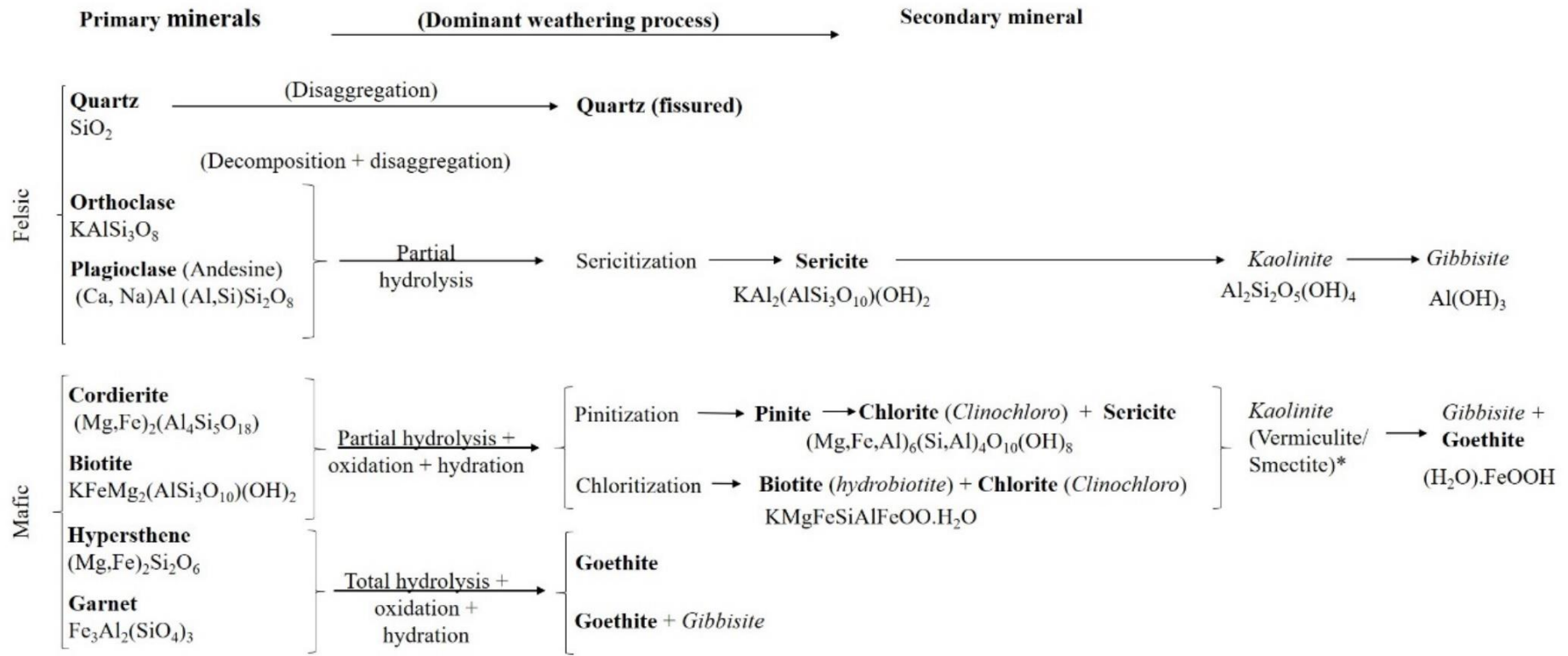


Figure 5.7 - Dominant weathering process affecting the gneissic rock minerals.

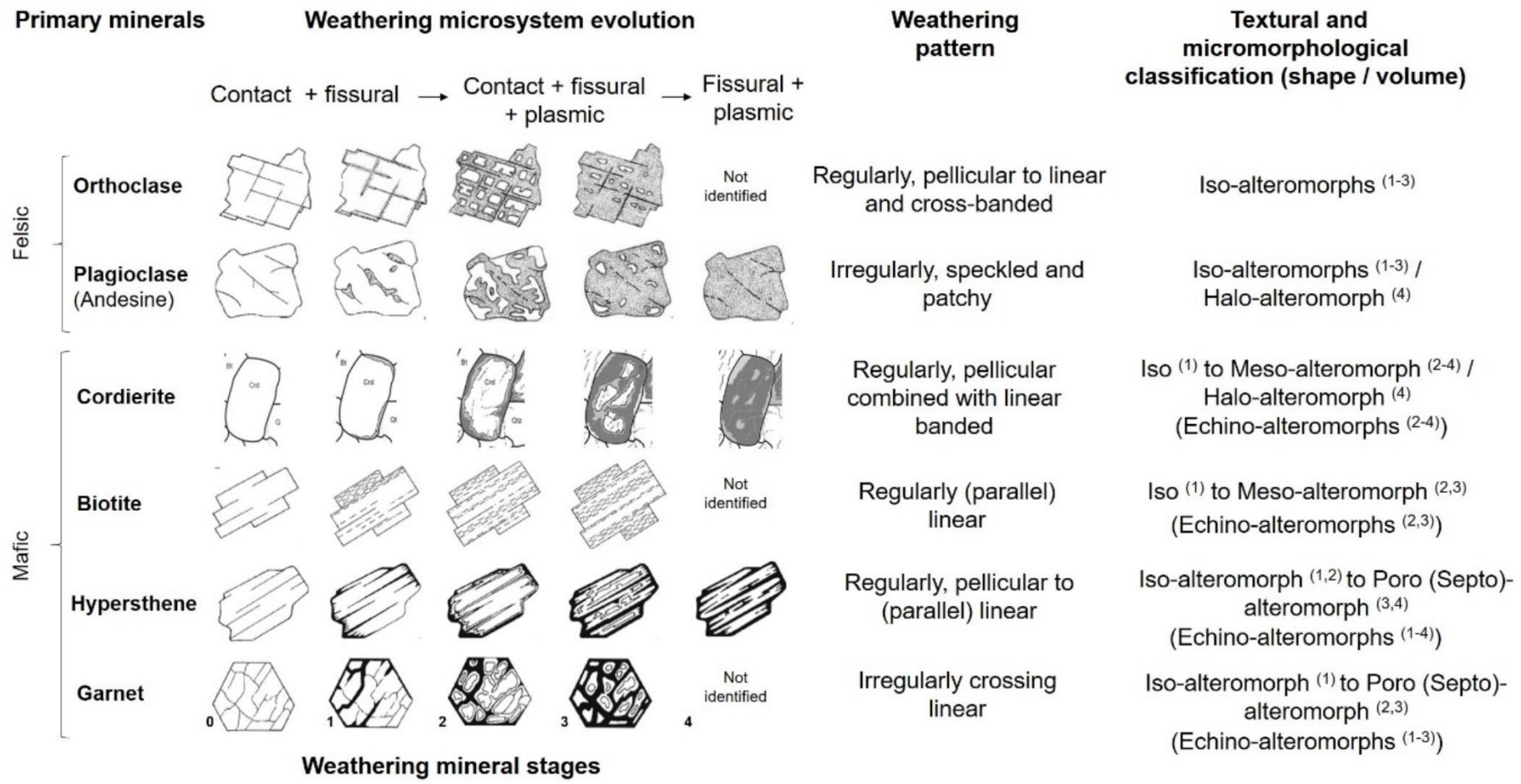


Figure 5.8 - Textural and micromorphological gneissic rock mineral classification.

5.4.2 Cordierite textural and micromorphological characterization

The most representative photomicrographs of the evolutionary stages of the cordierite alteromorphs and the respective values of E_a and I_f obtained for 60 minerals along their evolutionary stages are presented in Figure 5.9. The evolution of cordierite weathering is summarized in Table 5.3 in terms of its textural and micromorphological features, evolutionary stages, and petrographic index averages and intervals.

Cordierite is present in the contact microsystem formed by quartz, orthoclase, plagioclase, biotite and garnet and opaque minerals (Ot), overlain by another microsystem composed of intramineral fissures related to twinning planes in cordierite and transmineral fissures linked to the fracturing of the rock mass. This arrangement is considered the initial stage (stage 0) of the textural and micromorphological evolution of the cordierite located in the parental microsystem marked by lepido-granoblastic texture (Figure 5.9 – stage 0). The minerals identified in stage 0 contain 2.7 intramineral f/mm and are practically unweathered ($E_a = 0.82\%$), composing the gneiss parental microsystem. The microfissuring connects the weathering agents with the mineral, triggering pinitization in the alteromorph (Figure 5.9 and Table 5.3).

In stage 1 (Figure 5.9 – stage 1), alteroplasation (a type of pinitization) starts at the mineral rims and penetrates through fissures inward, consequently increasing the I_f and E_a values of the alteromorph. Alteroplasation is regular at the rims and along the fissures of the mineral, forming pinite, which is an isotropic material under polarized light. Twinning planes, when present, and intramineral to transmineral fissures are preferential areas for mineral weathering.

The weathering pattern is characteristically regular, pelicular combined with linear, the resultant alteroplasm or iso-alteromorph being formed by primary cordierite and pinite, with a well-defined geometry and shape. Pores were not observed in this microsystem. The 10 to 4 f/mm interval is determines the alteromorph textural evolution as well as the gradual increase in index E_a along the subsequent stages (Figure 5.9 and Table 5.3).

Table 5.3 - Evolutionary stages of the cordierite alteromorphs.

Stages	Microsystem	Weathering Pattern	Texture	Sketch	E _a (%)	I _f (f/mm)
0	Parental microsystem	-	Lepido-granoblastic (Gnaïsse)		0,8 (5 - 0)	2,7 (5,3 - 0)
1	Parental and fissural microsystem	Regular. Pelicular combined with linear.	Iso-Alteromorph.		14,2 (35 - 3)	7,2 (10 - 4)
2	Parental, fissural and plasmic microsystem	Regular. Pelicular combined with linear (parallel - banded).	Meso (Echino) - Alteromorph.		44,7 (54 - 35)	9,8 (12,4 - 7,4)
3	Parental, fissural and plasmic microsystem	Regular. Pelicular combined with linear (parallel - banded).	Meso (Echino) - Alteromorph.		80,8 (89 - 68)	> 10,0 (Minimum)
4	Parental, fissural and plasmic microsystem	Regular. Pelicular combined with linear (parallel - banded).	Meso-Alteromorph. Halo (Echino)-Alteromorph.		94,4 (100 - 86)	> 10,0 (Minimum)

Legend: light gray (pinite), dark gray (chlorite), pink (sericite) and yellow (goethite) and dotted lines (cracks).

In stage 2 (Figure 5.9 – stage 2), pinitization evolves and develops a kind of banding in the secondary minerals with the accumulation of iron oxides and hydroxides (possibly goethite) in the weathered minerals. In addition, the number of intramineral fissures in the alteromorph increases. Banding occurs with a fine pinite layer at the weathering front, accompanied by a crystallized portion of chlorite. Banding occurs both at the mineral rims and in the most expressive fissures. Pinitization evolves from the initial stages of cordierite weathering, forming chlorite, smectite and kaolinite. Sericite is a potassic mineral identified in the most weathered portions of the alteromorph, which are usually linked by transmineral fissures to the rock microsystem, where orthoclase and biotite are being decomposed.

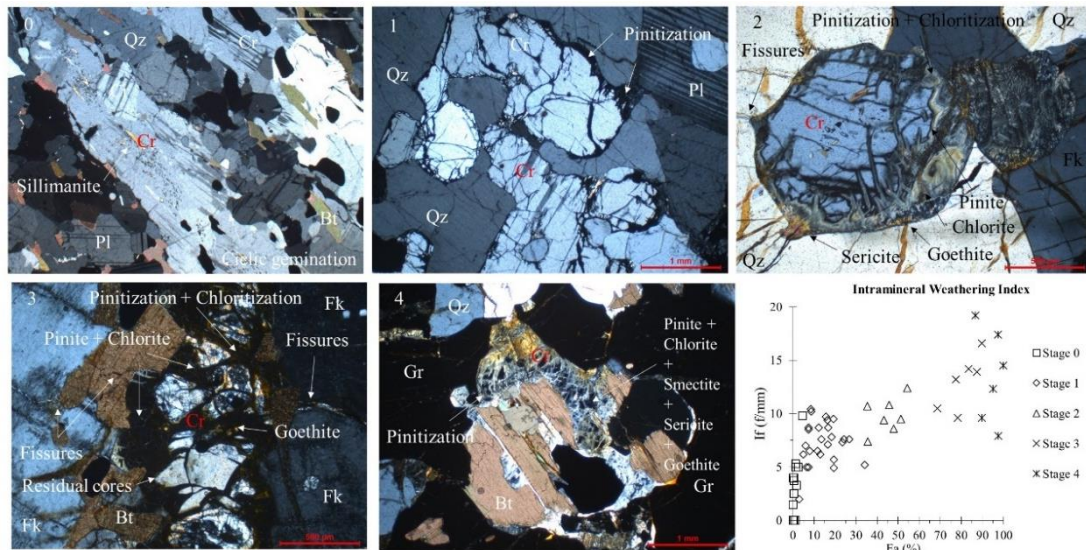


Figure 5.9 - Photomicrographs of the cordierite evolution stages (0, 1, 2, 3 and 4) with respect to the petrographic intramineral weathering indexes.

The intramineral fissures are oriented in two directions. The fissures in the most prominent orientation are filled with evolved minerals, such as chlorite and goethite; the secondary direction developed later, and the corresponding fissures may not be filled or filled only with pinite. The minerals in contact with the cordierite alteromorphs present intramineral fissures filled with secondary minerals that are oriented perpendicularly to the contact between these phases, roughly radially around the alteromorph. The analysis of the fissures indicates a change in size in one or more directions, which is corroborated by the secondary products, characterizing the meso-alteromorphic texture. When goethite forms past the cordierite rims and fills the fissures of adjacent minerals, the newly formed texture is echino(meso)-alteromorphic. However, in stage 2, the cordierite alteromorphs are found in a parental microsystem of superimposed fissural and plasmic microsystems. The I_f values present a subtle increase, while a gradual increase in E_a to values less than 50% are observed, i.e., a greater proportion of primary mineral (Figure 5.9 and Table 5.3).

In stage 3 (Figure 5.9 – stage 3), pinitization and chloritization are almost complete, isolating irregular, residual nuclei of the primary mineral inside the secondary plasma. Pinite and, specifically, chlorite are well crystallized, constituting the main secondary minerals of the alteromorph. Pinite is restricted to the weathering fronts and intramineral fissures, which propagate through primary mineral nuclei to the rims. Goethite mostly fills the fissures.

In stage 4 (Figure 5.9 – stage 4), pinitization and chloritization are complete in the alteromorph. Cordierite is completely weathered and is disaggregated, decomposed, and replaced by secondary products (pinite, chlorite, sericite, smectite and goethite). The primary mineral nuclei are now distinguished only by the differences in crystallinity among the constituting plasma. Mineral weathering makes both the visualization of the intramineral fissures and the quantification of I_f difficult. The alteromorph still preserves its original volume, despite being modified in shape. Under the microscope, no pores were identified in cordierite alteromorphs when they were completely replaced by secondary products, characterizing the final texture as holo-alteromorphic.

In stages 3 and 4, a great variation in the number of intramineral fissures, between 7.9 and 19.2 f/mm, is observed; these fissures superimpose those observed in stages 2 and 1. Nevertheless, a lower limit of approximately 10 f/mm can be established for textural evolution in these stages. In stages 3 and 4, the alteromorphs formed by secondary products are in a larger proportion than those from the primary mineral; the calculated E_a exceeded 68% and increases up to 100%, characterizing the holo-alteromorphic texture (Figure 5.9 and Table 5.3).

5.4.3 Petrographic aspects and weathering grade characterization

The main petrographic information regarding the textural and micromorphological modifications was gathered in Table 5.4 according to the weathering grades previously characterized. Table 5.4 also includes photomicrographs that illustrate the cordierite weathering evolution of the gneissic foliation microsystem.

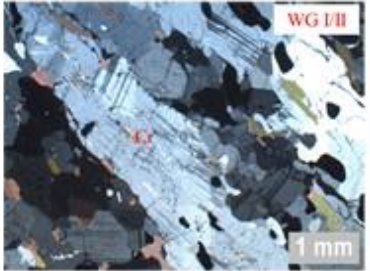

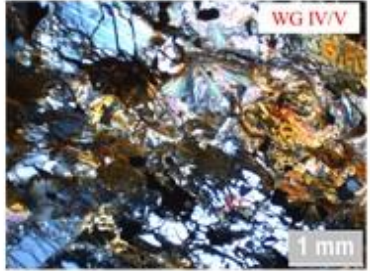
In the fresh to slightly weathering grades, W1, the gneissic rock matrix is formed by a lepido-granoblastic texture with incipient intramineral fissures, and the cordierite and plagioclase show incipient weathering. In the moderately weathering grade, W2, the weathering continues to the sericitization of the feldspars, orthoclase and plagioclase, and the pinitization and chloritization of cordierite and biotite alteromorphs.

The quartz appears to be fissured by formation of the secondary minerals produced by the cordierite and biotite alteromorph rims. The contact microsystem of the lepido-

granoblastic texture starts to be superimposed by fissural and plasmic microsystems. The cordierite alteromorphs begin to have a decisive impact because they increase intramineral fissuring, forming transminerals along the foliation plane. In the highly to completely weathering grade, W3, the rock matrix is completely modified due to weathering of the whole primary minerals in different development stages. Cordierite and plagioclase alteromorphs were found to be completely weathered to secondary minerals presenting meso(holo)- and holo-alteromorphic textures, while orthoclase and biotite alteromorphs showed partial development, showing iso- and meso-alteromorphic textures, respectively. The initial contact microsystem of the lepidogranoblastic texture is not easily recognized due to the superimposition of the fissural and plasmic microsystems, which now dominate the rock matrix.

Among the alteromorph textural modifications that occur with the progression of the mineral weathering stages, the main aspects controlling the degradation of the rock matrix are associated with the following stages: i) 3 and 4 for the orthoclase and plagioclase that are related to the isolation of nuclei of the fissured and cavernous primary minerals enveloped by secondary products (Figures 5.5 B-C and 5.8) that define weathering grade W3 (Table 5.4); ii) 2 to 4 for the cordierite and biotite that are related to the occurrence of fissures in the adjacent minerals and in the alteromorphs and to the textural modification classified as meso-alteromorphs (Figures 5.5 D-G and 5.8), which are observed in weathering grades W2 and W3, respectively (Table 5.4); and iii) 2 to 4 for the hypersthene and garnet that are related to the occurrence of intramineral pores, isolating cemented nuclei from the primary mineral via fissures (Figures 5.5 H-I and 5.8), considered due to the low mineral volumes of the petrographic analyses.

Table 5.4 - Petrographic aspects of the weathering grades.

Grades	Weathering process	Nature of rock matrix microsystems	Condition of alteromorphs stages	Textural classification	Rock matrix degradation
W1 (I - II)	Incipient pinitization of Cr; incipient sericitization of Pl	Contact with incipient intramineral fissures in Cr, Bt and Fk	Cr: 0 - 1; Pl: 0 - 1; Fk: 0; Bt: 0	Iso-altermorph (Cr, Pl)	
W2 (III)	Pinitization and chloritization of Cr; sericitization of Pl and Fk; chloritization of Bt. Quartz fissured.	Contact with the development of fissural and plasmic microsystems	Cr: 0 - 2; Pl: 0 - 1; Fk: 0 - 1; Bt: 0 - 1; Quartz fissured	Iso-altermorph (Cr, Pl, Fk, Bt); Meso-alteromorph (Cr); Echino-alteromorph (Cr)	
W3 (IV)	Complete weathering evolution of Cr and Pl to secondary products. Partial weathering stages development of Fk and Bt.	Dominant fissural and plasmic microsystems in the rock matrix	Cr: 1 - 4; Pl: 1 - 4; Fk: 1 - 3; Bt: 1 - 3; Quartz fissured	Iso-altermorph (Cr, Pl, Fk, Bt); Meso-alteromorph (Cr, Bt); Echino-alteromorph (Cr, Bt)	

Obs: Cordierite (Cr), plagioclase (Pl), orthoclase (Fk) and biotite (Bt).

5.5 Discussion and conclusion

The present research focused on a gneissic massif excavated for the construction of an unlined tunnel, which remained exposed to weathering for more than 50 years. The resulting block instability has affected the logistics of the iron ore railway transport. This research was based on mineral textural and micromorphological characterization and contributes to the understanding of the weathering and degradation stages that modified the mechanical properties of the gneissic rock.

The edge effect of the biotite alteromorphs that formed in the rock matrix deterioration and arenization processes, due to the meso-alteromorphic texture, were well documented in the literature to be one of the fabric modifications responsible for strength loss of gneissic rock, as observed in Le Pera et al. (2001) and Regmi et al. (2014), as well as for the granite rocks (Irfan and Dearman, 1978). However, the cordierite weathering behavior of some gneissic lithotypes seems to be relevant but still not fully considered properly. Marques et al. (2010) described weathering in Kinzigite, relating the oxidation and formation of iron oxides and hydroxides. In their work, the minerals pinitite, chlorite, sericite and smectite were not considered or described as secondary products, which are part of the mineralogy observed in the Nova Venécia gneissic rocks studied here.

In the foliation plane, under weathering of the gneissic rock studied, the microsystem formed of biotite and cordierite alteromorphs produced secondary minerals, such as chlorite and smectite, that contributed to the increase in fissuring, triggering weathering of the whole mineral; this weathering caused deep changes in the mineral bond, consequently decreasing the rock strength. The Monte Seco Tunnel was excavated in a gneissic rock mass that is in a tropical climate marked by wetting and drying cycles, which intensifies this type of weathering and rock matrix fragility, undoubtedly contributing to rock block instability problems.

Cordierite distributed in the rock mass (intact rock) and concentrated along the foliation planes is destroyed by pinitization, chloritization and replaced by pinitite, chlorite, sericite, smectite, kaolinite and goethite along cleavage planes, intramineral fissures and the alteromorph rims. The corresponding weathering pattern is characterized by the generation of secondary crystalline products that interfere in the intramineral fissuring of the adjacent minerals that form the rock microsystem, leading to a textural change

characterized by meso-alteromorphs and halo-alteromorphs.

The presence of the meso-alteromorphic texture in the cordierite and biotite characterize weathering grades W2 and W3, respectively. These weathered minerals contribute to the generation of a secondary fissural porosity, and the resulting textural change reflects the fragility mechanism of the crystalline fabric or the lepido-granoblastic texture. The tropical environment intensifies the effects of this type of fragility because wetting and drying cycles allow the secondary materials that fill the fissures to leach or expand and contract, further loosening the bonds between the minerals and compromising cohesion.

This analysis is fundamental to the understanding of the role played by the gneissic foliation in the instability of the blocks in a tunnel with no lining. Foliation is known to be a plane of minimal strength or traction, characterizing surfaces that favor the separation of blocks from the rock mass. When the minerals present in the foliation, such as biotite and cordierite, undergo weathering, they promote fissuring of the crystalline fabric and the subsequent loosening of the mineral bonds. Thus, biotite and cordierite textural modifications have a decisive influence on the loss of mechanical strength of wet rock, which deserves proper attention because of its relevance for determining the maintenance for and lifetime of the Monte Seco Tunnel.

5.6 References

- AREL E, TUGRUL A. 2001. Weathering and its relation to geomechanical properties of Cavusbasi granitic rocks in Northwestern Turkey. *Bull Eng Geol Environ* 60: 123–133.
- AZZONI A, BAILO F, RONDENA E, ZANINETTI A. 1996. Assessment of texture coefficient for different rock types and correlation with uniaxial compressive strength and rock weathering. *Rock Mech Rock Eng* 29: 39–46.

- BALTAZAR OF, ZUCCHETTI M, OLIVEIRA SAM, SCANDALARA J, SILVA LC. 2010. Report of São Gabriel da Palha and Lijnhares project, CPRM (Brazilian Geological Service). (in Portuguese)
- BARROSO EV, MARQUES EAG, CEZAR G, VARGAS EA. 1996. Caracterização física dos gnaisses intemperizados do município do Rio de Janeiro. In: 8º Congresso Brasileiro de Geologia de Engenharia, 1996. ABGE, Rio de Janeiro. (in Portuguese)
- BS 5930. 1999. Code of Practice for Site Investigations. British Standard. British Standards Institution, London.
- CACCIARI, P.P., FUTAI, M.M., 2016. Mapping and characterization of rock discontinuities in atunnelusing3dterrestrialallaserscanning. *Bull. Eng. Geol. Environ.* 75(1), 223–237. <https://doi.org/10.1007/s10064-015-0748-3>.
- CACCIARI, P.P., FUTAI, M.M., 2017. Modeling a shallow rock tunnel using terrestrial laser scanning and discrete fracture networks. *Rock Mech. Rock Eng.* 50 (5), 1217–1242. <https://doi.org/10.1007/s00603-017-1166-6>.
- CACCIARI, P.P., FUTAI, M. M. Assessing the tensile strength of rocks and geological discontinuities via pull-off tests. *Int J Rock Mech Min Sci.* 2018;105(380):44-52.
- CANTARELLA, V.P., MONTICELI, J.P., CACCIARI, P.P., FUTAI, M.M., 2016. JRC estimation with 3D laser scanner images. In: VII Brazilian Symposium on Rock Mechanics - SBMR 2016. Minas Gerais, Brazil.
- CERYAN S, TUDES S, CERYAN N. 2008. Influence of weathering on the engineering properties of Harsit granitic rocks (NE Turkey). *Bull Eng Geol Environ* 67: 97–104.
- COLE WF, SANDY MJ. 1980. A proposed secondary mineral rating for basalt road aggregate durability. *Aust Road Res* 10: 27–37.
- DEARMAN WR, BAYNES FJ, IRFAN TY. 1978. Engineering grading of weathered granite. *Eng Geol* 12: 345-374.
- DEERE DU, PATTON FD. 1971. Slope Stability in Residual Soils. In: 4th Panamerican Conference on Soil Mechanics and Foundation Engineering, 1971. State of the art papers, San Juan.

- DELVIGNE JE. 1998. Atlas of micromorphology of mineral alteration and weathering. The Canadian Mineralogist Special publication, Ontario, Canada, special publication., 494p.
- GUPTA AS, RAO KS. 2000. Weathering effects on the strength and deformational behaviour of crystalline rocks under uniaxial compression state. *Eng Geol* 56: 257–274.
- GUPTA AS, RAO KS. 2001. Weathering indices and their applicability for crystalline rocks. *Bull Eng Geol Environ* 60: 201–221.
- IRFAN TY, DEARMAN WR. 1978. The engineering petrography of a weathered granite in Cornwall, England. *Q J Eng Geol Hydrogeol* 11: 233–244.
- ISRM. 2015. The ISRM Suggested Methods for Rock Characterization, Testing and Monitoring: 2007-2014. Springer International Publishing, Cham. doi:10.1007/978-3-319-07713-0
- HOEK E. BROWN E. 1997. Practical estimates of rock mass strength. *Int J Rock Mech Min Sci* 34: 1165–1186.
- KLEIN C, DUTROW BD, JAMES DWIGHT K. 2007. The 23rd edition of the manual of mineral science: (after James D. Dana). J Wiley & Sons, New York, USA, 23rd ed., 675p.
- LE PERA E, CRITELLI S, SORRISO-VALVO M. 2001. Weathering of gneiss in Calabria, southern Italy. *Catena* 42: 1–15. doi:10.1016/S0341-8162(00)00117-X
- LUMB P. 1962. The properties of decomposed granite. *Geotechnique* 12: 226–43.
- MARQUES EAG, BARROSO EV, MENEZES FILHO AP, VARGAS EA. 2010. Weathering zones on metamorphic rocks from Rio de Janeiro-Physical, mineralogical and geomechanical characterization. *Eng Geol* 111: 1–18.
- MENDES FM, AIRES-BARROS L, PERES RODRIGUES F. 1966. The use of modal analysis in the mechanical characterization of rock masses. In: 1st International Society for Rock Mechanics Congress, 1966. ISRM, Lisbon.

- NESSE WD. 2012. Introduction to mineralogy. Oxford University Press, New York, USA, 2nd ed., 466p.
- ONODERA TF, YOSHINAKA ROM. 1974. Weathering and its relation to mechanical properties of granite. In: 3rd International Society for Rock Mechanics Congress Advances in Rock Mechanics, 1974. ISRM, Denver.
- PIMENTAL J, BARROSO EV. 1996. Condicionantes do desenvolvimento de perfis de intemperismo nos leptinitos da Serra da Carioca. In: 8^o Congresso Brasileiro de Geologia de Engenharia, 1996. ABGE, Rio de Janeiro. (in Portuguese)
- PRIDER R. T. 1945. Charnockitic and related cordierite-bearing rocks from Dangin, Western Australia. Geological Magazine 82: 145-172.
- SAJID M, COGGAN J, ARIF M, ANDERSEN J, ROLLINSON G. 2016. Petrographic features as an effective indicator for the variation in strength of granites. Eng Geol 202: 44–54.
- REGMI AD, YOSHIDA K, DHITAL MR, PRADHAN B. 2014. Weathering and mineralogical variation in gneissic rocks and their effect in Sangrumba Landslide, East Nepal. Environ. Earth Sci. 71: 2711–2727. doi:10.1007/s12665-013-2649-8
- VOGEL D. 1975. Precambrian weathering in acid metavolcanics rocks from the Superior Province Villebon Township, South-central Quebec. Canadian J. of Earth Sciences 12: 2080-2085.

6. THE INFLUENCE OF WEATHERING GRADES ON GNEISSIC ROCK⁴

Abstract

This paper presents the influence of weathering grade on gneissic rock behaviour under tropical climatic conditions. The studied rock mass, through which a tunnel was excavated, was not reinforced by lining during tunnel construction and thus has been exposed to weathering for more than fifty years. This rock mass is starting to present problems related to block instability, motivating the re-evaluation of the geotechnical properties of the rock mass (intact rock). The physical properties (density and porosity), rebound number (R_L), compressional wave velocity (V_p), uniaxial compressive strength (UCS), indirect tensile strength (ITS) and tangent elastic modulus (E) were correlated with the micropetrographic index (I_p), physical weathering degree (PWD), and strength ratio (R_s) for weathering grade characterization. The analyses indicated that mineral fragility influences the mechanical behaviour. A strength degradation relationship that is a function of weathering was suggested. A quantitative weathering grade was presented, which is important for tunnel maintenance, future engineering interventions and regional rock formation studies. Data from relevant literature were used to propose the normalized general degradation strength for gneissic rock and other rocks with the same mineralogical composition.

Keywords: Gneissic rock, Weathering grades, Strength degradation, Tunnel

⁴ Authors: Monticelli J.P., Futai M. M.

6.1 Introduction

The Monte Seco Tunnel (Espírito Santo State, Brazil) is a segment of the Vitória-Minas Railway (VMR) and was excavated in a gneissic rock mass; additionally, this tunnel has lining only at the entrance and exit. Since this tunnel was constructed in the 1950s, it has experienced a degradation of its initial mechanical characteristics due to the long-term exposure of the rock to weathering, resulting in rock falls from the ceiling and walls. VMR is responsible for the transport of iron ore from the Quadrilátero Ferrífero (Iron Quadrangle), in the state of Minas Gerais, to the Vitória ports, in the state of Espírito Santo, and its full operation is fundamental because ore supply interruption can cause logistical issues. Detailed assessment of the present geologic-geotechnical conditions of the Monte Seco Tunnel has indicated the risks associated with rock instability, constituting a fundamental part of several studies from GeoInfraUSP – EPUSP (Cacciari and Futai, 2016, 2017; Monticelli et al., 2019a,b).

A commonly studied subject is the rock weathering grade characterization and its relation to gneissic behaviour; however, the proposed classifications are usually qualitative graded from lowest to highest grade (hence, from highest to lowest mechanical strength), considering three to five grades (fresh, slightly weathered, moderately weathered, and highly weathered, for example) and based on weathering profiles and visual-tactile assessment of the intact rock (Deere and Patton, 1971 and ISRM, 2015). Weathering grades have been correlated with the uniaxial compressive strength (UCS) of rock (BS 5930, 1999; Hoek and Brown, 1997), thus assigning quantitative values. However, each rock type should be appropriately studied, and the classification of weathering grades should be based on existing experience and correct interpretation of local conditions and field and laboratory test results, appropriate to the level of the research project.

The focus of this study was the weathering grade characterization of a gneissic rock by the application of petrographic and physical-mechanical weathering indexes. The gneissic rock matrix was previously classified in terms of its petrographic facies in accordance with mineralogical properties and by means of tactile and visual weathering grade characterization. After classification, the samples were submitted to petrographic and physical-mechanical tests. The physical properties (density and porosity), rebound

number (R_L), compressional wave velocity (V_p), UCS, indirect tensile strength (ITS) and tangent elastic modulus (E) were correlated with the micropetrographic index (I_p) of Irfan and Dearman (1978), the physical weathering degree (PWD) of Esaki and Jian (1999), the coefficient of weathering (I_{Vp}) of Illiev (1966) and the unsound constituent (UC) and strength ratio (R_s) indexes of Gupta and Rao (2001).

The petrographic and the engineering weathering indexes could distinguish the gneissic petrographic facies behaviours; the results indicated that one of the facies exhibits a more moderate weathering grade than those of the other facies. The heterogeneity of the gneissic rock mass along the tunnel length may have allowed the geomechanical properties to be overestimated in previous investigations.

The analysis of these conditions and the results of the tests led to the proposition of a curve of the degradation of strength and stiffness related to the weathering of gneissic rock. The quantitative weathering information obtained in this research is fundamental for Monte Seco Tunnel maintenance, future engineering interventions and other applications related to the effect of weathering on the geomechanical behaviour of rock masses with the same lithology.

6.2 Background

Petrographic weathering indexes are used to qualify and quantify the intensity and the evolution of the decomposition and disintegration processes that affect the minerals that form the rock matrix. Engineering indexes are used to express the physical-mechanical property degradation along a continuous scale or range along the weathering grade scale, and if possible, define its limits.

Among the most widely used petrographic indexes is the I_p of Irfan and Dearman (1978). I_p relates the number of sound minerals (SM) to the UCs (unsound or weathered minerals, UMs; fissures, Fs; and pores, Vs) and characterizes both the decomposition and the disaggregation processes of the minerals according to Eq. 1.

$$I_p(ad) = \frac{SM}{UC} = \frac{SM}{UM+F+V} = \frac{SM(\%)}{UM+F_i+F_e+F_t+V(\%)} \quad (1)$$

The PWD was defined by Esaki and Jian (1999); it relates the secondary porosity of a weathered sample to the total secondary porosity of the rock acquired after weathering and could provide additional information in rock characterization. However, the PWD application requires knowledge of the variation in porosity (η) along the weathering profile. The PWD is calculated according to Eq. 2, where η_f represents the fresh rock, η_w is the weathered rock and η_u represents the ultimate weathering product, usually the complete or the extreme weathering grade.

$$PWD (\%) = \left(\frac{\eta_w - \eta_f}{\eta_u - \eta_f} \right) 100 \quad (2)$$

The index usually used to quantify weathering aspects is the coefficient of weathering (I_{Vp}) proposed by Iliev (1966); this index quantifies the V_p loss in the weathered rock and is calculated according to Eq. 3, where V_{pf} represents the fresh rock and V_{pw} represents the weathered rock. The index is multiplied by 100 to obtain its value as a percentage. The author suggested an I_{Vp} value of approximately 0% for weathering grade I, between 0-20% for grade II, 20-40% for grade III, 40-60% for grade IV and 60-100% for grade V. Weathering grades I-V are comparable to those of the ISRM (2015) classification.

$$I_{Vp} (\%) = \left(\frac{V_{pf} - V_{pw}}{V_{pf}} \right) 100 \quad (3)$$

Among the mechanical weathering indexes, the strength ratio (R_S) was introduced by Gupta and Rao (2001) to characterize and quantify weathering grades with a rapid assessment of the effects of mechanical degradation. Although this index did not develop through research in gneissic lithotypes, the authors demonstrated that the index (R_S) is a useful tool in the assessment of the variation in elastic modulus due to the weathering of quartzite, basalt and granite. In addition, I_{Vp} could be used to estimate the UCS in R_S calculations. R_S relates the UCS of the rock in weathering states (UCS_w) with the fresh rock (UCS_f), and it is calculated according to Eq. 4.

$$R_S (\%) = \left(\frac{UCS_w}{UCS_f} \right) 100 \quad (4)$$

6.3 Materials and methods

Samples of the rock mass were obtained from blocks from the Monte Seco Tunnel; the different weathering grade samples were collected manually in the outcrop. The samples were collected from the same rock mass in the Monte Seco Tunnel and included all weathering grades.

The rainfall varies from 100 to 120 cm in the summer and from 50 to 20 cm in the winter, and the temperature varies from 28 to 26 °C in the summer and from 22 to 20 °C in the winter. Dearman et al. (1978) define this climate condition as tropical because there are dry and rainy seasons. In tropical conditions, such as the climate of the studied area, the physical-chemical weathering intensity varies from moderate to very slight and controls the disaggregation and decomposition of rock.

The characterization of the gneissic rock was carried out by means of tactile-visual inspection and petrography. The fresh gneissic rock of the study area is light grey to bluish dark-grey and predominantly fine- to medium-grained with a secondary coarse-grained texture. Centimetre- to metre-sized bands that correspond to the mesosome are characterized by a lepidogranoblastic texture and a biotite-rich gneiss foliation, interspersed with millimetre-sized light (felsic) and centimetre-sized quartz-feldspathic lenses. Well-formed bands of granoblastic texture correspond to the medium- to coarse-grained leucosome composed of feldspar, quartz, cordierite, garnet and opaque minerals. The presence of these features, which are closely related to the metamorphism of a sedimentary prototype, leads to the heterogeneity of the rock matrix.

This gneissic banding was classified into petrographic facies B1, B2 and B3, according to mineral composition, structure, texture and grain size (Table 6.1). The samples were carefully collected from drilling cores and outcropping rock blocks in the vicinity of the southern part of the Monte Seco Tunnel to represent the three alteration horizons of the rock mass. The weathering grades of the samples were characterized according to the proposal presented in Table 6.2, which was based on the Hoek and Brown (1997), the BS 5930 (1999), and the ISRM (2015) weathering classifications. To consider the abrupt weathering changes observed in field investigations (Monticelli et al. 2019a) and the rock heterogeneity, the fresh grade (I) and slightly weathered grade (II) were

grouped into grade W1, while the highly weathered grade (IV) and completely weathered grade (V) were grouped into grade W3. The moderately weathered grade (III) was maintained in W2. In this proposal, the W1 and W3 grades could be distinguished, by their tactile features, through the results of laboratory tests.




Petrographic analysis and physical-mechanical testing (physical property testing, rebound hardness testing, ultrasonic, in their tactile features, UCS and ITS analysis) were carried out at the laboratories of the Institute of Geosciences (IGc), EPUSP and the Engineering School of São Carlos at the University of São Paulo. The textural and micromorphological characterization of the rock-forming minerals was presented in Monticeli et al. (2019b). The mineral composition, structure, texture and grain size of the rock were described, as well as an accurate description of the grades and types of weathering and mineral cracking.

The I_p ratio was modified in Eq. 5 to capture the development of fissures and the coalescence of intramineral fissures in the formation of transmineral fissures due to the mineral fragility of the cordierite and biotite alteromorphs (Figure 6.1, blue boxes), which are determinant for the rock matrix modifications. Figure 6.1 illustrates the criteria used to calculate the modified micropetrographic index ($I_{p\ mod}$) of the gneissic rock of the Monte Seco Tunnel based on the Delvigne (1998) standardized classification of weathered minerals.

$$I_{p\ mod} = \frac{SM_{Fk,Pl(0-2\ stages)} + SM_{Bt,Cr(0-1\ stages)} + SM_{Hp,Gr(0-1\ stages)}(\%)}{UM_{Fk,Pl(3-4\ stages)} + UM_{Bt,Cr(2-4\ stages)} + UM_{Hp,Gr(2-4\ stages)} + F_i + F_e + F_t + V(\%)} \quad (5)$$




The modal composition of SM and UC was obtained by counting points for each sample. The point counting was performed using the *JMicroVision* software following a random mesh in representative microsites of the thin sections, analysed under the *Leica Zeiss Axioplan* optical microscope. The counting ended when the proportions became constant at 200 points. Approximately 12 microsites were investigated in each thin section, totalling 2400 points analysed in this way. A total of fifteen thin sections were used to characterize the weathering grades. The photomicrographs were captured using the Leica Application Suite V4.7 software.

Table 6.1 - Description of the petrographic facies of the gneissic rock

Facies	Structure	Texture	Grain size	Mineralogical assembly			
B1 	Finely banded and foliated	Equigranular to inequigranular	Fine-grained	Qz	+++	Cr	++
		Lepidogranoblastic	0.1-3 mm	Fk	++	Hp	+
				Pl	++	Gr	+
				Bt	++	Ot	+
B2 	Clear intercalation of light (L) and dark (D) bands; foliated	Inequigranular	Fine- to medium-grained	Qz	++	Cr	++
		Lepidogranoblastic to granoblastic	(L) 1-5 mm (D) 0.1-3 mm	Fk	++	Hp	+
				Pl	++	Gr	+
				Bt	++	Ot	+
B3 	Massive (without foliation)	Inequigranular porphyroblastic	Coarse-grained	Qz	+++	Cr	++
		Granoblastic	5-20 mm	Fk	+++	Hp	+
				Pl	++	Gr	+
				Bt	+	Ot	+

Obs: Minerals: quartz (Qz), orthoclase (Fk), plagioclase (Pl), biotite (Bt), cordierite (Cr), hypersthene (Hp), garnet (Gr) and other minerals (Ot).

Table 6.2 - Intact rock weathering grades (modified after Hoek and Brown, 1997; BS 5930, 1999 and ISRM, 2015)

Grades	Visual-tactile features	Images (size: 54.5 mm)	UCS by simple means (MPa)
W1 (I - II) fresh to slightly weathered	Fresh to incipient weathering. Macroscopically, there is no evidence of mineral weathering. Minerals have lustre. Slabs with difficulty with various hammer blows, resists cutting by a steel knife and finger pressure.		100 - 200 (> 200)
W2 (III) moderately weathered	Shows signs of mineral weathering. Minerals show a lack of lustre and noticeable discolouration, sometimes occurring with a yellow film (iron oxides and hydroxides). Breaks with some difficulty from a hammer blow. Steel knife scratches the surface and removes crystals. Resists finger and nail pressure.		50 - 100
W3 (IV/V) highly to completely weathered	Rock and minerals are significantly weathered and friable. Minerals lacking lustre and are strongly discoloured; iron oxides and hydroxides impregnate the sample. Breaks easily with a hammer blow*. Minerals are removed by finger and nail pressure; steel knife easily cuts grooves in the sample**.		12.5 - 50 (*) 1.25 - 12.5 (**)

Representative specimens of each petrographic facies (Table 6.1) and weathering grade (Table 6.2) were submitted to physical tests. Porosity, density and apparent absorption were obtained following the ISRM (1979a) guidelines. MTS equipment was used to determine the UCS of the 53 dry samples. The UCS testing was performed

following the ISRM (1979b) guidelines. The tangent elastic modulus (E) of the 17 dry samples was also obtained by using local instrumentation with a strain gauge. The angle (β) between the foliation and load direction for weathering grades W1, W2 and W3 was approximately 60° , 0° and 90° , respectively. The ITS testing of 44 dry samples was carried out by using the EMIC test equipment with curved loading jaws, following the procedures recommended by the ASTM D 3967-08 (2008) guidelines. The angle (β) between the foliation and load direction was either 0° (parallel) or 90° (perpendicular).

In the sclerometry test, a *Proceq*, type L (0.735 Nm), digital Silver Schmidt hammer, which has a system for rebound correction in relation to the orientation of the device application, which is the main advantage of this sclerometer over other hammers, was used in the rock weathering characterization. Ample debate on the method to obtain the rebound number is observed in the literature; single or continuous impacts are usually performed (Hucka, 1965; Poole and Farmer, 1980; ASTM D5983-00, 2001; Kahraman et al., 2002; Aydin and Basu, 2005; Buyuksagis and Goktan, 2007; Aydin, 2009). In this work, the methodology of ASTM (2001) was used, which proposes 10 single impacts separated by at least the diameter of the sclerometer point and collected away from the sample edges to avoid effects.

Following the guidelines of Aydin (2014), the compressional wave velocity test was carried out on the cylindrical specimens using the Pundit Lab+ equipment from *Proceq*, positioned in a direct transmission manner with transducers of 250 kHz, where the average of five measurements was recorded for weathering characterization. After the laboratory tests, the physical-mechanical weathering indexes were calculated with Eqs. 2 to 4. Based on the R_s index proposed by Gupta and Rao (2001) (Eq. 4), the indirect tensile strength ratio (R_{ITS}) and compression elastic modulus ratio (R_E) were calculated and introduced in the same manner in this study.

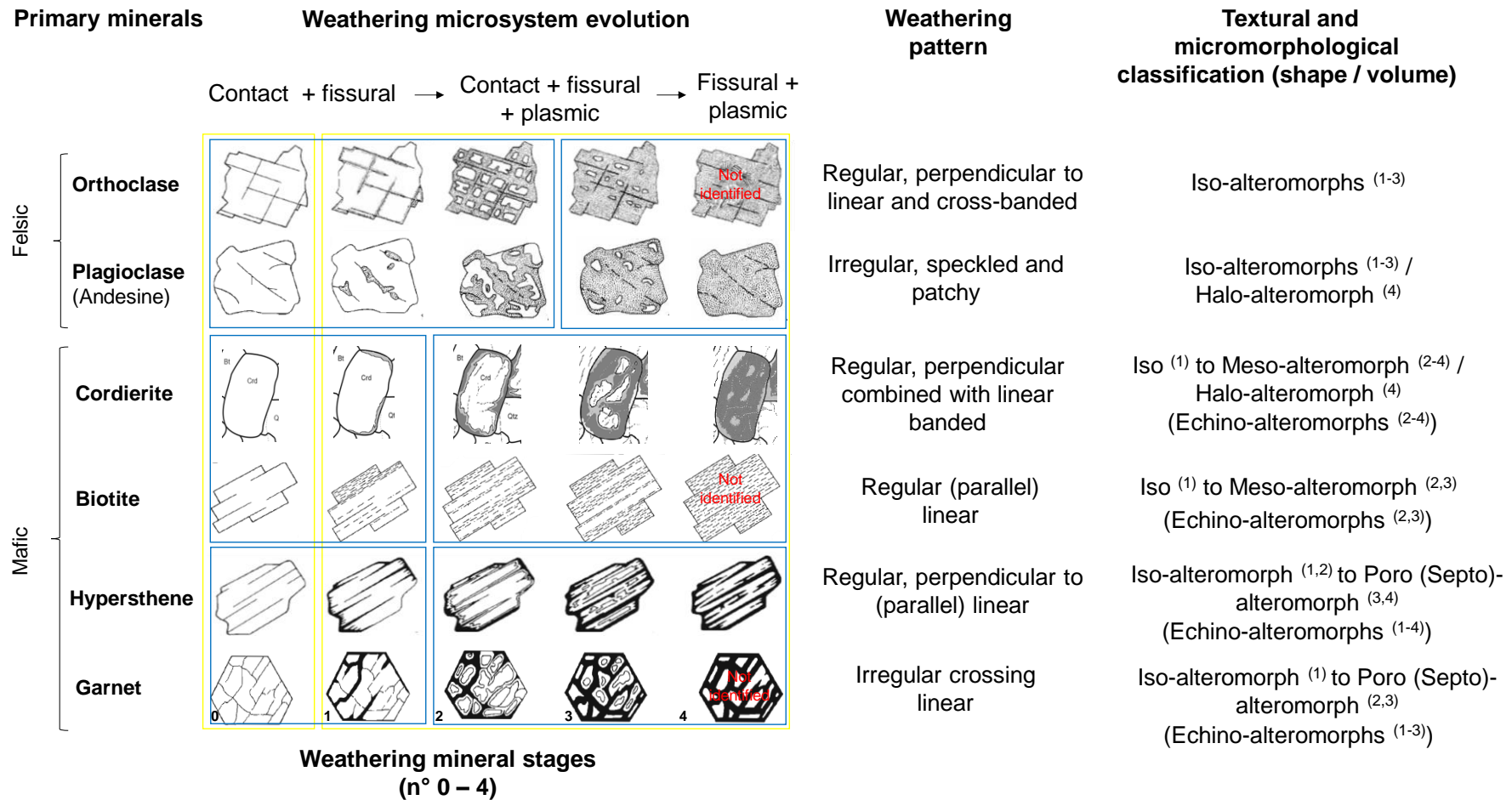


Figure 6.1 - Illustration of the criterion used for the petrographic weathering index application (modified after Monticelli et al. 2019a). Yellow boxes represent what could be classified as UM, while the blue boxes are related to the criterion applied based on textural and micromorphological modifications.

6.4 Influence of weathering on the petrographic and physical properties of gneissic rocks

The result of the SC and UC counting points showed that the gneissic I_{ps} values, compared to those of granite, do not indicate a weathering evolution and descriptions that are the same nor reflect the same petrographic characteristics of those determined by Irfan and Dearman (1978). For these reasons and seeking to adapt and calibrate a weathering grade classification (I-V, from fresh to completely weathered) to the gneissic rock matrix evolution, the most representative photomicrographs of the petrographic facies, their respective I_{pmod} and the previously associated weathering grade (Table 6.2) are shown in Figure 6.2.

There is a clear difference between the I_{pmod} values among the weathering grades and petrographic facies. Compared to facies B1 and B2, the B3 thin samples previously characterized by grade W1 (Table 6.2) present many intra- to transmineral fissures related to cordierite and orthoclase alteromorphs, which decreases the fit of the I_{pmod} values for the moderately weathered grade W2 (III) and highly weathered grade (IV) (Figure 6.2, sample numbers 11-14). On the other hand, the decrease in I_{pmod} for the petrographic facies B1 and B2 is due the development of intra- to transmineral fissures related to the meso-alteromorph textural and micromorphological modification presented in the cordierite and biotite alteromorphs.

This textural modification influences the fissuring of the adjacent minerals, consequently connecting plasmic microsystems and increasing the whole mineral decomposition (Figure 6.2, samples numbers 1-10). These aspects are fundamental to understanding the influence of mineralogical characteristics on the gneissic rock behaviour after calibration of the relation among the petrographic facies and weathering intensity with a continuously decreasing I_{pmod} .

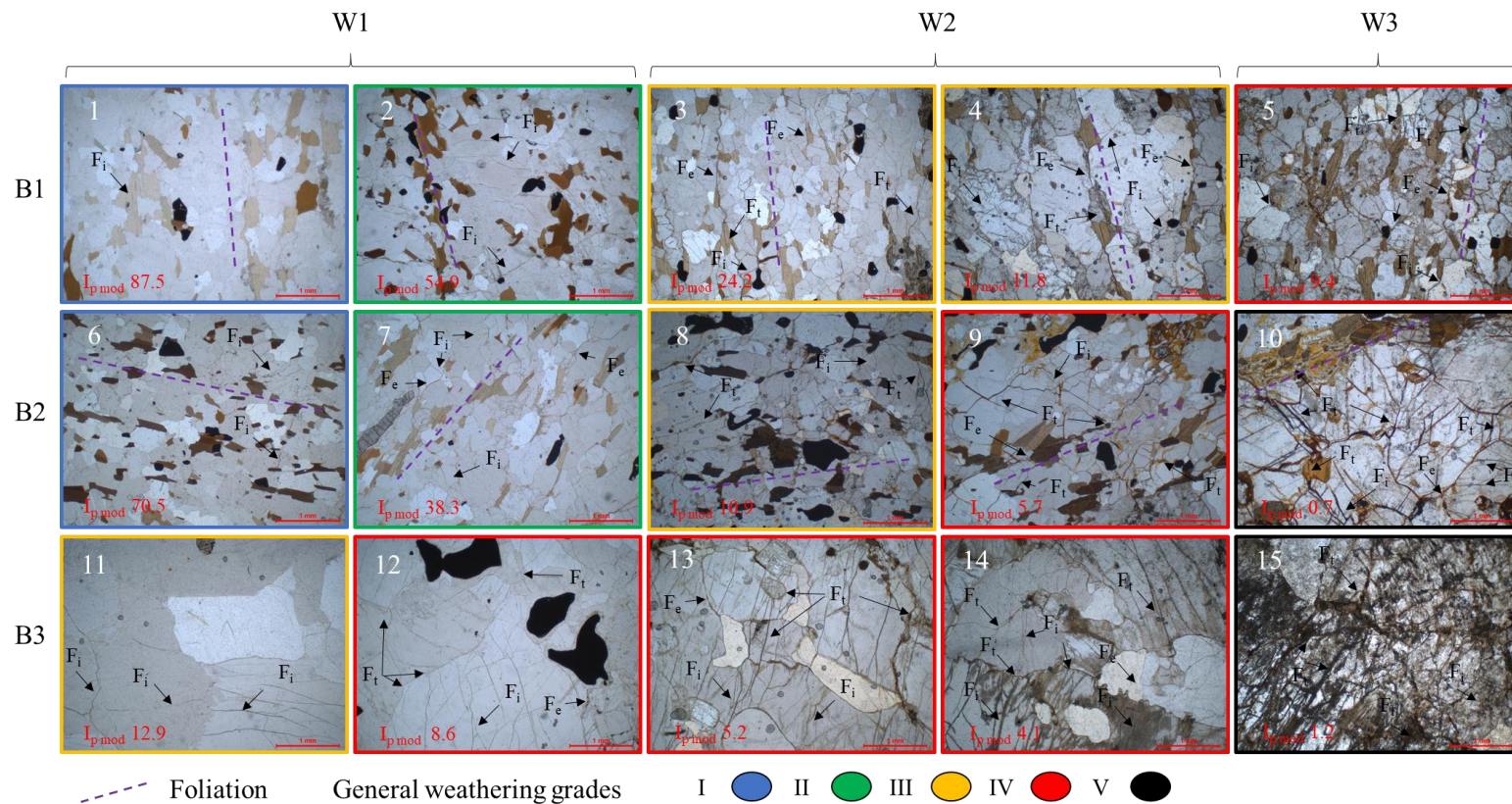


Figure 6.2 - Photomicrographs illustrating the evolution of the fissures in facies B1 (sample numbers 1-5), B2 (sample numbers 6-10) and B3 (sample numbers 11-15) according to the $I_{p\ mod}$ and the comparison between the initial (Table 6.2) and the general (I-V) weathering grade classifications. The samples numbers 1 to 15 are denoted in white, and the values of $I_{p\ mod}$ are denoted in red. Intramineral (F_i), intermineral (F_e) and transmineral (F_t) fissures are indicated.

Notably, the behaviour observed in facies B3 is influenced by the granulometry (Table 6.1), which, due to the high quantities of coarse-grained minerals, increases the mineral embrittlement, resulting in open cleavages in the orthoclase and fissures in the cordierite alteromorphs.

The petrographic aspects of the gneissic banding (Table 6.1), which are closely related to the suggested weathering grade rearrangement (Figure 6.2), are also responsible for the variation in the physical properties, density and porosity, as presented in Figure 6.3. Facies B1 and B2, rich in mafic minerals with tight intramineral fissures, such as those found in biotite, are more dense than facies B3, rich in felsic coarse-grained minerals with incipient intra- to transmineral fissuring, for the same porosity range in the low weathering grades (0.2-2%). Due to the development of secondary porosity related to the increase in fissuring and mineral decomposition, the variation in density among the petrographic facies decreases with the porosity, although some B3 densities seem to be outside the limits of density determined for previously studied gneissic rock.

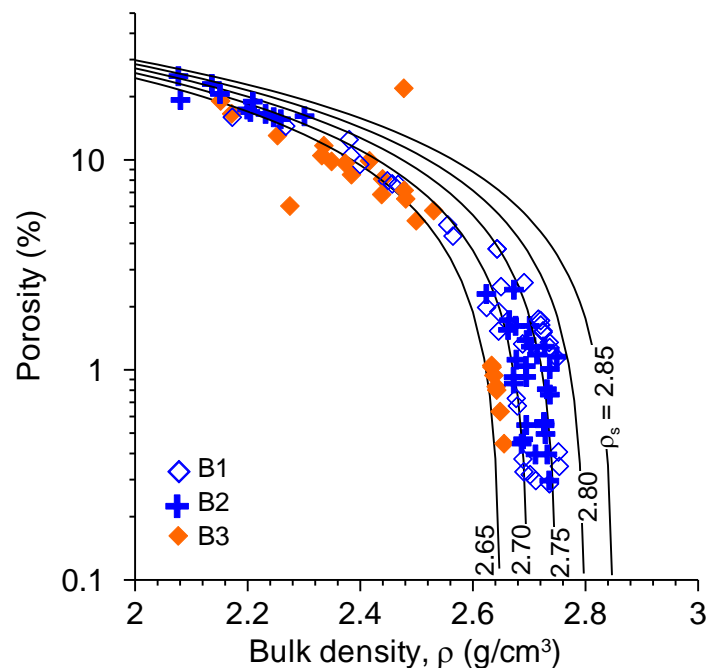


Figure 6.3 - Relationship between physical properties, porosity and bulk density, for the petrographic facies of the gneissic rock mass.

The average results of the petrographic analyses, $I_{p\ mod}$, physical properties (bulk density and porosity), V_p and R_L were organized in Figure 6.4. The average values were calculated based on $I_{p\ mod}$ and R_S for general weathering grade classification (I, II, III, IV and V, from fresh to completely weathered). Basically, facies B3 were grouped into grades III, IV and V, unlike facies B1 and B2, due to the petrographic characteristic data (Figure 6.2), and further considerations will be given for mechanical degradation. In terms of the major petrographic and physical aspects of the effect of weathering on gneissic rock, it can be observed that $I_{p\ mod}$ density, V_p and R_L decrease and porosity increases as weathering becomes more severe. The resultant significant coefficients of determination support the rearrangement of the gneissic rock weathering grades and the observed modifications to the rock matrix. These relationships provide useful and accessible information to characterize gneissic weathering grades (Figures 6.2 and 6.4), although a preliminary heterogeneity classification may be needed to comprehensively evaluate the gneissic behaviours.

Regarding the sclerometry test results, a comparison between the rebound values obtained on the surfaces of the weathered rock blocks (R_{Lsur}) and the average of the samples extracted from them (R_{Lint}) was performed (Figure 6.5). Under ideal conditions, there would be no difference between R_{Lsur} and R_{Lint} . However, in general, the R_{Lsur} values of the weathered rock blocks were observed to be lower than the R_{Lint} values, and this trend was observed for a continuous range of known rebound values.

In the rock blocks that are more homogeneously weathered or exhibit an advanced weathering condition, e.g., block J, this difference seems to be smaller, but often the samples extracted from such rock blocks are broken during the sclerometry test. This indicates a possible limit in the rebound values of cylindrical samples due to sample breaking. On the other hand, in heterogeneously weathered rock blocks, for rock blocks presenting less advanced weathering conditions with exfoliation weathering, the difference is slightly greater, e.g., block H, reflected by the data point plotting farther from the 1:1 line in Figure 6.5. In general, the broken samples were re-utilized to produce ITS samples to determine the approximate relationships between R_L , V_p , and UCS and the rock indirect tensile strength, as shown below.

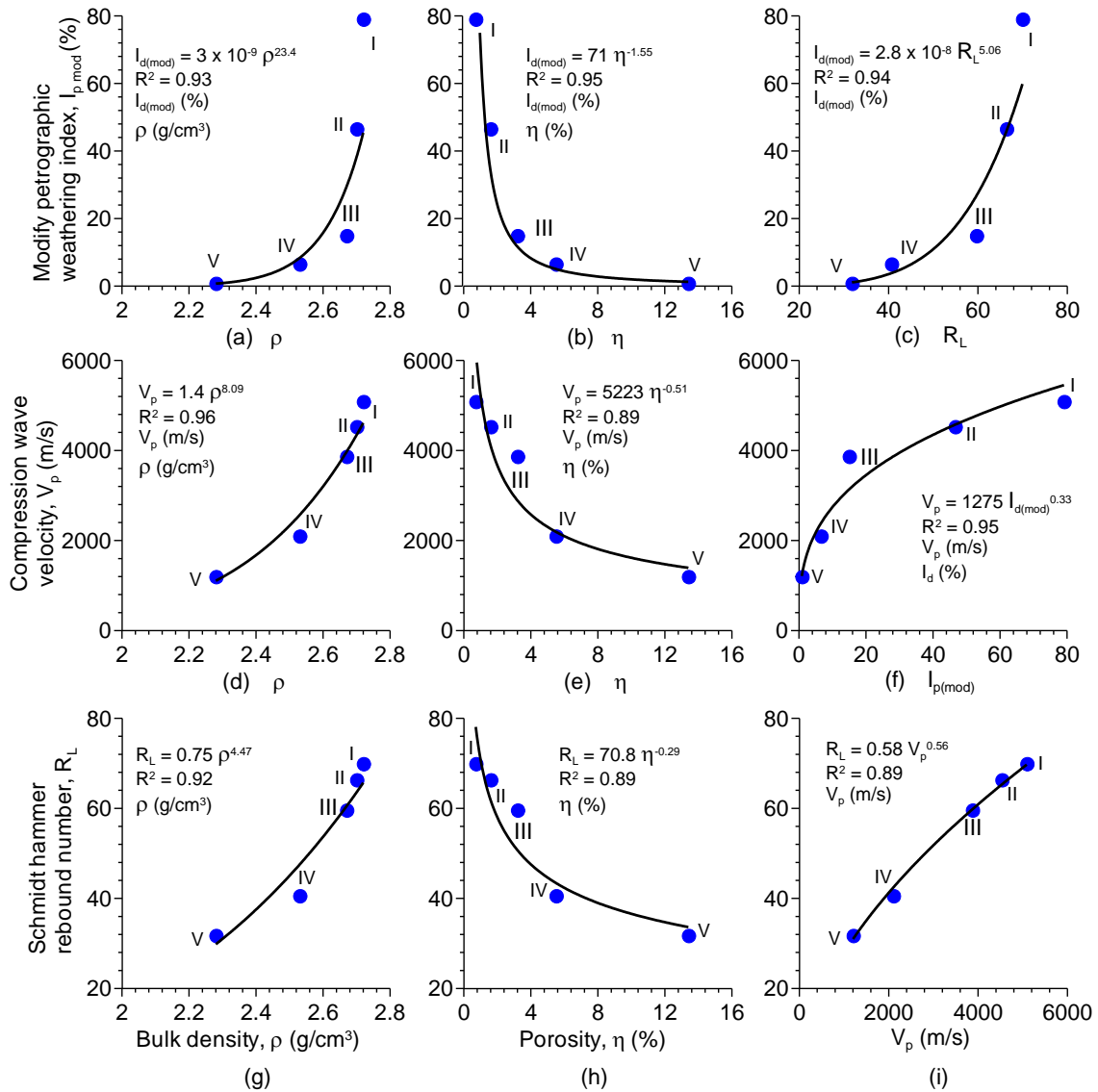


Figure 6.4 - Relationships among the average values of the petrographic index, physical properties (bulk density and porosity), compression wave velocity and rebound number with the general weathering grades.

The relationship between R_{Lsur} and R_{Lint} shows that it is important to consider that the extracted samples of a weathered rock block can be weak enough to be broken with a few rebounds, in a sense, setting the expectations for the rebound results of the samples (R_{Lep}) and indicating that a weaker sclerometry device may be used to improve the weathering characterization. In addition, the joint compressive strength (JCS) estimation of the Barton and Choubey (1977) criterion is incorporated once the cylindrical specimens that were extracted close to a weathered discontinuity surface show rebounds higher than the true weathering condition of the discontinuity surface, and this estimate is more significant in heterogeneously weathered rock blocks.

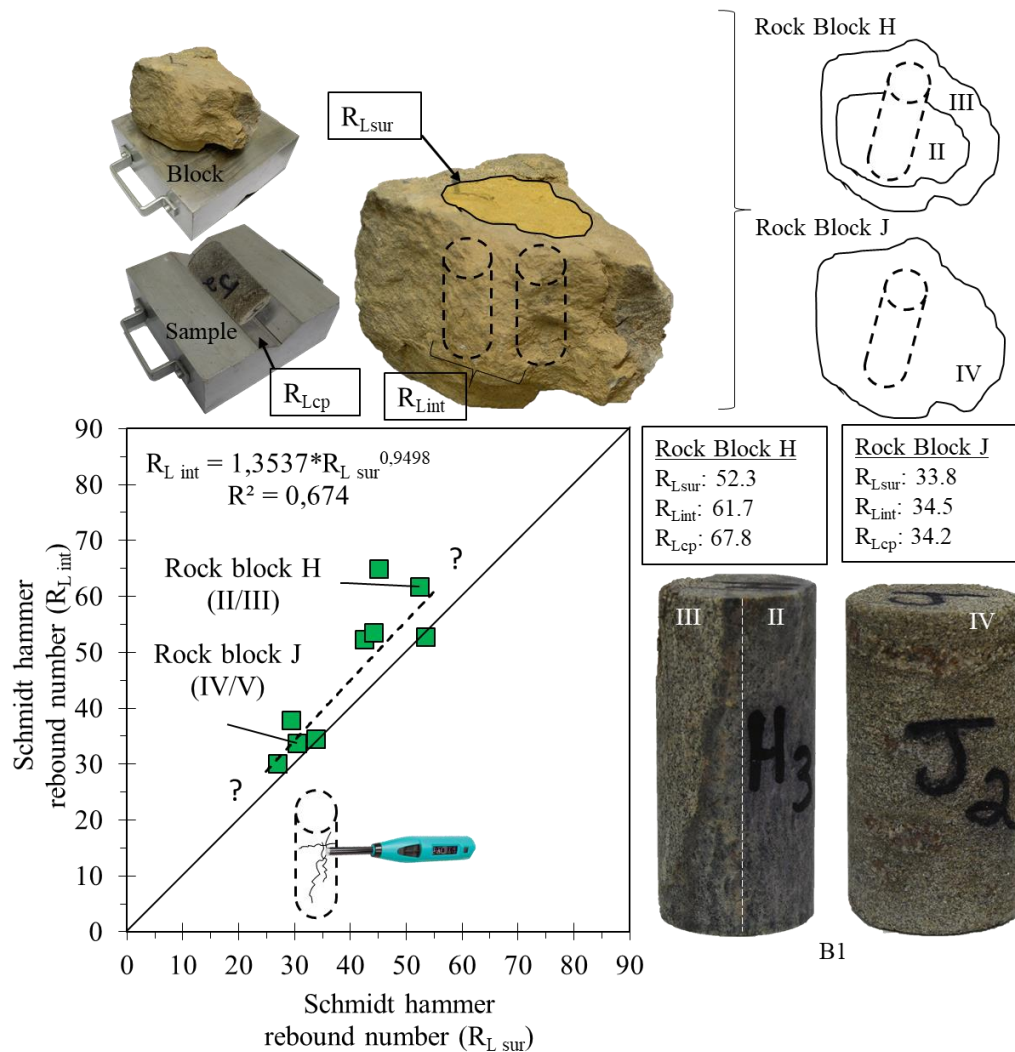


Figure 6.5 - Results of sclerometry tests carried out in heterogeneously weathered rock blocks. Rebound numbers were obtained from the rock block surface ($R_{L\text{sur}}$), the extracted sample ($R_{L\text{cp}}$) and the average values of the extracted samples ($R_{L\text{int}}$).

6.5 Influence of weathering on strength and deformability

The photographic records of the UCS and ITS samples in weathering grade W3 (IV-V) and the representative stress-strain (displacement) curves for the general weathering grades are shown in Figure 6.6. The comparison of the ITS values obtained parallel and transverse to foliation in the extreme weathering grades is shown in Figure 6.7. The UCS, ITS and E values were correlated with bulk density and porosity in Figure 6.8 and with R_L and V_p in Figure 6.9. Figure 6.10 shows the relationship between E and ITS with UCS along the general weathering grade classification. Unfortunately, it was

not possible to characterize E with confidence in the moderately weathering grade because the material became deformable, and it was difficult to fix the local instrumentation. Figures 6.6 to 6.10 summarize the geomechanics results and are discussed below.

The axial and splitting rupture modes were observed in the UCS tests for all the petrographic facies, but for the material with advanced weathering conditions, one shear failure was usually observed in facies B1, while multiple shear failures were observed in facies B2 and B3 (Figure 6.6a-c).

The foliation of the gneissic rock studied weakly influenced the UCS values in weathering grade W1 (I-II) of facies B1 and B2, as was noticed by one rupture along the foliation plane oriented at 60° , resulting in a UCS of 77 MPa, was disregarded in the relationships between the physical and mechanical properties shown below.

Dobereiner et al. (1993) noted that the difference between parallel and transverse UCS values increases with weathering, but Marques et al. (2010) argued that the gneissic rock becomes more isotropic. The foliation effect was not fully addressed in the UCS characterization; however, the ratio between the transverse and parallel ITS values of facies B1-B2 in the extremes weathering grades indicated an increase in the foliation effect with weathering (Figure 6.7).

In general, the ITS is higher in specimens loaded in a direction transverse to foliation than those loaded parallel to foliation. However, when the weathering grades increase, the effect of anisotropy increase, and the ratios of parallel to transverse ITS results can be compared. This ratio is 0.65 for grades I-II and decreases to 0.37 for grades IV-V. This result indicate that weathering reduces the strength along the foliation planes.

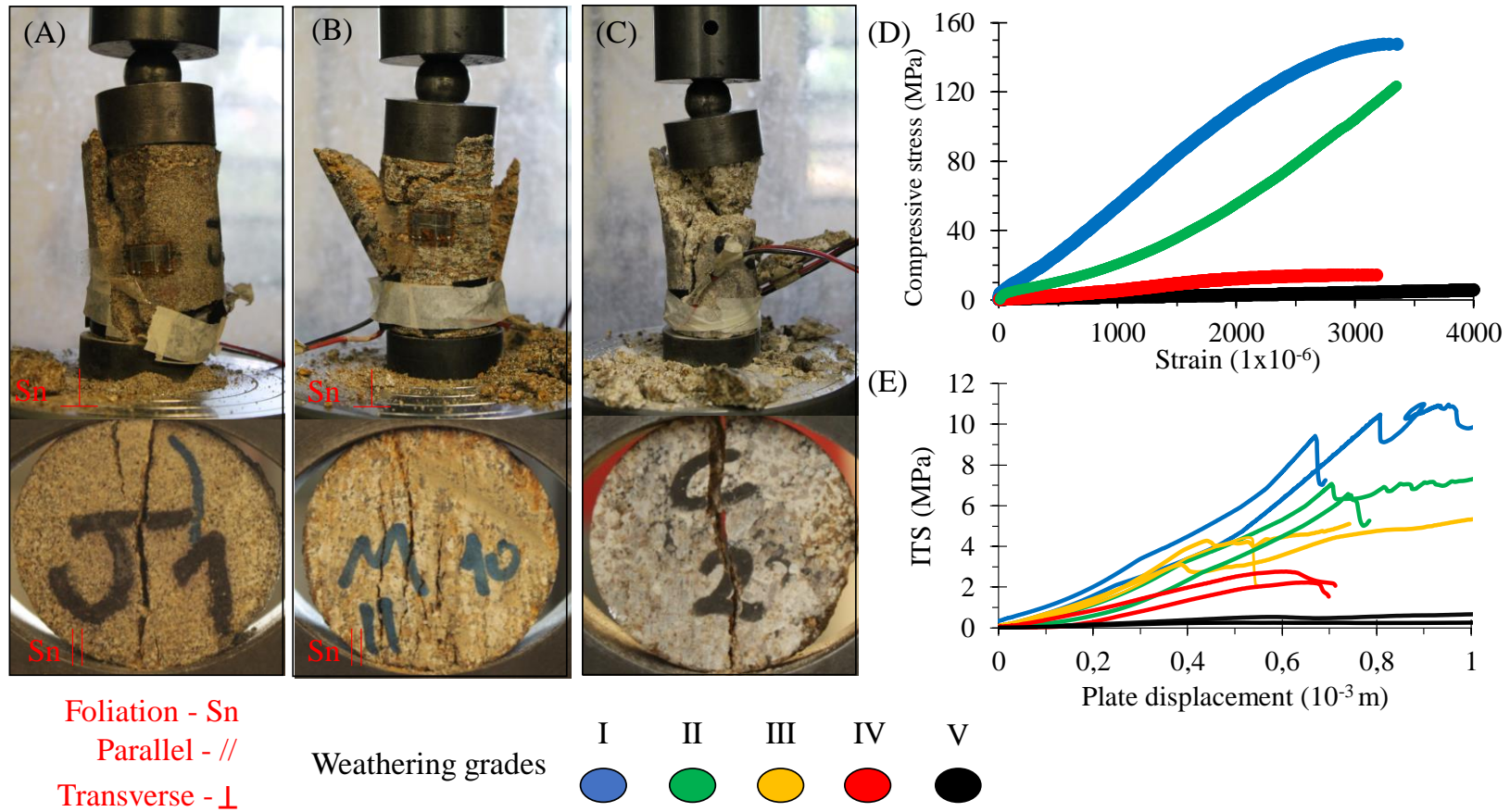


Figure 6.6 - Photographic record after the UCS and ITS tests for the completely weathering grade of petrographic facies B1 (A), B2 (B) and B3 (C). Illustrations of the typical compressive stress-strain (displacement) curves from the UCS (D) and ITS (E) tests highlighting the different weathering grade behaviours.

The increase in the effect of foliation on the ITS values could be related to the cordierite and biotite textural modifications. The aligned contact microsystem of the biotite-cordierite foliation plane in the low weathering grades or the lepidogranoblastic texture is superimposed by parallel and transverse transmineral fissuring triggered by the weathering of these minerals in the advanced weathering grade.

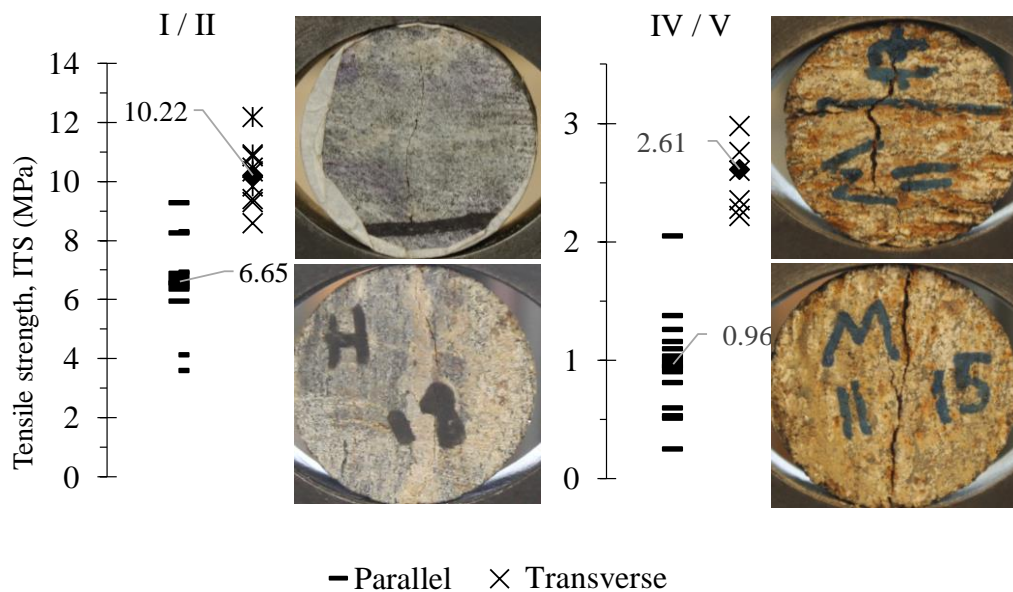


Figure 6.7 - Comparison between parallel and transverse tensile strength values obtained for the extreme weathering grades.

The difference in the mineralogical conditions among the petrographic facies was easily recognized in the relationships between the UCS and ITS results and the physical properties. The petrographic facies B3 samples presented UCS and ITS maximum values of approximately 100 MPa and 6 MPa, respectively, while those of the B1-B2 facies were approximately 160 MPa and 11 MPa (Figure 6.8a-d). For granite, according to Sajid et al. (2016), the increase in mineral grain size decreases the UCS and ITS strengths in the less advanced weathering grades. This aspect also influenced the variation in strength observed in facies B1-B2 to B3 in the UCS and ITS tests. Facies B3 presents UCS and ITS values that plot roughly in the middle of the mechanical degradation trend in relation to facies B1-B2 (Figure 6.8a-b).

The mechanical responses of UCS, ITS and E have practically the same tendency (Figure 6.8); the value increases with bulk density, and the opposite trend is observed with porosity. For bulk densities higher than 2.6 g/cm^3 or porosities lower than 2%, the strength and stiffness of the rock increase rapidly. The fit of the proposed correlation equation is better with porosity than with bulk density.

In the estimation of the mechanical properties by non-destructive testing, the foliation and heterogeneity effects increase the variation in the data (Figure 6.9); thus, the average gneissic rock behaviour is characterized. High coefficients of determination were observed for the relationships among UCS, ITS and E from the non-destructive tests (R_L and V_p values), despite the low amount of E data used for the correlation (Figure 6.9). The sclerometry device used was a useful tool for the rock weathering characterization, although a weaker sclerometry device could have been used for the characterization of advanced weathered grade rock materials, as interpreted above; however, when correlated with mechanical properties, the variation in rebound number was most significant in the low weathering grades (Figure 6.9a).

The rock samples broken in the sclerometry tests were recycled and used in the ITS tests, which providing information for rock weathering characterization in field inspections, although the foliation effect was not fully assessed (Figure 6.9c-d). The I_{VP} index was not capable of distinguishing grades W1 and W3, and its relationship with V_p was consistent with those of the other properties (Figure 6.9b, d, e). The correlations using R_L and V_p to determine UCS, ITS and E were represented by power functions. These relationships are important in practical applications because R_L and V_p can be used to determine in situ conditions and mechanical parameters indirectly.

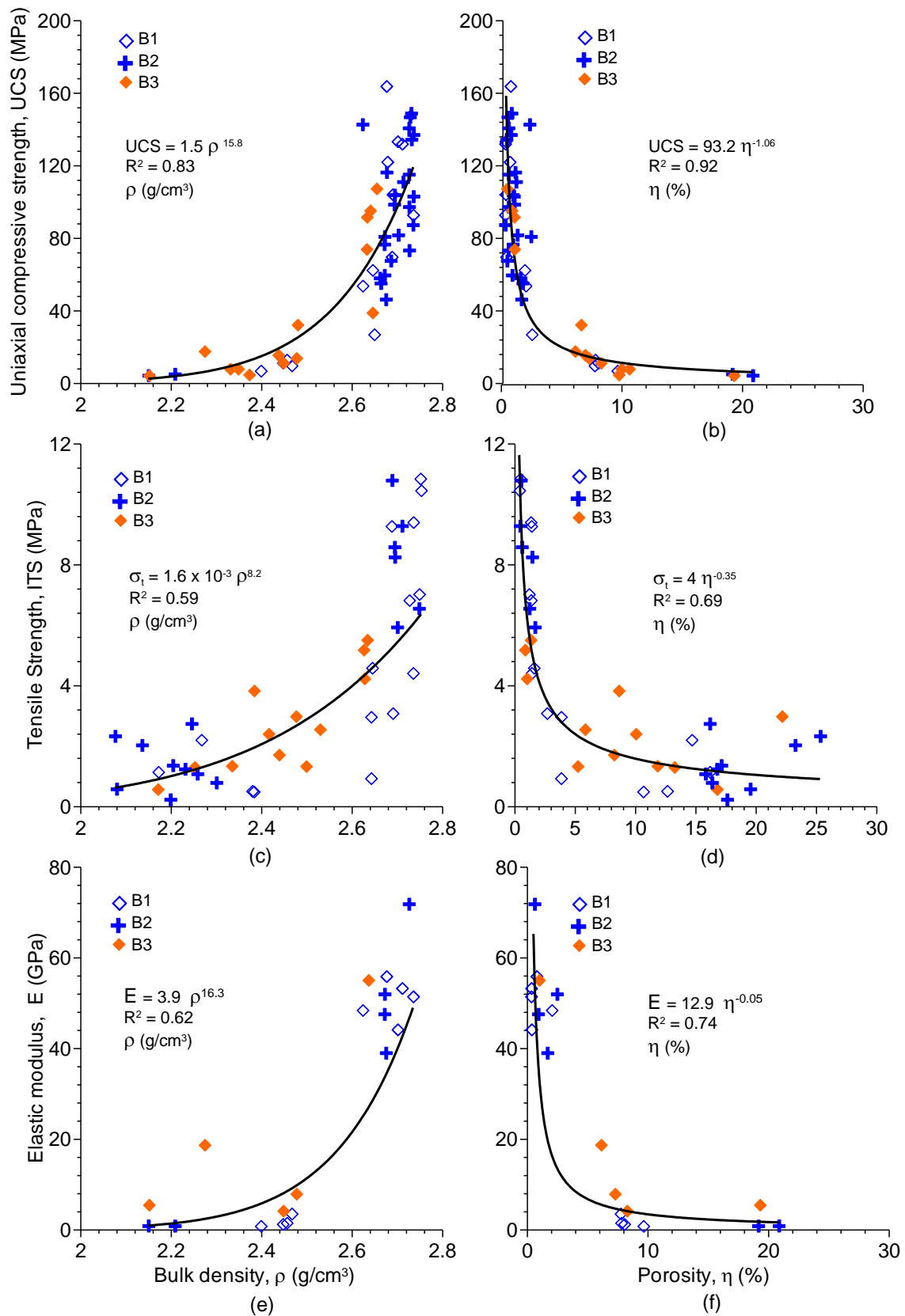


Figure 6.8 - Relationships between the UCS, tensile strength and elastic modulus with the bulk density and porosity.

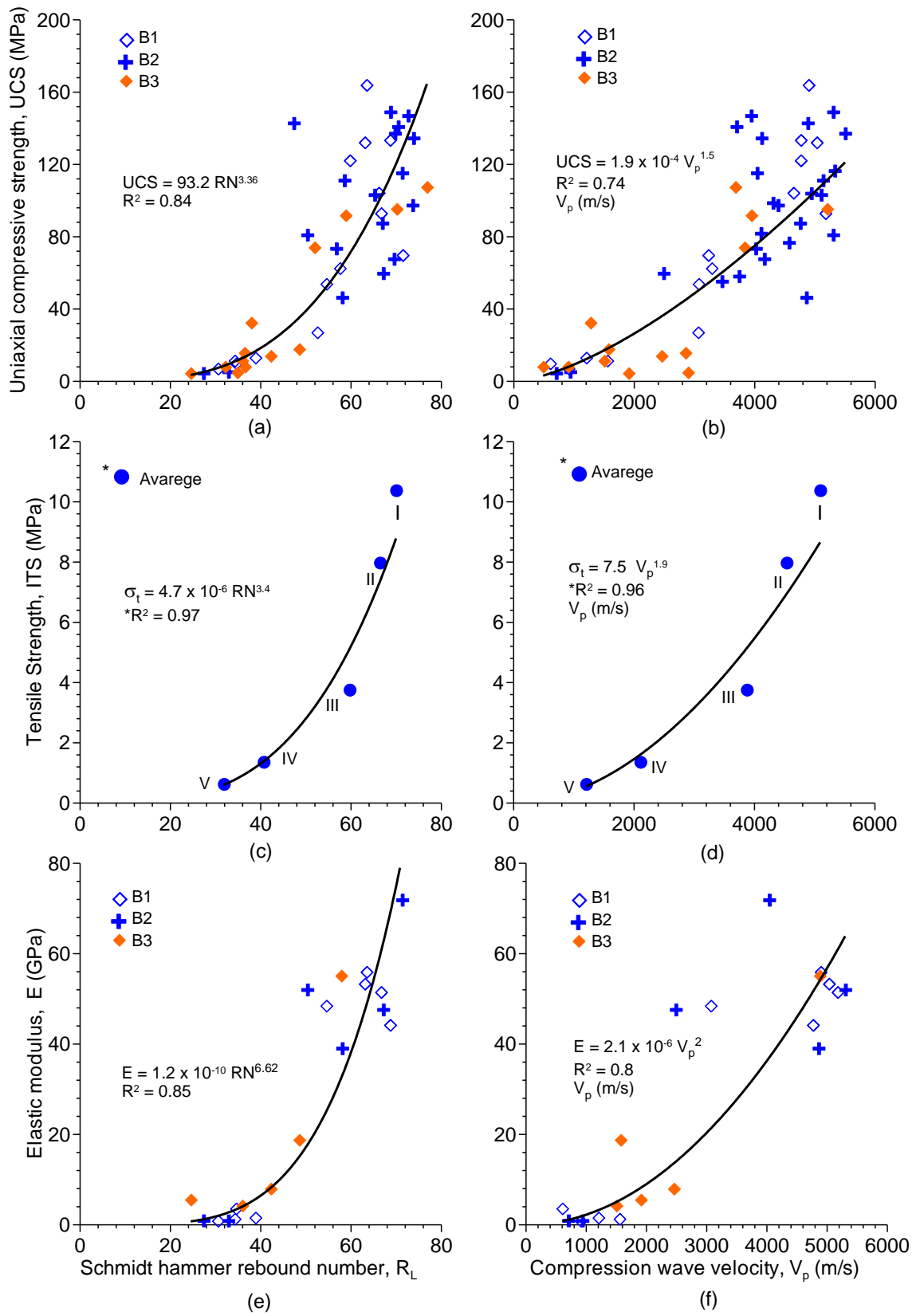


Figure 6.9 - Relationships between the UCS, tensile strength and elastic modulus with the rebound number and compression wave velocity.

One of the major topics discussed in rock mechanics is the proportionality between the UCS and ITS and the UCS and E (Perras and Diederichs, 2014). These proportionalities are not well known for gneissic rocks, especially in the characterization of weathering grades, but good results were obtained for the studied gneissic rock (Figure 6.10). The ratio between ITS and UCS is 0.066, and that between E and UCS is 380. It is useful to estimate ITS and E by using UCS.

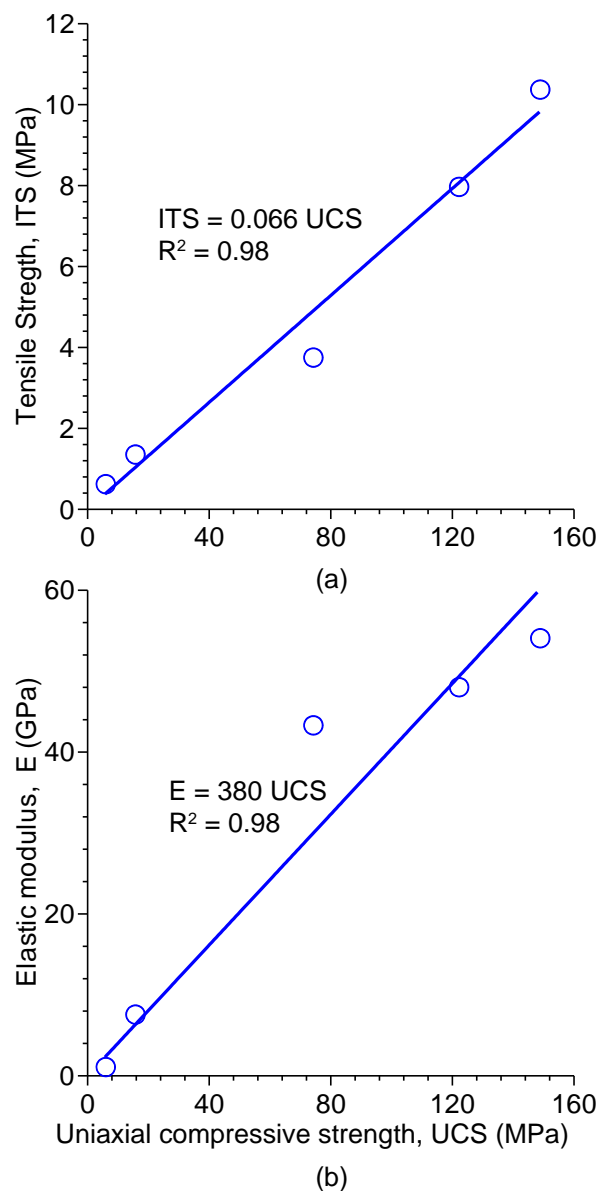


Figure 6.10 - Relationships between the tensile strength (a) and elastic modulus (b) with the UCS.

For gneissic rocks, usually, either petrographic or geochemical indexes are used for physical-mechanical properties in rock weathering characterization. Here, the petrographic weathering indexes ($I_{p \text{ mod}}$ and UC_{mod}) of the studied gneissic rock were correlated with the mechanical parameters (UCS, ITS and E) for weathering grades I-V, as shown in Figure 6.11. $I_{p \text{ mod}}$ showed slightly higher coefficients of determination than UC_{mod} , which demonstrates that the $I_{p \text{ mod}}$ can also characterize heterogeneous and metamorphic rocks, such as the gneissic rock of the Monte Seco Tunnel. In addition, the ratio (SC/UC) seems to be a better alternative to relating the mineralogical constituents and their respective textural modification effects than considering only UC as the petrographic weathering index.

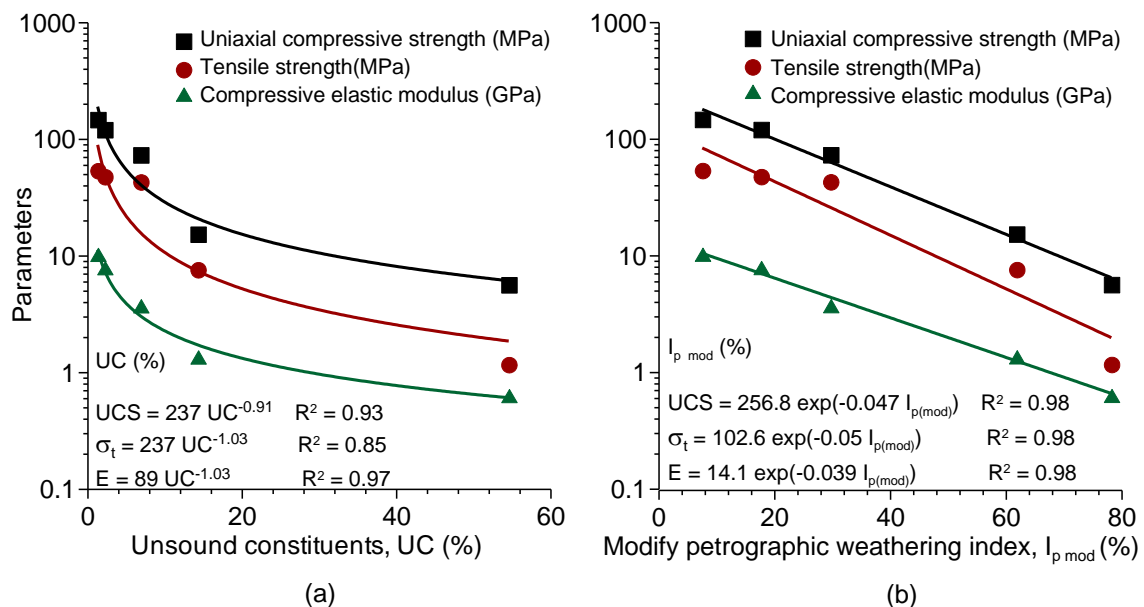


Figure 6.11 - Relationships between the mechanical parameters (UCS, ITS and E) and the modified petrographic weathering indexes, UC_{mod} (a) and $I_{p \text{ mod}}$ (b).

6.6 Discussion

The quantification of the gneissic rock weathering in terms of UCS, ITS and elastic modulus (E) can be obtained through the physical index PWD and petrographic index I_p (micropetrographic index). According to the presented methodology, it is necessary to correctly identify the extreme porosity values (maximum, η_u , and minimum, η_f) for the correct application of the PWD index, as well as the maximum strength and elastic

modulus values (UCS_{max} , ITS_{max} and E_{max}) and the $R_{(S,ITS,E)}$ index. In addition, the application of petrographic indexes, such as I_p , it should be supported by textural and micromorphological criteria. A petrographic index based on a ratio of mineralogical characteristics seems better relates the weathering increase than a single aspect.

The results presented previously can explain the influence of weathering on the petrographic, physical and other measures and on the mechanical properties of the rock; there are sufficient tests results to explore deeply. The index properties of the rock were tested, and the PWD presented results that better represent the weathering grade, which can be determined by simple tests. The strength has to be normalized, as proposed by Gupta and Rao (2001), and the same principle was used to normalize not only the UCS but also the ITS and E (Eq. 6).

$$R = \frac{UCS_w}{UCS_f} = \frac{ITS_w}{ITS_f} = \frac{E_w}{E_f} \quad (6)$$

where R is the strength and stiffness degradation, UCS is the uniaxial compressive strength, ITS is the indirect tensile strength, E is the elastic modulus, the subscript w denotes weathered samples, and the subscript f denotes fresh samples.

Both the porosity and strength (or E) were normalized for the normalized curve, which represents the effect of weathering on the gneissic rock mass of the Monte Seco Tunnel. The result of the normalized UCS, ITS and E versus PWD is presented in Figure 6.12. Figure 6.12a is plotted on an arithmetical scale, and PWD is presented in the log plot in Figure 6.12b.

The results indicate that one unique curve can be used to represent the degradation weathering effect (Figure 6.12). It is an interesting and innovated result that should be tested for other rock lithologies, and in the future, the general behaviour of mechanical degradation under weathering should be determined. The degradation curve can be represented by Eq. 7:

$$R = \frac{100}{1+0.1 PWD^{1.4}} \quad (7)$$

Note that the UCS, ITS and E degradation curves of the Monte Seco Tunnel rock mass have the same form (Eq. 7) and depend on PWD only. Therefore, the same degradation function will be able to determine all parameters. For example, the weathered UCS is obtained by Eq. 8, and the same procedure can be performed for ITS and E.

$$UCS_w = R UCS_f = \frac{100}{1+0.1 PWD^{1.4}} UCS_f \quad (8)$$

These preliminary results motivated us to infer the application of this theory to other rock masses with similar mineralogical and textural characteristics. Five data points were selected from the literature to represent UCS results for a large range of weathering conditions (PWD): gneiss (Dobereiner et al., 1993), quartzite and kinzigite (Gupta and Rao, 2001), augen gneiss and leptinite (Marques et al., 2010). The literature data were normalized by using the same approach as that used for the Monte Seco Tunnel test data (Eq. 4 and Eq. 6), and the results are presented in Figure 6.12c (arithmetic scale) and Figure 6.12d (PWD plot in log scale). The parameters used to normalize the mechanical parameters are shown in Table 6.3. The normalized literature data plot in the same range as the Monte Seco Tunnel data and can be represented by a unique function. The innovative result is that Eq. 8 can be used with the results of all the data. Figure 6.12a indicates that Eq. 8 can represent the normalized results of UCS, ITS and E, and Figure 6.12c shows the Eq. 8 fit result of UCS for different rocks with the same characteristics.

A general, qualitative and quantitative synthesis of Monte Seco gneissic rock weathering is presented in Table 6.4. Table 6.4 was constructed for weathering grades I to V, for which the rock matrix mineralogical modifications were related to the geotechnical parameters. For example, cordierite (Cr) and biotite (Bt) are minerals that control the matrix bond loss of the gneissic rock of the Monte Seco Tunnel because they trigger cracks in the adjacent minerals in grades III and IV (more intense cracking in degree IV), a situation that does not occur in grades I and II. The weathering grades III and IV present significant reductions in their strength parameters, for example, grade III

has a UCS between 100-30, whereas grades I and II have a UCS > 100 MPa. Quantitative information about weathering (Table 6.4) is important for Monte Seco Tunnel maintenance and future engineering interventions.

The PWD and R-value of Table 6.4b should be considered a general result for gneissic rock and similar lithologies and could be used to define the degradation effect on mechanical properties.

Table 6.3 - The porosity and uniaxial compression strength values

References	Rock	η_f (%)	η_u (%)	UCS _f (MPa)
This study	Gneiss	0.2	22	165
Dobereiner et al. (1993)	Gneiss	1.0	13	200
Gupta and Rao (2001)	Quartzite and Kinzigite	0.02	17	210
Marques et al. (2010)	Augen Gneiss and Leptinite	0.2	20	120
		0.5	15	120
		0.5	14	160

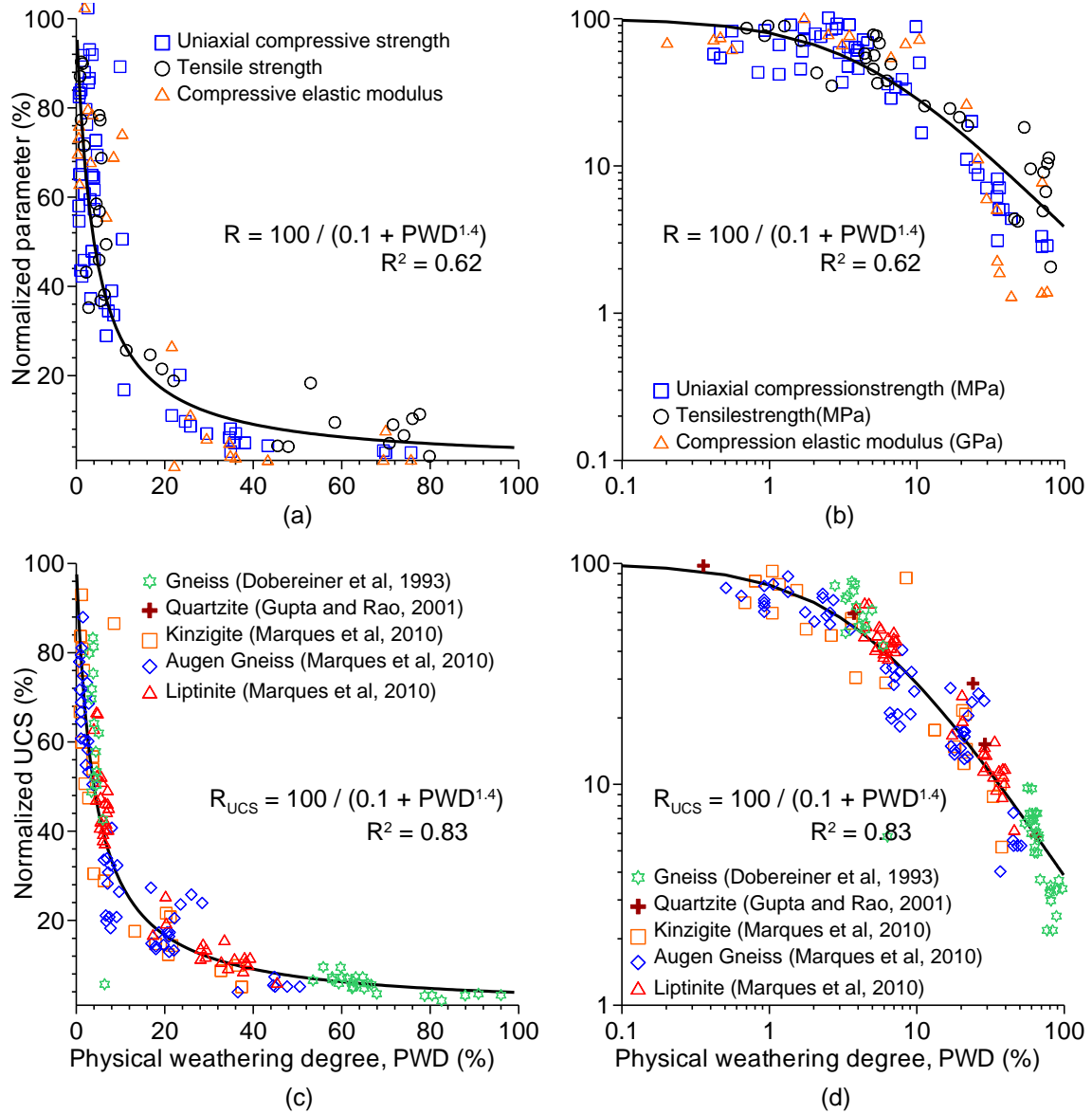


Figure 6.12 - The degradation curves of rock mechanical parameters due to weathering of the Monte Seco Tunnel and of similar lithotypes.

Table 6.4a - Weathering grades of gneissic rock matrix in terms of petrographic modifications

PF	WG	Staining	Nature of rock matrix microsystems	Condition of alteromorphs boundaries	Condition of alteromorphs stages	$I_{p \text{ mod}}$	
B1 - B2	W1	I	No penetration of brown iron staining.	Contact. Fissural nonexistent to very short/fine F_i .	Completely tight and sharp.	No weathering.	> 100
				Contact. Fissural, very short/fine F_i .		Cleaved minerals showing intramineral fissures (Bt and Fk).	100 - 60
	II	Iron staining only along the joint walls, influenced by the foliation.	Increasing length and number of F_i . Formation of F_e . Incipient formation of plasmic microsystems.	Tight and sharp with faintly stained mineral boundaries. Start of bond loss between some alteromorphs.	Cr (1) is slightly weathered by pinitization process, followed by incipient sericitization of Pl (1) and Fk (1) and chloritization of Bt (1).	60 - 30	
B1 - B2 - B3	W2	III	Penetration of iron staining into the rock matrix along the fissures. Rock and mineral discolouration.	Formation of branches of F_i and F_e . Formation and extension of branches of F_t . Plasmic microsystems are connected ($I_p < 15$).	Embrittlement of Cr alteromorphs boundaries. Higher quantities Fk and Bt with boundaries affected by the open cleavages. Increasing bond loss between alteromorphs.	Weathering increases in Cr (1-2) by pinitization and chloritization processes, followed by an increase in the quantities of Pl (1), Fk (1) and Bt (1) alteromorphs. Qz fissured.	30 - 10
B1 - B2 - B3	W3	IV	More inward penetration of brown iron staining along fissures. Rock and minerals discoloured.	High quantities of branches of F_i , F_e and F_t forming a complex fissure network with the dendritic to parallel pattern of fissures. Plasmic microsystems are connected, isolating contact microsystems.	Disaggregation of Cr and embrittlement of Pl, Fk and Bt alteromorphs boundaries. Fk and Bt presenting open and weathered cleavages. The alteromorphs boundaries are considerably open.	Complete weathering of Cr (1-4) to secondary products. Increasing of Pl and Fk (1-2) alteromorphs stages. Increasing quantities of Bt (1-2) with open cleavage appearance. Qz fissured.	10 - 2
		V	Complete discolouration of rock and minerals. Whole rock is stained with iron.	Dominant fissural and plasmic microsystem in the rock matrix. Complex dendritic to parallel pattern of fissure network dominated by F_t , unfilled to filled by secondary products.	Decomposition and disaggregation of whole alteromorphs boundaries. The alteromorphs boundaries are open and isolated by secondary products.	Complete weathering of Cr (1-4) and Pl (1-4) to secondary products. Partial weathering stage development of Fk (1-3) and Bt (1-3). Qz fissured.	< 2

Obs: Petrographic facies (PF), weathering grade (WG); intramineral (F_i), intermineral (F_e) and transmineral (F_t) fissures; and quartz (Qz), orthoclase (Fk), plagioclase (Pl), cordierite (Cr) and biotite (Bt). Modified micropetrographic index ($I_{p \text{ mod}}$).

Table 6.4b - Weathering grades of gneissic rock matrix in terms of physical-mechanical parameters and indexes

PF	WG	ρ	η	PWD	R_L	V_p	UCS	ITS	E	$R_{S, ITS, E}$	
		(g/cm ³)	(%)	(%)	(%)	(m/s)	MPa	MPa	GPa	(%)	
B1 - B2	W1	I	> 2.68	< 0.8	< 2.5	> 68	> 4800	> 140	> 9.2	> 53	> 85
		II	2.68 - 2.65	0.8 - 1.6	2.5 - 8	68 - 62	4800 - 4200	140 - 100	9.2 - 6.6	53 - 38	85 - 60
B1 - B2 - B3	W2	III	2.65 - 2.52	1.6 - 4.0	8 - 25	62 - 46	4200 - 2700	100 - 30	6.6 - 2	38 - 12	60 - 20
B1 - B2 - B3	W3	IV	2.52 - 2.27	4.0 - 10	25 - 45	46 - 36	2700 - 1600	30 - 10	2.0 - 0.66	12 - 4.0	20 - 5
		V	< 2.27	> 10	> 45	< 36	< 1600	< 10.0	< 0.66	< 4.0	< 5

Obs: bulk density (ρ), porosity (η), physical weathering degree (PWD), rebound number (R_L), compressive wave velocity (V_p), uniaxial compressive strength (UCS), indirect tensile strength (ITS), elastic modulus (E) and mechanical weathering index ($R_{S, ITS, E}$).

6.7 Conclusion

The paper presents data on a complete range of weathering conditions, index properties and mechanical properties of the Monte Seco Tunnel gneissic rock mass. A mineralogical and petrological study was performed to explain the effect of weathering on the rock microstructure. Three petrographic facies (B1, B2 and B3) were identified. The weathering index of the gneissic rock mass was associated with its microsystem evolution, weathering pattern, textural and micromorphological classification.

Facies B1 and B2 are rich in mafic minerals with tight intramineral fissures (biotite), resulting in higher density values than those for facies B3, which include felsic coarse-grained minerals with incipient intra- to transmineral fissuring.

$I_{p \text{ mod}}$ was used to quantify the mineralogical weathering effect. The relationships among $I_{p \text{ mod}}$, physical properties (bulk and porosity), R_L and V_p were defined, and the index clearly depended on both these rock properties and the weathering grade.

The anisotropy was determined from the transverse and parallel ITS results. The effect of anisotropy increases with weathering grades.

The mechanical properties (UCS, ITS and E) and the bulk density, R_L and V_p decrease with increasing of porosity. These results directly reflect the influence of weathering on the mechanical properties.

A general degradation curve for this gneissic rock mass and correlated lithology was proposed. The normalized UCS, ITS and E of the Monte Seco Tunnel rock mass fit the same function and depend on PWD. The degradation curve can represent the weathering effect of 6 lithologies. This result may be different for rocks from other rock formations or with different microstructural arrangements, textures, mineralogies, etc. However, this paper introduces an approach for grouping normalized data and can be used to create a general classification of weathering grade associated with quantitative information.

6.8 References

- ASTM D3967-08, 2008. Standard Test Method for Splitting Tensile Strength of Intact Rock Core Specimens 1 D3967-08. ASTM Int. West Conshohocken, PA, 20–23. doi:10.1520/D3967-08.2
- ASTM D5983-00, 2001. Standard Test Method for Determination of rock hardness rebound number method D 5983 - 00. ASTM Int. West Conshohocken, PA.
- Aydin, A., 2014. Upgraded ISRM suggested method for determining sound velocity by ultrasonic pulse transmission technique. *Rock Mech. Rock Eng.* 47, 255–259. doi:10.1007/s00603-013-0454-z
- Aydin, A., 2009. ISRM Suggested method for determination of the Schmidt hammer rebound hardness: Revised version. *Int. J. Rock Mech. Min. Sci.* 46, 627–634. doi:10.1016/j.ijrmms.2008.01.020
- Aydin, A., Basu, A., 2005. The Schmidt hammer in rock material characterization. *Eng. Geol.* 81, 1–14. doi:10.1016/j.enggeo.2005.06.006
- Barton N, Choubey V (1977) *The Shear Strength of Rock Joints in Theory and Practice.* *Rock Mech.* 10:1-54. doi: 10.1007/BF01261801.
- BS 5930, 1999. Code of Practice for Site Investigations, British Standard. British Standards Institution, London.
- Buyuksagis, I.S., Goktan, R.M., 2007. The effect of Schmidt hammer type on uniaxial compressive strength prediction of rock. *Int. J. Rock Mech. Min. Sci.* 44, 299–307. doi:10.1016/j.ijrmms.2006.07.008
- Cacciari, P.P. and Futai, M.M. 2016. Mapping and characterization of rock discontinuities in a tunnel using 3D terrestrial laser scanning. *Bulleting of Engineering Geology and Environment*, 75: 223–237. doi:10.1007/s10064-015-0748-3
- Cacciari, P.P. and Futai, M.M. 2017. Modeling a Shallow Rock Tunnel Using Terrestrial Laser Scanning and Discrete Fracture Networks. *Rock Mechanics and Rock Engineering*, 50: 1217–1242. doi:10.1007/s00603-017-1166-6
- Dearman W.R., Baynes F.J., Irfan T.Y. 1978. Engineering grading of weathered granite. *Engineering Geology*, 12: 345–374. doi:10.1016/0013-7952(78)90018-2

- Deere, D.U., Patton, F.D., 1971. Slope Stability in Residual Soils. 4th Panam. Conf. Soil Mech. Found. Eng. States art Pap. 525, 87–170. doi:10.1016/0267-7261(96)00001-2
- Delvigne, J.E., 1998. Atlas of Micromorphology of Mineral Alteration and Weathering, The Canadian Mineralogist. Ontario, Canada.
- Dobereiner, L., Durville, J.L., Restitutito, J., 1993. Weathering of the massiac gneiss (massif central, France). Bull. Int. Assoc. Eng. Geol. - Bull. l'Association Int. G  ologie l'Ing  nieur 47, 79–96. doi:10.1007/BF02639596
- Esaki, T., Jiang, K., 1999. Comprehensive study of the weathered condition of welded tuff from a historic stone bridge in Kagoshima, Japan. Eng. Geol. 55, 341–350.
- Gupta, A.S., Rao, K.S., 2001. Weathering indices and their applicability for crystalline rocks. Bull. Eng. Geol. Environ. 60, 201–221. doi:10.1007/s100640100113
- Hoek, E., Brown, E., 1997. Practical estimates of rock mass strength. Int. J. Rock Mech. Min. Sci. 34, 1165–1186. doi:10.1016/S1365-1609(97)80069-X
- Hucka, V., 1965. A rapid method of determining the strength of rocks in situ. Int. J. Rock Mech. Min. Sci. Geomech. 2, 127–134.
- Iliev, I., 1966. An attempt to estimate the degree of weathering of intrusive rocks from their physico-mechanical properties, in: 1^o ISRM Congress: International Society for Rock Mechanics.
- Irfan, T.Y., Dearman, W.R., 1978. The engineering petrography of a weathered granite in Cornwall, England. Q. J. Eng. Geol. Hydrogeol. 11, 233–244. doi:10.1144/GSL.QJEG.1978.011.03.03
- ISRM, 2015. The ISRM Suggested Methods for Rock Characterization, Testing and Monitoring: 2007-2014. Springer International Publishing, Cham. doi:10.1007/978-3-319-07713-0
- ISRM, 1979a. Suggested Method for Determination of Water Content, Porosity, Density, Absorption and Related Properties and Swelling, Slake Durability Index Properties. Int. J. Rock Mech. Min. Sci. 16, 141–156.

- ISRM, 1979b. Suggested methods for determining the uniaxial compressive strength and deformability of rock materials. *Int. J. Rock Mech. Min. Sci. Geomech.* 16.
- Kahraman, S., Fener, M., Gunaydin, O., 2002. Predicting the Schmidt hammer values of in-situ intact rock from core sample values. *Int. J. Rock Mech. Min. Sci.* 39, 395–399. doi:10.1016/S1365-1609(02)00028-X
- Marques, E.A.G., Barroso, E. V., Menezes Filho, A.P., Vargas, E. do A., 2010. Weathering zones on metamorphic rocks from Rio de Janeiro-Physical, mineralogical and geomechanical characterization. *Eng. Geol.* 111, 1–18. doi:10.1016/j.enggeo.2009.11.001
- Monticelli, J.P., Cacciari, P. P., Futai, M. M., 2019a. Concept model of weathering advance in the Monte Seco Tunnel region, Espírito Santo State, Brazil. (paper to submission)
- Monticelli, J.P., Sígolo, J.B., Futai, M.M., 2019b. Textural and micromorphological characterization of gneissic rock alteromorphs resulting from the degradation under tropical climate conditions - A pioneer cordierite alteromorphs characterization (paper to submission)
- Perras, M.A., Diederichs, M.S., 2014. A Review of the Tensile Strength of Rock: Concepts and Testing. doi:10.1007/s10706-014-9732-0
- Poole, R.W., Farmer, I.W., 1980. Consistency and repeatability of Schmidt Hammer rebound data during field testing. *Int. J. Rock Mech. Min. Sci.* 17, 167–171. doi:10.1016/0148-9062(80)91363-7
- Sajid, M., Coggan, J., Arif, M., Andersen, J., Rollinson, G., 2016. Petrographic features as an effective indicator for the variation in strength of granites. *Eng. Geol.* 202, 44–54. doi:10.1016/j.enggeo.2016.01.001

7. GENERAL REMARKS

In the weathering study of the gneissic rock mass, the geological and geotechnical investigations focusing on structural geology were of fundamental importance to develop the concept model of weathering advance in the Monte Seco Tunnel. The study of the genesis of the structures along the geologic time helped explain the difference of intensity and type of fracturing that affects the rock mass in depth, permitting characterize specific weathering profiles along the tunnel. The weathering advance in the gneissic rock mass is clearly structurally controlled.

In the critical sector C, ca. 120 m far from the southern entrance, the weathering advanced via foliation S_n and discontinuity set F2 of the Precambrian age, reactivated during the Cretaceous, and via discontinuity set F1 of Cenozoic age. The Neotectonism (Cenozoic age) is responsible the changing the drainage pattern in the study area and for originating discontinuity set F1, which currently conditions water infiltration in sector A. This process is also responsible for the denudation and uplift of the rock mass, which helped the formation of relief fractures (discontinuity set F3) related to the foliation, parallel to hillside in sector B. These geologic events trigger the destabilization of rock blocks that impact iron ore transport logistics by the VALE S.A. Vitória-Minas Railway in the Monte Seco Tunnel. The sector D there is no conditions to weathering advance and the fall of blocks can be disregarded comparatively to sectors A, B and C.

Once the weathering was recognized throughout the rock mass, the heterogeneity of the intact rock was classified in petrographic facies and analyzed by thin sections and physical-mechanical tests. The use of standardized classification of the textural and micromorphological modification of the minerals helped characterize the increase of intra to transmineral fissures and the mineral weathering stages related to the mechanical degradation in each weathering grade. These procedures were needed to understand the gneissic rock matrix transformations and identify the minerals - and modifications in their crystal fabric - responsible for the alterability of the petrographic facies and the influence in the strength degradation in the tropical environment.

The cordierite and biotite Meso-alteromorphs textural modifications acts as an edge effect triggering the increase of intra to transmineral fissuring processes of gneissic rock

matrix, which conducts a significant bond loss among whole minerals and progressively drops in the gneissic mechanical values in the weathering grades II-III and III-IV, respectively. The increase of grain size of the minerals from facies B1 to B3 influenced the fissure increasing and the cordierite weathering conducting higher disaggregation process to facies B3, comparatively to facies B1 and B2. Based on the petrographic and physical-mechanical indexes, such as I_p , I_{d4° and R_s , facies B3 was placed at the start of the moderately weathered grade (III), thus an unfavorable rock matrix characteristic to the Monte Seco Tunnel.

The development of this work also made it possible to propose an equation for estimating the alterability parameter in the RMR 2014 update, which contributes to a better distribution of its values and allows the distinction of geomechanical sections of heterogeneous geological substrates, such as the Monte Seco Tunnel. However, the assessment of this parameter by slake durability test needs to be further investigated by the geological engineering community for define the number of cycles, his applicability and influences in tunneling projects.

A general degradation curve for this gneissic rock mass and correlated lithology was proposed. The normalized UCS, ITS and E of the Monte Seco Tunnel rock mass fit the same function and depend on PWD. The degradation curve can represent the weathering effect of 6 lithologies. This result may be different for rocks from other rock formations or with different microstructural arrangements, textures, mineralogies, etc. However, this dissertation introduces an approach for grouping normalized data and can be used to create a general classification of weathering grade associated with quantitative information.

The methodology developed herein to the weathering study of a gneissic rock mass can be applied to unsupported tunnels with problems of block instability, not only along the Vitória-Minas Railway, but also in other geologically similar regions. The present study of the Mantiqueira Complex is of interest to Southern Brazil, where important metropolitan regions are located, and which may demand projects and construction of underground works, such as highway and railway tunnels.